NCC1-01010

Sliding-Mode Control Applied for Robust Control of a Highly Unstable Aircraft

By
Travis Kenneth Vetter

B.S. Mech. Engineering & Material Science (University at California at Davis) 2000
B.S. Aeronautical Engineering (University of California at Davis) 2000

MASTERS THESIS

Submitted in partial satisfaction of the requirements for the degree of

MASTERS OF SCIENCE

In

Mechanical and Aeronautical Engineering

in the
OFFICE OF GRADUATE STUDIES

of the
UNIVERSITY OF CALIFORNIA
DAVIS

Approved:

_____

_____

_____

Committee in Charge
2002

Acknowledgments

In my undergraduate college admission, as with most university students, an essay was required. In that essay I explained and expounded on a "becoming a 'they'". The group of people so often referred to when questions arise. "How do they do that?" and the so common answer to the why question, "Because that is how they do it!" After years of study occasionally I have an answer. But perhaps the larger victory has been in beginning, ever so slightly, to understand the questions. In this project, one with a scale and complexity I have never attempted, the part I enjoyed the most, was always the question, what is 'x' doing and why? How can we optimize this? How does this help? What's next? It has been with much pleasure that I was a part of asking these questions for this project. However, a project of this magnitude cannot be accomplished alone. The hours and resources required have taxed all those around me and also built and reinforced so much.

I wish to thank my advisor, Prof. Hess for his support, guidance and notable efforts to provide funding and the computer resources required for this endeavor. To NASA, this research was supported by grant NCC1-01010 from NASA Langley Research Center. The grant technical manager was Dr. Barton Bacon. And to Prof. Baughn who generously allowed Scott and I to occupy a corner of his lab. Thanks, too, to Dr. Major Scott Wells who has been instrumental in the completion of this project. He is insightful, generous, and patient. But more importantly, a year and a half of study, philosophy and humor, often over lunch on the quad, have made him a valued friend.

Special thanks to my immediate and extended family for all their support, guidance and above all, their love and caring. They have been and continue to be my strongest asset. There many contributions have shaped me and made this project possible, my mother's strength and leadership, my father's wisdom, and humor, and my stepfather's many years as an engineering role model, and life support. To my sister Ashley, whose search through life and ever growing wisdom has been challenging and wonderful. My brother once said he was "born to save me from permanent dweebdum", he later added that I was "born to save him from jockdum". Perhaps this is true, for since day one we have been best friends and admiring brothers. Finding adventures, challenges, both mental and physical, and support beyond what I could have imagined. And to my dearest Christina, whose smile, kindness and intelligence continue to make my life a wonderful place to be. This project could not have been completed without the valued support from the school, faculty, family, and friends. Thank you.

Table of Contents

Abstract

An investigation into the application of an observer based sliding mode controller for robust control of a highly unstable aircraft and methods of compensating for actuator dynamics is performed. After a brief overview of some reconfigurable controllers, sliding mode control (SMC) is selected because of its invariance properties and lack of need for parameter identification. SMC is reviewed and issues with parasitic dynamics, which cause system instability, are addressed. Utilizing sliding manifold boundary layers, the nonlinear control is converted to a linear control and sliding manifold design is performed in the frequency domain. An additional feedback form of model reference hedging is employed which is similar to a prefilter and has large benefits to system performance. The effects of inclusion of actuator dynamics into the designed plant is heavily investigated. Multiple Simulink® models of the full longitudinal dynamics and wing deflection modes of the forward swept aero elastic vehicle (FSAV) are constructed. Additionally a linear state space models to analyze effects from various system parameters. The FSAV has a pole at +7 rad/sec and is non-minimum phase. The use of 'model actuators' in the feedback path, and varying there design, is heavily investigated for the resulting effects on plant robustness and tolerance to actuator failure. The use of redundant actuators is also explored and improved robustness is shown. All models are simulated with severe failure and excellent tracking, and task dependent handling qualities, and low pilot induced oscillation tendency is shown.

List of Figures

Chapter 1

Introduction

1.1 Introduction

The ability to stabilize and control aircraft has been one of the great successes of the aeronautical field. From the beginning, extreme attention and effort was expended to achieve desired stability properties, whether the aircraft, alone, was stable or not (Wright Flyer). For almost the entire history of aeronautics engineers have relied on the physical configuration of the aircraft to provide both desired performance and stability, including damage tolerance and changes in the flight regime. All flight profiles had to be stabilized and obtained by changing the shape of the airplane. This leads to a combination of three problems, poor performance, small flight envelope, and extreme mechanical complexity. The introduction of stability augmentation systems began to deal with all these issues in a beneficial way, greatly increasing the flight envelope, while allowing for simpler, lighter mechanical configurations.

The benefits obtained by stability augmentation systems (SAS), particularly digital systems, stem from the ability to tailor an airframe to design requirements other than stability and control, such as stealth, payload shape or a particular flight condition. The SAS could be designed to modify the dynamics of the aircraft, yielding an aircraft with satisfactory behavior in a given flight condition. A shortcoming of stability augmentation systems is quickly realized when one must account for varying aircraft dynamics at a variety of different flight conditions. A feedback structure on take off

may be far too aggressive at mach 2. Previously this task was performed by over-designing surfaces, pilot adaptation, and gain scheduling to compensate for changes in flight regime. However, a key assumption in gain scheduling is that the plant behavior is known and a predesigned controller can be chosen. What about plant failures or changes which are not foreseen? What about changes to the airplane which are not part of the decision parameters? The motivation for adaptive or reconfigurable control becomes glaringly apparent.

1.2 Why and What: Reconfigurable Control

In the past 20 years a huge increase in the volume of literature on the subject has followed an increasing need for research in this area. Ever- increasing demand for performance and initial improvements in SAS has lead to the design of extremely high-performance airplanes with unstable airframes and divergent behavior beyond the capability of a pilot to control. In addition, the drastic increase in pilot workload suggests the need for SAS systems which can improve the handling qualities and reduce the workload requirements on the pilot. Furthermore, in a military setting, "Lessons learned from the Vietnam Era show 20% of aircraft losses were due to flight control damage. Loss of hydraulics, actuator damage, and surface damage are responsible for most of the flight control system losses,"[1] and in the civilian sector, huge increases in air travel have driven increases in safety and tolerance of aircraft to damage and failure. The economics of flight also dictate an increased need for both performance and robustness. As aircraft become more and more complicated and capable, their cost increases and the loss of an aircraft, even without the human cost, becomes a high

economic burden. All of these factors motivate research into failure and damage tolerance.

While robustness to plant variation and failures has been synonymous with compromised performance, perhaps it is possible to construct a feedback scheme or algorithm which adapts and reconfigures the control laws to the aircraft behavior? Such a system might have excellent performance over a wide range of flight regimes and failures. This is the basis and hopes for a reconfigurable controller.

A reconfigurable controller can be defined as any controller which is able to tolerate sudden, large changes to parameter variation and unmodeled dynamics in real-time by variation or modification of the error dynamics. There are many avenues of research currently being investigated to achieve these ends.

1.3 Types of Reconfigurable control

1.3.1 Failure detection

Failure detection followed by control law selection was employed in the past and continues to be used today. A set of hypothesized failures is considered and then some sort of detection system is created. Other issues arise because of the necessity of measuring many parameters. In measuring parameters like actuator position, a seemingly simple task, it become quite difficult when one considers that the measurement system may be as prone to failure as the actuator itself. If an improper reconfiguration is chosen, it may then drive the aircraft unstable. While there are many other ways to perform failure detection [1-4] and some are quite effective, they all struggle with the same problem; the actual failures must match an anticipated failure. The more

classes of failures anticipated, the harder it is to distinguish which failure occurred, and the complexity of the system increases extremely quickly.

1.3.2 Control allocation

Conventional aircraft have controls designed to apply only one moment to the aircraft. For example: the elevator controls pitch, the rudder yaw, and the aileron roll. And while a certain amount of coupling occurs, each particular effector is significantly more powerful in its primary direction than any other. This makes allocation of control moments a fairly simple process. However, as aircraft become less conventionally shaped and begin to include many redundant and highly coupled control surfaces, allocation becomes vastly more complicated. Ideally a control allocation should be defined in such a way that decoupled moments result. In order for such a system to be considered reconfigurable, it would have to dynamically change that allocation based on tests or algorithms.

Control allocation schemes can follow the same reconfigurable concepts of failure detection or can use a more adaptive approach. However, the basic concept is that by changing how and which actuators are used, the response of the aircraft can be tailored. If a failure is detected in an aileron, perhaps the gain to the opposite aileron will be doubled. This is an extremely simple example, and many more sophisticated systems exist and including varied cost functions, attainable moment subsets, facet searches, pseudo inverse, and many others, including simple ganging or daisy chaining techniques.

1.3.3 Parameter Identification

Parameter identification is a very active area of research in reconfigurable control. It is generally divided into two main categories, indirect adaptive and direct adaptive. Indirect adaptive schemes generally rely on reconstructing the plant, or a lower order approximation, by observing the input output characteristics and then constructing or choosing a control scheme which will be appropriate. This class of adaptive laws includes Receding Horizon Optimal control, Multiple Model Adaptive Control, and many others. Whether the method solves the problem in the time or frequency domain, there will be some required amount of time, or some sort of averaging over time. Some methods can deduce the primary system parameters within one period of the dominant mode.[5] However, in some highly unstable designs this may be too long to maintain controlled flight.

Direct adaptive schemes generally try to reconfigure the controller based on the error between what was actually achieved and what was expected without reconstructing the plant. For this reason they often include an internal model of the system to which it compares the actual states. Examples of these systems include linear and nonlinear dynamic inversion. It should be noted that many types of a nonlinear dynamic inversion use an indirect method of parameter identification to manage and reduce the inversion error, particularly in the event of a failure. An example can be found in Siwakosit.[6] A type of indirect parameter identification which has shown great promise is Sliding Mode Control (SMC). Previous work by Shtessel[7-10] and Utkin.[11,12] SMC is invariant to certain types of parameter variation, and can be robust to other types and does so without

any parameter identification at all. These features make it very attractive option among reconfigurable designs.

1.4 Thesis overview

In previous works Sliding Mode Control has shown great promise in robustness to model uncertainty, adaptation to unknown and potentially large parameter changes due to failure events while maintaining a low pilot induced oscillation tendency and retaining near design handling qualities. The purpose of this research is to expand the understanding and applicability of Sliding Mode Control. Investigation into observer design criteria, hedging effects, and the effect of inclusion and exclusion of actuator dynamics in the sliding manifold design is performed using a highly unstable aero elastic vehicle.

Chapter 1 provides a cursory introduction to the concept of reconfigurable control and places sliding mode control relative to other control architectures. Chapter 2 introduces SMC theory and parasitic dynamics. Chapter 3 begins to investigate the issues and concerns in SMC design and implementation in all systems but focuses on issues pertaining to the current design challenge. Chapter 4 introduces the Forward Swept Aero Elastic Vehicle (FSAV) model and the setup chosen to be tested. This introduces a general SMC design procedure using the frequency domain and then applies that approach to three variations of the FSAV utilizing two different sliding manifolds and varying actuator configurations. Chapter 5 discusses the results of the simulations, investigates effects of design choices and compares the benefits and drawbacks of the three design variations. Chapter 6 summarizes and concludes this research along with recommendation for further investigation.

The FSAV model used was introduced by Gilbert in 1982.[13] In his recommendations he stated that his analysis could be extended in a number of ways including, "Further investigation of the integrated flight control and aero elastic wing stabilization aspects of aircraft control system design."[13] Little could he have suspected that the dynamics which challenged the FSAV model could be neglected without any performance degradation by designing an appropriate reconfigurable control system.

After highlighting a few types of reconfigurable control structures, and deciding that Sliding Mode Control is a serious option for future control schemes, it is now necessary to introduce the basics of Sliding Mode Control.

Chapter 2

SMC

2.1 Introduction to SMC

In chapter 1 a very brief overview of control was given. While the number of ideas presented only constitutes a fraction of the control schemes available, SMC tantalizes the designer with instantaneous and complete adaptation to matched uncertainty. Parameter identification and error detection, along with the logic to support them, presents enormous challenges to the control designer. SMC has no adaptation algorithm and no failure detection scheme, its very construction makes it invariant to matched uncertainty. Thus, any failure or noise or plant variation which is matched will result in zero performance degradation and require zero adaptation time.

Using terms like 'zero adaptation time' and 'instantaneous' quickly raise eyebrows and suggest an absence of parasitic dynamics and time delays. In fact, as will be shown the inclusion of parasitic dynamics is a restriction on ideal SMC's. Therefore, when implementing SMC with real actuators, digital computers and other parasitic effects, a more complicated system is formed.

The fundamental concepts of SMC were first seen in Russia as early as the 1930's. However, it was not seen outside Russia until the 1970's when papers by Itkis[14] (1976) and Utkin[12] (1977) were released in English. (Authors Note: I am continually amazed at both SMC's youthfulness and its age every time I consider that I was born 1977!) Since then, SMC has been investigated and implemented in a wide range of

applications, from servo motor control, spacecraft control, to power converters, multiple object formation flights, flexible structure control, robotic control, missile guidance and even neural net learning algorithms. Of importance to this work is SMC's application to flight control. During the 1990's available works and attention on SMC have greatly increased through publications by Slotine[15], Young[11], and a book devoted entirely to SMC by Edwards and Spurgeon.[16] Recent works by Shtessel, Hess, Wells, and Vetter have forwarded the use of SMC in flight control applications directly relevant to this work.[7-10,17-28]

2.2 The Ideal Sliding Mode

SMC is a type of variable structure control system (VSC). These systems are a class of control whereby the control law is changed during control as a function of some decision parameter based on the state of the system. Much of the presentation here is based on Edwards & Spurgeon.[16] For the purpose of demonstration consider the double integrator

$$\ddot{y}(t) = u(t) \tag{2.1}$$

Define a non-VSC control law of

$$u(t) = -ky(t) \tag{2.2}$$

where k is strictly positive scalar. Checking the response of the system in Fig. 2-1 using a phase plane portrait, a highly undesirable limit cycle behavior occurs. While varying k can change the eccentricity of the ellipse, it cannot drive the system states to zero.

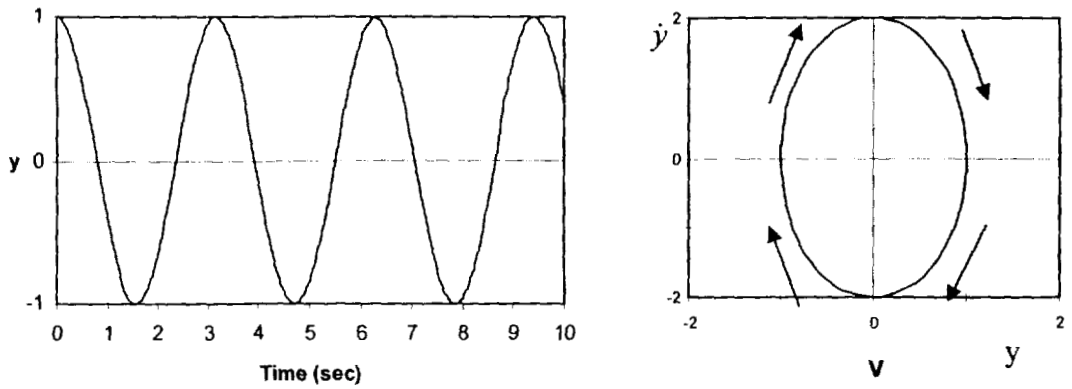

Figure 2-1: Time and Phase Plot of Double Integrator using Gain feedback.

Consider now, using a control structure where $0 < k_1 < 1 < k_2$ to capitalize on the variation of eccentricity with changing k.

$$u(t) = \begin{cases} -k_1 y(t) & \text{if } y\dot{y} < 0 \\ -k_2 y(t) & \text{otherwise} \end{cases} \qquad (2.3)$$

Thus, multiple control laws are being used, decided by the quadrant of the phase plane where the states lie. $y\dot{y}$ is negative in the II and IV quadrants, where defined k_1 is defined such that the eccentricity makes the state get closer to zero. The resulting response and phase portrait is shown in Fig. 2-2

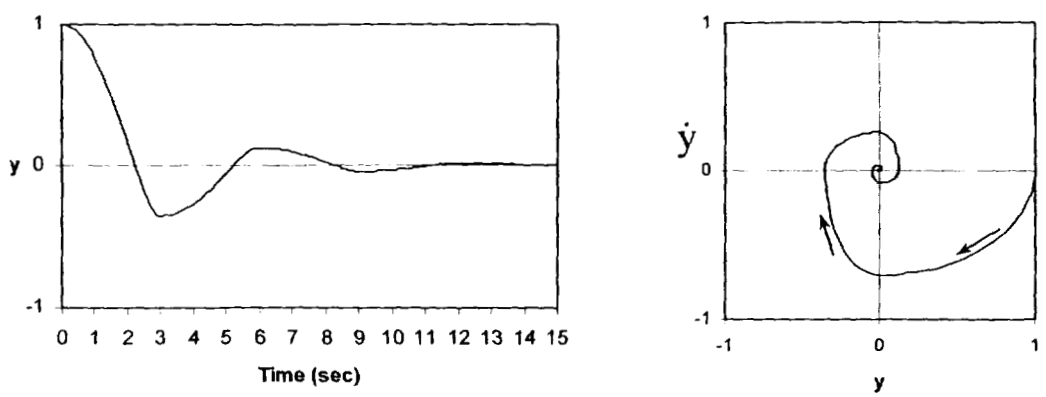

Figure 2-2: Time and Phase Plots under VSC using a quadrant dependent switching function[28]

The resulting system is stable and converges to the origin despite the fact that neither of the individual systems converge!

Here is the interesting part, instead of switching the control at the quadrants, use a switching function, in this case a line, and the control defined as in Eq. (2.4)

$$u(t) = \begin{cases} -1 & if\ \sigma(y,\dot{y}) > 0 \\ 1 & if\ \sigma(y,\dot{y}) < 0 \end{cases} \qquad (2.4)$$
$$\sigma(y,\dot{y}) = my + \dot{y}$$

The second equation is termed the switching function because it is used to decide which control structure is implemented at the time. A concise form of Eq. (2.4) is:

$$u(t) = -sign(\sigma(t)) \qquad (2.5)$$

where sign(x) is the signum function which simply finds the sign of the argument. The resulting time response and phase diagram is show in Fig. 2-3. Note that the function $\sigma(t)$ is undefined on the sliding surface. When the solution is near zero the control will switch at infinite frequency between 1 and -1 as it drive the states to the origin. The response of the system while on the sliding surface is governed *only* by the surface! In this case, as seen in Fig. 2-3, this line represents first order decay, one order below the order of the system. This is a common feature of sliding behavior. In fact leting $\sigma = 0$ and solving for the response of the system it can be shown that:

$$\dot{y} = -my(t) \qquad (2.6)$$

Note that the original plant parameters do not appear! The resulting response is only governed by the sliding surface.

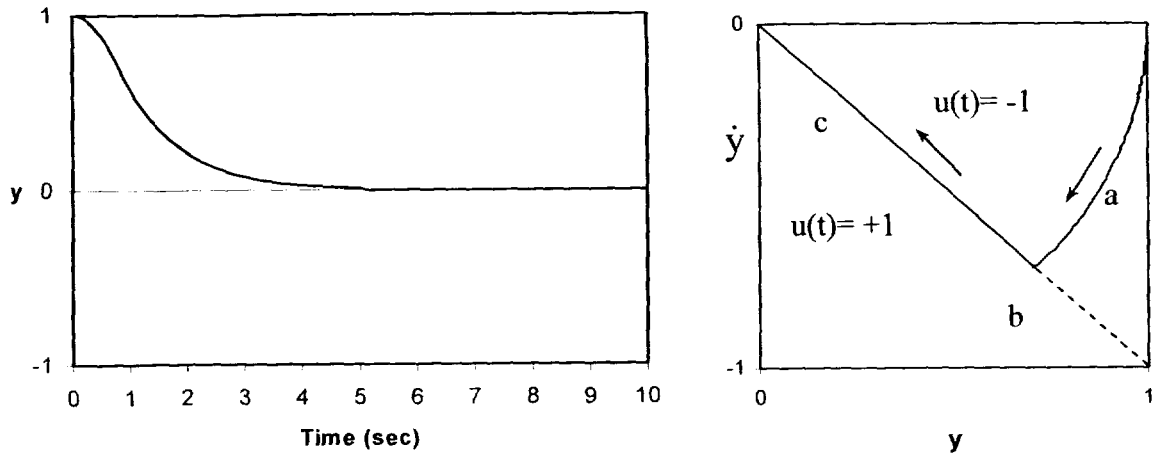

Figure 2-3: Time and Phase plots of Sliding behavior[28].

Figure 2-3 also shows the three main areas of SMC. Label 'a' marks what is termed the "reaching phase". During this time sliding is

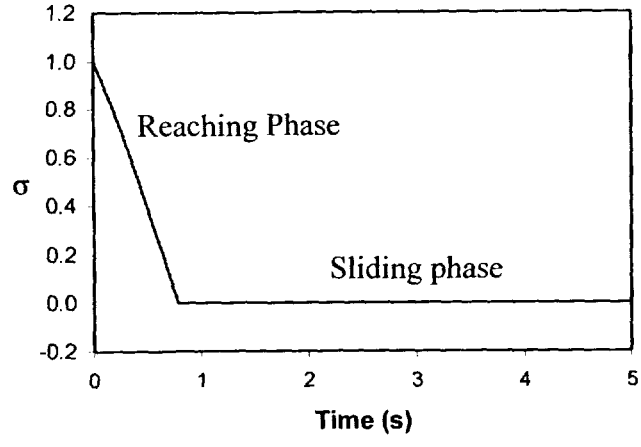

Figure 2-4: Plot of σ vs. Time.[28]

not occurring and the system

response is controlled by the system dynamics and the control chosen. Label 'b' marks the sliding surface, in this case a line. And label 'c' marks the sliding mode or period during which sliding is occurring.

Note that the control defined in Eq. (2.4) is maintaining $\sigma=0$ for all $t>$ time of intersection with the sliding mode. This is shown in Fig. 2-4.

It was stated earlier that SMC is *invariant* to matched uncertainty. Let us modify the original double integrator with a nonlinear term while using the exact same control laws.

$$\ddot{y}(t) = -a\sin(y) + u(t) \qquad (2.7)$$

Let us look at the resulting phase trajectory.

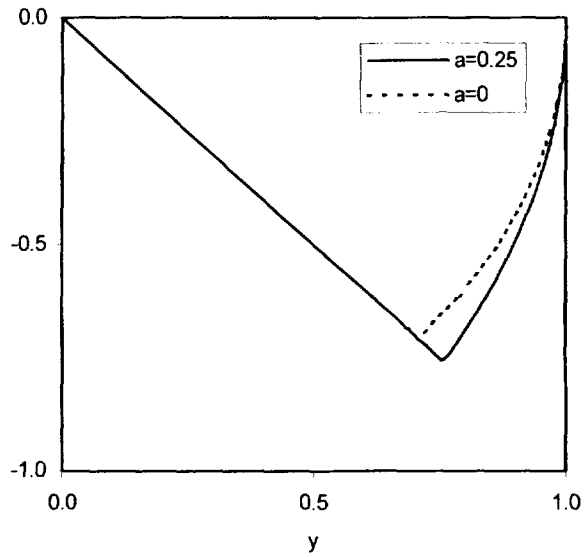

Figure 2-5: Effect of nonlinearity on phase trajectory[28]

During the reaching phase, the effect of the nonlinearity does affect the response. However, no difference is observed once the sliding surface is reached.

So under an ideal Sliding Mode Controller, the following important points are in evidence:

a) The response which results from the VSC is not inherent in either of the two control laws.

b) Control laws must drive the states to the sliding surface for stability and sliding to occur.

c) The resulting dynamics are one order less than the original system

d) Once the system is driven to the sliding surface, infinite switching occurs since the control signal is undefined on $\sigma=0$ and therefore the control switches back and forth.

e) Unmodeled dynamics and matched uncertainty only affect the response during the reaching phase.

An additional element to sliding mode control is that if the system is square, the uncontrolled states are stable and there are no transmission zeros in the right half plane, then SMC acts as a feedback linearizer. The benefit of this is that the control variables become completely decoupled.

It seems as though the world's control problem has been solved! Since there are many pages left in this thesis, there must be more to it.

2.3 Equivalent Control

Because the control input to the system is nonlinear and discontinuous, attempting to perform any analysis of robustness, uniqueness, or performance becomes extremely difficult. In continuous control schemes Lipshitz conditions are usually used. This is improper to apply here since any function which satisfies Lipshitz is necessarily continuous.[16,29] Filippov proposed a method for solving differential equations with

discontinuous right hand sides by averaging the solutions obtained at a discontinuity when approaching from opposite directions.[29] A significantly more intuitive approach was proposed by Utkin, and called equivalent control. This is the control action which would be required to maintain $\sigma=0$.[12]

The equivalent control will be found for Eq. (2.7). Sliding surface is defined as:

$$\sigma(y,\dot{y}) = my + \dot{y} \qquad (2.8)$$

Since $\sigma=0$ on the sliding surface for any time after ignition of sliding, $t>t_s$, then $\dot{\sigma} = 0$. So taking the derivative of Eq. (2.8) and substituting Eq. (2.7) returns:

$$\begin{aligned} &\dot{\sigma}(t) = m\dot{y}(t) + \ddot{y}(t) \quad \textit{Substituting for } \ddot{y}(t) \textit{ gives :} \\ &\dot{\sigma}(t) = m\dot{y}(t) - a\sin(y) + u(t) \end{aligned} \qquad (2.9)$$

Setting the left hand side to zero and solving for u(t) yields u_{eq}.

$$u_{eq}(t) = a\sin(y) - m\dot{y}(t) \qquad (2.10)$$

Note that the equivalent control contains the control required to completely remove the nonlinearity.

In general, it can be shown for an LTI system, given a sliding surface of

$$\begin{aligned} &\sigma(\mathbf{x}) = \mathbf{S}\,\mathbf{x} \\ &S \in \Re^{mxn} \end{aligned} \qquad (2.11)$$

that the equivalent control, u_{eq} is unique and can be written as:

$$u_{eq}(t) = -(SB)^{-1} SAx(t) \qquad (2.12)$$

So why isn't this control used? This control is only effective in maintaining the sliding mode if the exact nonlinearity is known. Any unmodeled, or unknown dynamics will drive the system off the sliding mode. This can be easily seen in the equivalent

control in Eq. (2.10) where the exact nonlinearity is seen that was inserted in Eq. (2.7) If the nonlinearity had been slightly different, the result would be non-sliding behavior under that equivalent control. Using the original variable control law found in Eq. (2.4) would, however, maintain the sliding mode. So the equivalent control tool, while not directly applicable as a control law, is useful for analysis and some proofs, as will be seen.

2.4 Relative Order

Of critical importance to a practical understanding of SMC is the more general concept of relative order. The relative order is defined as the number of times the output of a system must be differentiated for the input to appear. In the double integrator problem the input is u(t) and the output is y(t). Thus the output needs to be differentiated twice to see u(t) in the equation, as in Eq. (2.1) and the relative order is two. The resulting switching, or sliding, surface will always be one order less than the relative order of the system.

It can be shown with ease that a first order actuator has a relative order of one. Simple state space analysis shows us that relative order is additive, and thus, a first order actuator added to this system would increase the relative order by one, to a total of three. The resulting sliding surface would be

$$\sigma(y, \dot{y}, \ddot{y}) = my + n\dot{y} + \ddot{y} \qquad (2.13)$$

The sliding surface should be one less than the relative order of the feedback variable. Other orders, higher or lower, will almost always cause instability. In a linear system, the relative order can be easily found by subtracting the number of zeros from

the number of poles in the transfer function. This can be easily seen in the bode diagram as the slope of the magnitude plot at high frequency, in units of -20 dB/dec.

2.5 Parasitic Dynamics

2.5.1 Issues with Parasitic Dynamics

SMC has one primary design issue, dealing with unmodeled parasitic dynamics. These can be considered as any unmodeled dynamics which add phase lag to the system, or limit the control bandwidth, including unmodeled actuators, limited bandwidth actuators, time delays, and structural modes. All of these issues limit the frequency at which the states can be controlled. This allows the states to leave the sliding surface faster than the controller can drive them back. Most of the research into SMC design is focused on methods to deal with parasitic dynamics. Some of the more prevalent concepts are Boundary Layers, Observer based SMC, Hedging and second order SMC.

2.5.2 Boundary layers & Pseudo Sliding

One solution to the high-frequency commands produced by SMC is the use of a continuous approximation to the VSC. Instead of using infinite frequency control to maintain the states exactly on the sliding surface, to do this a continuous approximation which will keep the states arbitrarily close to the sliding surface is proposed. The continuous approximation near the sliding surface is often called a boundary layer. Since pure sliding behavior is no longer in evidence, the sliding motion is considered 'pseudo-sliding'. This will remove the benefit of strict invariance but produce a continuous control signal of finite bandwidth.

Throughout the literature, the high frequency switching behavior of pure SMC is often referred to as chattering. This is highly unfortunate since this term historically has

been defined as a noticeable chattering of the states. However, in pure SMC, with infinite frequency switching, the states are continuous after being passed through a finite bandwidth plant. The infinite frequency control is, nonetheless, a large problem for finite bandwidth actuators.

While there are many choices to approximate the signum function, as long as the controller does not hit the saturation limits, the exact shape is largely irrelevant. The basic saturation element boundary layer is shown in Fig. 2-6. Some other options are the Power law approximation, sigmoidal function and inverse tangent function. (not shown).

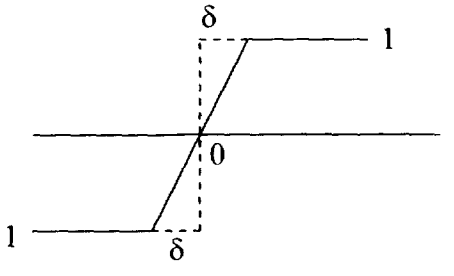

Figure 2-6: Saturation Approximation of Signum Function.

It is shown later that the application of boundary layer methods do eliminate the infinite frequency switching, providing a continuous control signal to the actuators. Depending on actuator speed, in some cases inclusion of actuator dynamics which were not included in the design of the controller can be tolerated. This is so despite the fact that inclusion of these dynamics leads to an improper relative order of the sliding surface.

2.5.3 Observers

The inclusion of an observer in the feedback path as shown in Fig. 2-7 has been shown to drastically increase the ability of the SMC controller to tolerate unmodeled dynamics, especially when used with a boundary layer scheme.

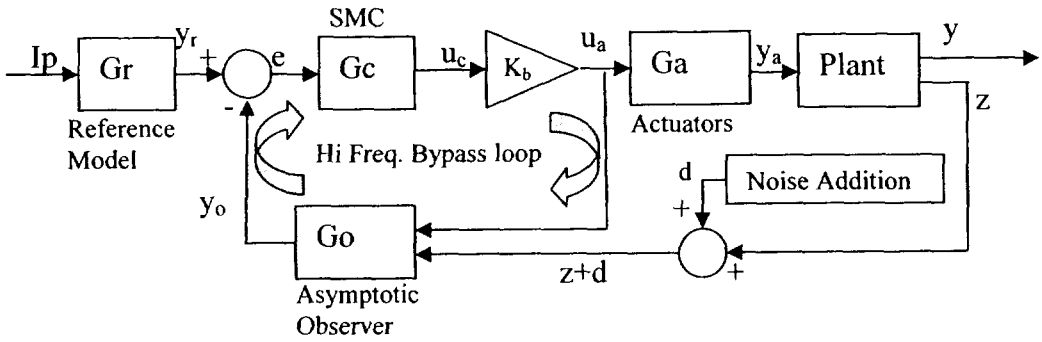

Figure 2-7: Block Diagram Showing Observer Location

In order to understand how the "high frequency bypass loop" works, it is first necessary to understand the feedback properties of an observer when considered in the entire system. The transfer function investigated is from the control output to the observer feedback, $\frac{y_o}{u_c}$, in a single-input, single-output system.

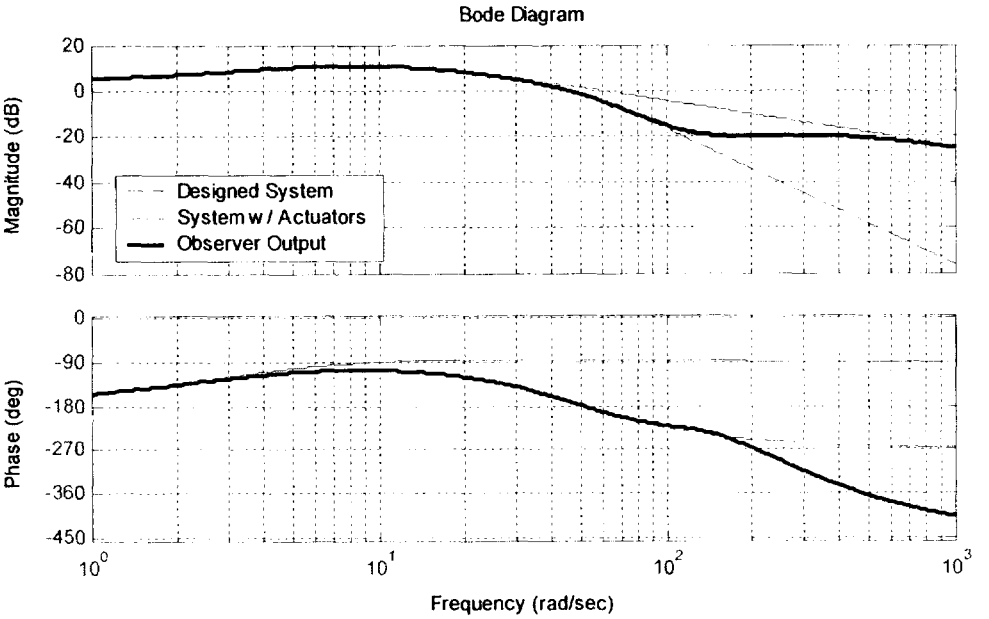

Figure 2-8: Bode Plot of Observer Output $\frac{y_o}{u_c}$.

In first analyzing Fig. 2-8, basic features will be highlighted. Throughout this thesis, observer speeds will be defined by their smallest eigenvalue. For example, if the 'q' observer is running at eigenvalues of λ=10,11,12,13 then it will be referred to as 'Pq1=10'. An airspeed observer with eigen value at λ=0.5, would be designated Pa1=0.5. It is assumed that the rest of the eigen values increase above that. The increment used is usually unity, but larger increments are sometimes used for very fast observers.

From the slope of the magnitude plot at high frequency, in Fig. 2-8, it is concluded that the relative order of the plant (solid line) is one. The actuators are not included in the design and have relative order two. This leads to a plant&actuator relative order of three as seen from the -60 dB/dec decay at high frequency of the dashed

line. This observer is running extremely fast at 200 rad/sec. Note how the observer replicates the dynamics of the actual plant until, at some point, dictated by the eigenvalues of the observer, it relies on the internal model which has a relative order of the plant only. This plot shows how, at very high frequencies, the relative order of the feedback y_o is the designed relative order and not the actual relative order of the system. This is exactly the feature required by the SMC in the high frequency bypass loop.

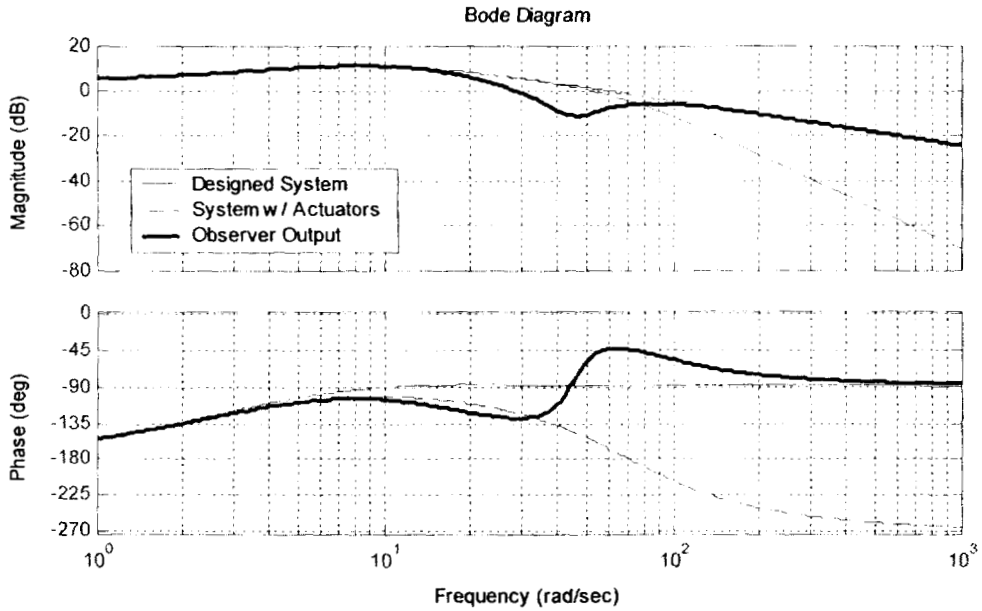

Figure 2-9: Slow Observer: Proper Phase and Low Frequency Magnitude Drop.

Fig. 2-9 shows the same model with a slower observer and faster actuators. This corresponds to the models which will be designed later. At this observer speed two different features are in evidence. First, the phase behavior is significantly better, indeed the phase lags evident by the solid black line in Fig. 2-9 indicates instability of that system. In this diagram it can be seen how the observer tries to track the increased phase

roll-off of the system with actuators but at some frequency resorts to its internal model with the designed phase lag. Again, this is exactly the desired behavior.

The second feature is that the "follow as long as you can then jump" behavior is not observed in the magnitude plot. The sharp drop comes from a pair of very lightly damped zero's resulting from the observer dynamics. There is no actual system feature at 36 rad/sec. This is a good example of why a designer must tweak the system during the design phase.

The two figures combined show how the high-frequency bypass loop operates, the observer allows the SMC to "see" a system which at low frequencies is the actual system, but at high frequencies has the designed relative order. This largely hides the actuator dynamics and increased relative order from the SMC. This has shown itself to be a very effective method and is used throughout this research.

2.5.4 Hedging

2.5.4.1 Hedging Development

Observers successfully hide the high-frequency actuator dynamics, but do nothing for nonlinear actuator effects like position and rate limits.

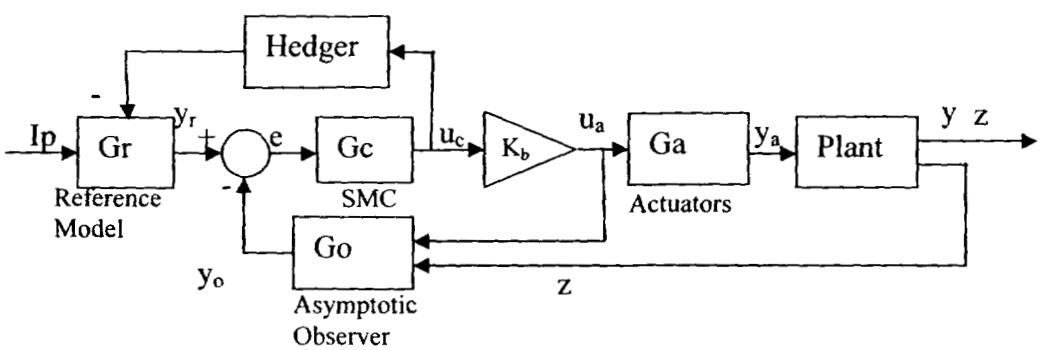

Figure 2-10: Block Diagram of Original Hedging

Initial concepts of model reference hedging, as shown in the block diagram in Fig. 2-10 are based on the following idea: The reference model is slowed, or "hedged", by an amount that hides dynamics which the adaptive control cannot attain. This approach was used successfully on a model of the X-33 by Johnson et al.[30] by hedging the commanded acceleration given to a dynamic inversion controller.

Initial investigation found that running the command signal u_c through a model of the plant with an appropriate gain and subtracting this directly from the states of the reference model as in Fig. 2-11 could drastically improve the robustness of the SMC system.

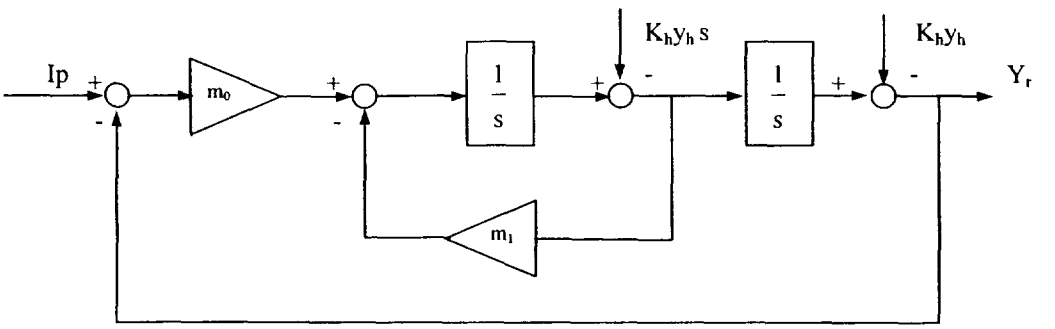

Figure 2-11: Block Diagram of Original Hedge Inputs to Reference Model

This approach is invalid in models with unstable plants because the output y_h is unbounded. It was also realized, and can be easily shown, that the inputs from the hedge plant can be run through a transfer function and moved outside the reference model. This is shown in Fig. 2-12

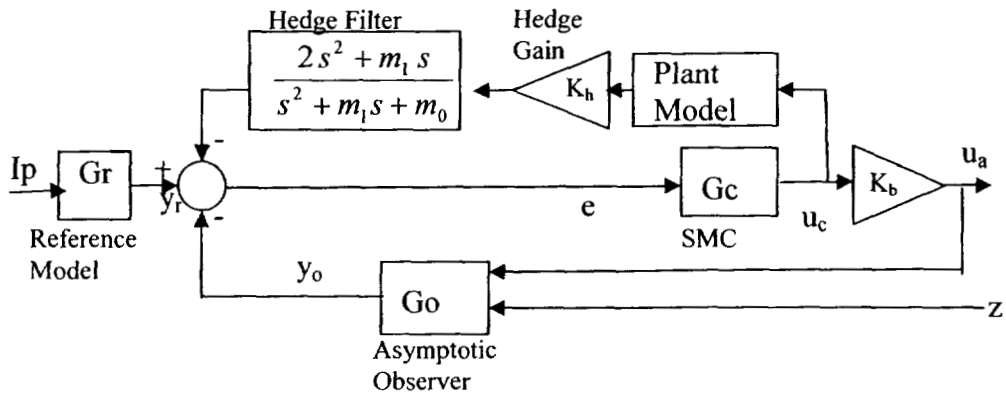

Figure 2-12: Block Diagram of Hedging With Hedge Filter

Investigation of the resulting feedback structure, *hedge plant*hedge gain*hedge filter* transfer function, revealed that the resulting bode plots all exhibited a similar shape. The concept of Model Reference Hedging as previously described was abandoned. The new hedge structure, Fig. 2-13 is equivalent to the old structure but allows significantly better understanding of the dynamics, and shows that hedging is in parallel with the observer and is modifying the shape of the feedback to the SMC.

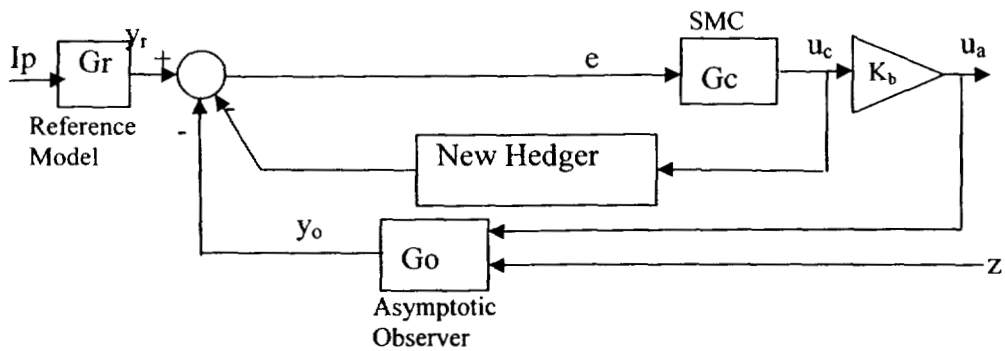

Figure 2-13: Block Diag. of Simplified and Reduced Hedger, Parallel to Observer.

2.5.4.2 Hedge Design

The Basics of hedge design are found by understanding the observer plots in §2.5.3. The hedger will attempt to modify the deviation from the designed response such that the SMC controller 'sees' the system for which it was designed.

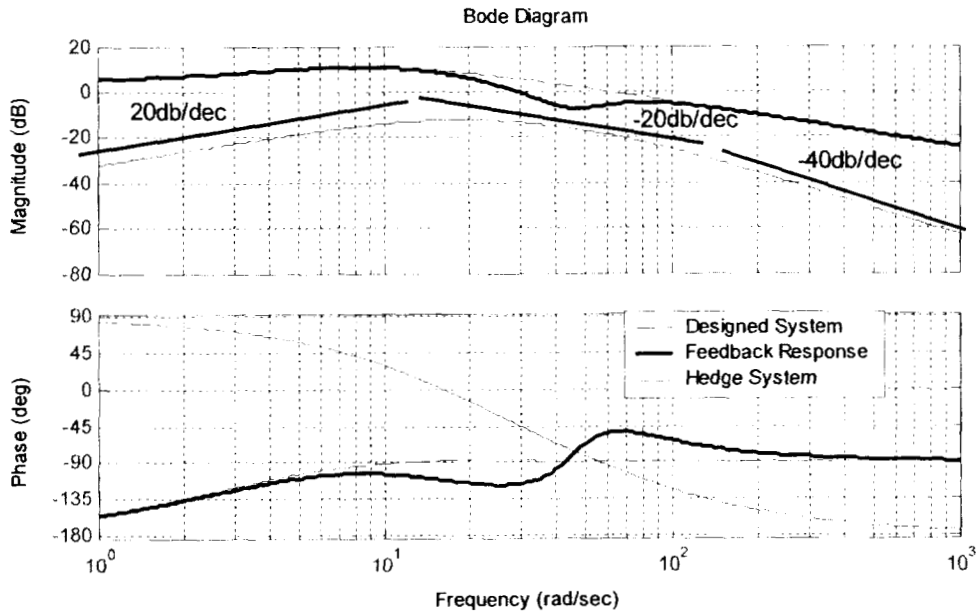

Figure 2-14: Hedge Shape Guidelines. K_h=10,Pq1=10. FSAVro

Figure 2-14 shows the guidelines for designing hedge transfer functions, which should have the following characteristics.

- +20 dB/dec slope at low frequencies
- -20*r dB/dec slope at frequencies where the actuators distort the magnitude curve (r = relative order of designed system without addition actuator dynamics)
- -20*r-20 dB/dec slope at high frequencies

The hedge system shown is going to be added to the existing feedback response of the observer. This has the effect of 'pushing up' the feedback response closer to the designed system. The hedge system shown is

$$y_h = K_h\left(\frac{70s}{s+70}\right)\left(\frac{1}{(s+20)(s+20)}\right) \qquad (2.14)$$

Increasing K_h to the final design value provides the response shown in Fig. 2-15.

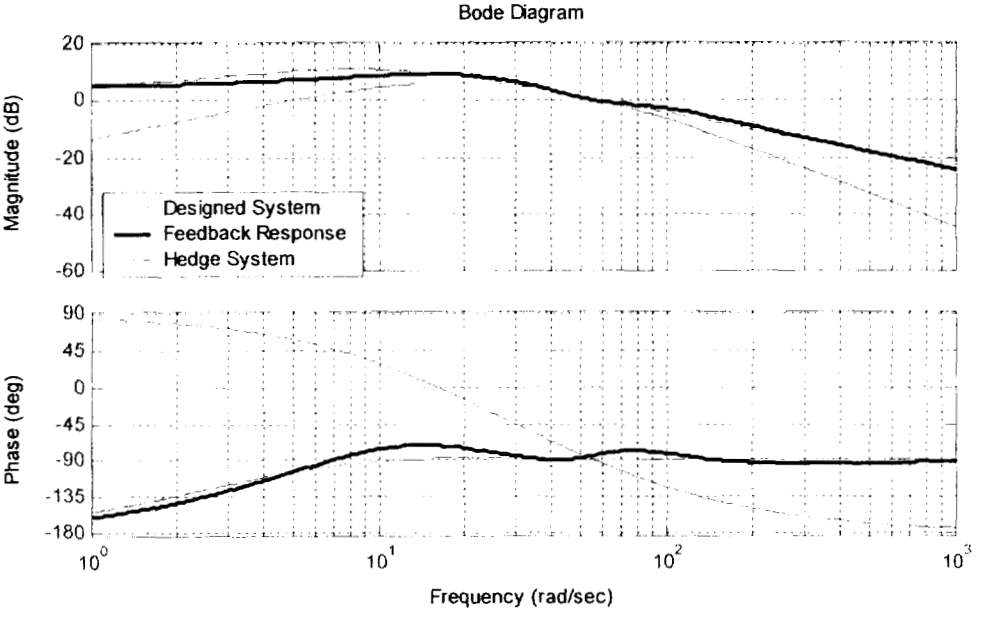

Figure 2-15: Bode Plot of Feedback Response. K_h=85, Pq1=15. FSAVro

This plot shows that, despite the inclusion of second order actuators in the design, most of the parasitic dynamics they introduce are removed from the feedback response "seen" by the SMC controller. The combination of the observer and hedger has made a system with relative order three, appear to the controller like a system with a relative order one. The phase of the resultant system is often an important design issue. The results of this design are near ideal as the resulting feedback system has no additional lag from the designed system.

Now that the actuator dynamics can be hidden from the controller, consideration of the effect of these modifications on robustness and performance must be performed. The phase and magnitude depression seen in all the above plots is heavily dependent on

the actuator bandwidth. In an actuator failure, which is often modeled as reduced actuator bandwidth, this depression grows and shifts to lower frequencies. This would suggest that the middle portion of the hedge signal, (the part that should reflect the designed relative order) should be as broad a region below the nominal depression as possible. However, simulation reveals and intuition suggests that making a broader 'working' area in the hedge signal, which is subtracted from the feedback, reduces tracking performance by hiding more and more of the system to which the controller could adapt. Thus, for optimum tracking performance, the smallest hedge gain and 'working' area should be employed. A balance between the two must be sought and the variables at the designer's disposal in the hedger are the shape and gain of the hedge signal.

It should also be noted that as the hedge gain increases, the system can become unstable as more dynamics become hidden. In addition, under piloted flight, high hedge gains cause outer-loop phase lag and overshoot which can lead to Pilot Induced Oscillation (PIO) tendencies.

In Fig. 2-15 the observer speed was increased from that in Fig. 2-14. This observer speed results in an unstable system without hedging. Thus, one of the benefits of hedging is its ability to stabilize faster observers. It does mean however, that there is a minimum hedge gain which is required for a given observer speed. This also goes to demonstrate how intimately the hedger is intertwined with the observer.

While this hedging model has strayed from the initial concept of hiding unobtainable commands from the adaptive controller, it has migrated into a very beneficial observer loop shaping tool with large effects on system robustness and

performance. It also suggests that a system capable of performing the tasks sought originally could be implemented in addition to the current method.

Chapter 3

Design Decisions

3.1 Introduction to Design Decisions

In the previous chapter, the fundamental concepts of sliding mode controllers were established. In addition, some real-world implementation considerations, including boundary layers, high-frequency bypass loops using observers, and reference model hedging were introduced. The options available in these strategies create a huge range of design parameters and system characterization options. The complexity and strong interaction of the components within the proposed SMC design is exactly how it improves upon past designs. This interaction, however, makes parameterization quite difficult. While understanding and precisely predicting the behavior of this system on a fundamental level is quite difficult, an attempt to at least understand the behavior of some pieces of the system through empirical analysis, is now undertaken.

3.2 The State Space Model

Initially, all of the investigation into the design parameters was done through simulation. As evidence mounted that the system could be modeled as a very high gain PID controller once the boundary layer was introduced and pseudo-sliding was occurring, the problem of forming a state space model of the entire system became tractable. The benefit of creating the state space models, besides the joy of state space arithmetic, is the ability to analyze the systems and its components in the frequency domain. Transfer functions and bode plots can be generated to examine the effects of

measurement noise and parameter identification, in addition eigenanalysis can be performed on the model.

The use of the state space analysis is the basis of selecting many of the design parameters shown below. The main block diagram used in the derivation is shown in Fig. 3-1,

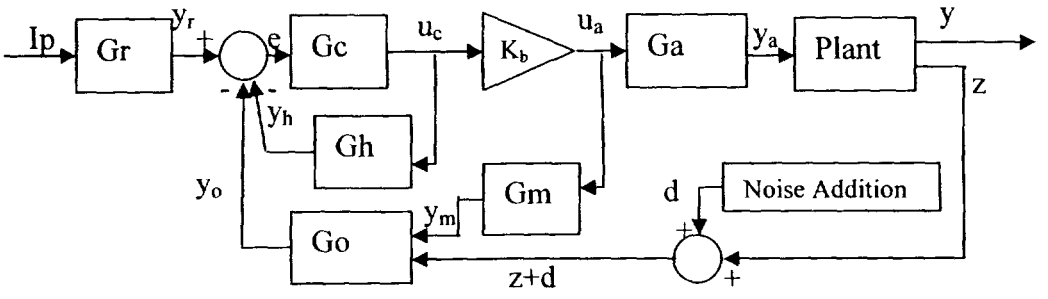

Figure 3-1: Block Diagram with Signal Names. FSAVfo

The individual state space representations of each block were reduced until a standard A,B,C,D formulation was achieved, named as above in Fig. 3-1 and below in Eq. (3.1).

$$x \in \Re^{n},\ x_a \in \Re^{n_a},\ x_c \in \Re^{n_c},\ x_r \in \Re^{n_r},\ \hat{x}_o \in \Re^{n_o},\ x_m \in \Re^{n_m},\ x_h \in \Re^{n_h} \qquad (3.1)$$

$$y \in \Re^{m_y},\ y_a \in \Re^{m},\ y_c \in \Re^{m_y},\ y_r \in \Re^{m_y},\ \hat{y}_o \in \Re^{m_y},\ y_m \in \Re^{m_m},\ y_h \in \Re^{m_h}$$

$$z \in \Re^{m_z}$$

Linear Plant

$$\dot{x} = \mathbf{A}\,x + \mathbf{B}\,y_a$$

$$y = \mathbf{C}_y\,x + \mathbf{D}_y\,y_a$$

$$z = \mathbf{C}_z\,x + \mathbf{D}_z\,y_a$$

Actuators

$$\dot{x}_a = \mathbf{A}_a\,x_a + \mathbf{B}_a\,\mathbf{K}_b\,y_c$$

$$y_a = \mathbf{C}_a\,x_a + \mathbf{D}_a\mathbf{K}_b\,y_c$$

Reference Model

$$\dot{x}_r = \mathbf{A}_r x_r + \mathbf{B}_r Ip$$
$$y_r = \mathbf{C}_r x_r + \mathbf{D}_r Ip$$

Hedge Filter

$$\dot{x}_h = \mathbf{A}_h x_h + \mathbf{B}_h y_c$$
$$y_h = \mathbf{C}_h x_h \quad let\ \mathbf{D}_h = 0$$

Model Actuators

$$\dot{x}_m = \mathbf{A}_m x_m + \mathbf{B}_m \mathbf{K}_b y_c$$
$$y_m = \mathbf{C}_m x_m + \mathbf{D}_m \mathbf{K}_b y_c$$

Linear Controller

$$\dot{x}_c = \mathbf{A}_c x_c + \mathbf{B}_c e$$
$$u_c = \mathbf{C}_c x_c + \mathbf{D}_c e$$

Observer

$$\dot{\hat{x}}_o = \mathbf{A}_o \hat{x}_o + \mathbf{B}_o y_m + \mathbf{G}_o z$$
$$y_o = \mathbf{C}_o \hat{x}_o \quad let\ D_o = 0$$

$\mathbf{A_o}$, $\mathbf{B_o}$, $\mathbf{G_o}$, $\mathbf{C_o}$, are defined in Eq. (3.2)

Output Feedback

$$\tilde{y} = y_o + y_h$$

Controller Input

$$e = y_r - \tilde{y}$$

Observers were written in the form shown in Eq. (3.2). This formulation made it very easy to use multiple observers and collapse them into a single state space model as introduced later.

$$\dot{x}_o = \left[\mathbf{A}_1 - \mathbf{G}_1\mathbf{C}_1\right]x_o + \left[\mathbf{B}_1 \quad \mathbf{G}_1\right]\begin{bmatrix} y_m \\ z+d \end{bmatrix}$$
$$y_o = \left[\mathbf{C}_1\right]x_o \qquad (3.2)$$
$$Where\ \ \mathbf{A}_1 - \mathbf{G}_1\mathbf{C}_1 \quad Getsset\,to: \mathbf{A}_o$$

In most blocks the signals have widths greater than one. However within each block the signals are operated on by some dynamic system, and then reformed as a vector at the output. This is shown in Fig. 3-2 with a general pair of compensators or models.

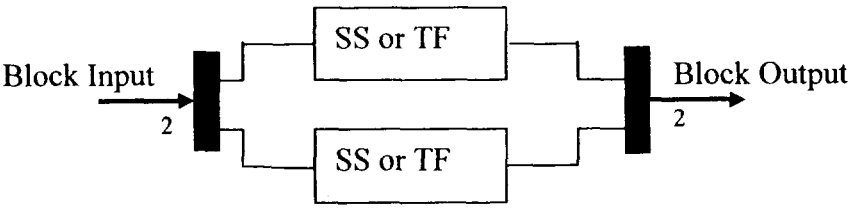

Figure 3-2: Sub-block Example.

Clearly, system elements can be in state space or transfer function form, however to finally describe the model in state space, all the transfer functions must be proper. This becomes an issue in some cases and can only be dealt with by adding a very high frequency pole. It must be significantly above the crossover frequency of the controller which can be quite fast, in excess of 500 rad/sec! If it is set too high, numerics demand prohibitively small time steps in simulation.

In the analysis of feedback and performance, it is desired to be able to determine the effective plant that the controller is attempting to control. Using block diagrams and state space algebra the system in Fig. 3-1 can be transformed to the system shown in Fig. 3-3. This effective plant includes the actual plant, actuators, model actuators, hedge system and the observer.

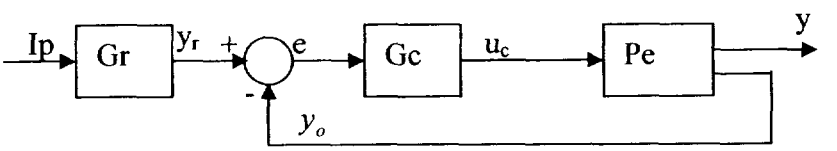

Figure 3-3: Block Diagram Of Equivalent System

The equivalent state space representation is shown in Eq. (3.3).

$$\begin{aligned} \dot{x}_c &= \mathbf{A}_e x_e + \mathbf{B}_e y_c \\ \begin{bmatrix} y \\ y_o + y_h \end{bmatrix} &= \mathbf{C}_{cl} x_{cl} + \mathbf{D}_{cl} u_c \end{aligned} \qquad (3.3)$$

Where $\mathbf{A_e}$, $\mathbf{B_e}$, $\mathbf{C_e}$, $\mathbf{D_e}$ are defined as follows:

$$\mathbf{A}_e = \begin{bmatrix} \mathbf{A} & \mathbf{BC}_a & \mathbf{0}_{n\times n_m} & \mathbf{0}_{n\times n_o} & \mathbf{0}_{n\times n_h} \\ \mathbf{0}_{n_a\times n} & \mathbf{A}_a & \mathbf{0}_{n_a\times n_m} & \mathbf{0}_{n_a\times n_o} & \mathbf{0}_{n_a\times n_h} \\ \mathbf{0}_{n_m\times n} & \mathbf{0}_{n_m\times n_a} & \mathbf{A}_m & \mathbf{0}_{n_m\times n_o} & \mathbf{0}_{n_m\times n_h} \\ \mathbf{G}_o\mathbf{C}_z & \mathbf{G}_o\mathbf{D}_c\mathbf{C}_a & \mathbf{B}_o\mathbf{C}_m & \mathbf{A}_o & \mathbf{0}_{n_o\times n_h} \\ \mathbf{0}_{n_h\times n} & \mathbf{0}_{n_h\times n_a} & \mathbf{0}_{n_h\times n_m} & \mathbf{0}_{n_h\times n_o} & \mathbf{A}_h \end{bmatrix} \begin{bmatrix} x \\ x_a \\ x_m \\ x_o \\ x_h \end{bmatrix}$$

Plant States
Combined Actuator States
Combined Model Act. States
Combined Observer States
Combined Hedger States

$$\mathbf{B}_e = \begin{bmatrix} \mathbf{B}\mathbf{D}_a\mathbf{K}_b \\ \mathbf{B}_a\mathbf{K}_b \\ \mathbf{B}_m\mathbf{K}_b \\ \mathbf{B}_o\mathbf{D}_d\mathbf{K}_b + \mathbf{G}_o\mathbf{D}_z\mathbf{D}_a\mathbf{K}_b \\ \mathbf{B}_h \end{bmatrix} [u_c]$$ *Output From Controller*

$$\mathbf{C}_e = \begin{bmatrix} \mathbf{C}_y & \mathbf{D}_y\mathbf{C}_a & \mathbf{0}_{n_y\times n_m} & \mathbf{0}_{n_y\times n_o} & \mathbf{0}_{n_y\times n_h} \\ \mathbf{0}_{n_h\times n} & \mathbf{0}_{n_h\times n_a} & \mathbf{0}_{n_h\times n_m} & \mathbf{C}_o & \mathbf{C}_h \end{bmatrix} \begin{bmatrix} x \\ x_a \\ x_m \\ x_o \\ x_h \end{bmatrix} \quad y = \begin{bmatrix} y \\ y_o + y_h \end{bmatrix}$$

State Output
Feedback States

$$\mathbf{D}_e = \begin{bmatrix} \mathbf{D}_y\mathbf{D}_a\mathbf{K}_b \\ \mathbf{D}_h \end{bmatrix} [u_c]$$

An additional state space system was created which modeled the entire system, and could also be used to analyze the effect of noise on system output y and on the control signal u_c. This system is referred to as the 'CL' system or "System CL" because it represents the entire Closed Loop system.

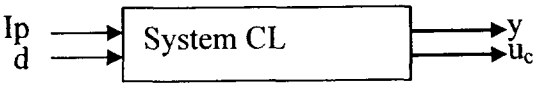

Figure 3-4: Block Diagram of SysCL

The state space representation is shown in Eq. (3.4).

$$\dot{x}_{cl} = \mathbf{A}_{cl}\, x_{cl} + \mathbf{B}_{cl} \begin{bmatrix} \mathrm{Ip} \\ \mathrm{d} \end{bmatrix}$$
$$\begin{bmatrix} y \\ u_c \end{bmatrix} = \mathbf{C}_{cl}\, x_{cl} + \mathbf{D}_{cl} \begin{bmatrix} \mathrm{Ip} \\ \mathrm{d} \end{bmatrix} \qquad (3.4)$$

Where $\mathbf{A_{cl}}$, $\mathbf{B_{cl}}$, $\mathbf{C_{cl}}$, $\mathbf{D_{cl}}$ are defined as follows:

$$\mathbf{A}_{cl} = \begin{bmatrix} \mathbf{A} & \mathbf{B}\,\mathbf{C}_a & \mathbf{B}\,\mathbf{D}_a\mathbf{K}_b\mathbf{C}_c & \mathbf{0}_{n\times n_m} & -\mathbf{B}\,\mathbf{D}_a\mathbf{K}_b\mathbf{D}_c\mathbf{C}_o & -\mathbf{B}\,\mathbf{D}_a\mathbf{K}_b\mathbf{D}_c\mathbf{C}_h & \mathbf{B}\,\mathbf{D}_a\mathbf{K}_b\mathbf{D}_c\mathbf{C}_r \\ \mathbf{0}_{n_a\times n} & \mathbf{A}_a & \mathbf{B}_a\mathbf{K}_b\mathbf{C}_c & \mathbf{0}_{n_a\times n_m} & -\mathbf{B}_a\mathbf{K}_b\mathbf{D}_c\mathbf{C}_o & -\mathbf{B}_a\mathbf{K}_b\mathbf{D}_c\mathbf{C}_h & \mathbf{B}_a\mathbf{K}_b\mathbf{D}_c\mathbf{C}_r \\ \mathbf{0}_{n_c\times n} & \mathbf{0}_{n_c\times n_a} & \mathbf{A}_c & \mathbf{0}_{n_c\times n_m} & -\mathbf{B}_c\mathbf{C}_o & -\mathbf{B}_c\mathbf{C}_h & \mathbf{B}_c\mathbf{C}_r \\ \mathbf{0}_{n_m\times n} & \mathbf{0}_{n_m\times n_a} & \mathbf{B}_m\mathbf{K}_b\mathbf{C}_c & \mathbf{A}_m & -\mathbf{B}_m\mathbf{K}_b\mathbf{D}_c\mathbf{C}_o & -\mathbf{B}_m\mathbf{K}_b\mathbf{D}_c\mathbf{C}_h & \mathbf{B}_m\mathbf{K}_b\mathbf{D}_c\mathbf{C}_r \\ \mathbf{G}_o\mathbf{C}_z & \mathbf{0}_{n_o\times n_a} & \mathbf{B}_o\mathbf{D}_m\mathbf{K}_b\mathbf{C}_c & \mathbf{B}_o\mathbf{C}_m & \mathbf{A}_o - \mathbf{B}_o\mathbf{D}_m\mathbf{K}_b\mathbf{D}_c\mathbf{C}_o & -\mathbf{B}_o\mathbf{D}_m\mathbf{K}_b\mathbf{D}_c\mathbf{C}_h & -\mathbf{B}_o\mathbf{D}_m\mathbf{K}_b\mathbf{D}_c\mathbf{C}_r \\ \mathbf{0}_{n_h\times n} & \mathbf{0}_{n_h\times n_a} & \mathbf{B}_h\mathbf{C}_c & \mathbf{0}_{n_h\times n_m} & -\mathbf{B}_h\mathbf{D}_c\mathbf{C}_o & \mathbf{A}_h - \mathbf{B}_h\mathbf{D}_c\mathbf{C}_h & \mathbf{B}_h\mathbf{D}_c\mathbf{C}_r \\ \mathbf{0}_{n_r\times n} & \mathbf{0}_{n_r\times n_a} & \mathbf{0}_{n_r\times n_a} & \mathbf{0}_{n_r\times n_m} & \mathbf{0}_{n_r\times n_o} & \mathbf{0}_{n_r\times n_h} & \mathbf{A}_r \end{bmatrix} \begin{bmatrix} x \\ x_a \\ x_c \\ x_m \\ x_o \\ x_h \\ x_r \end{bmatrix}$$

$$\mathbf{B}_{cl} = \begin{bmatrix} \mathbf{B}\,\mathbf{D}_a\mathbf{K}_b\mathbf{D}_c\mathbf{D}_r & \mathbf{0}_{n\times n_y} \\ \mathbf{B}_a\mathbf{K}_b\mathbf{D}_c\mathbf{D}_r & \mathbf{0}_{n_a\times n_y} \\ \mathbf{B}_c\mathbf{D}_r & \mathbf{0}_{n_c\times n_y} \\ \mathbf{B}_m\mathbf{K}_b\mathbf{D}_c\mathbf{D}_r & \mathbf{0}_{n_m\times n_y} \\ \mathbf{B}_o\mathbf{D}_m\mathbf{K}_b\mathbf{D}_c\mathbf{D}_r & \mathbf{G}_o \\ \mathbf{B}_h\mathbf{D}_c\mathbf{D}_r & \mathbf{0}_{n_h\times n_y} \\ \mathbf{B}_r & \mathbf{0}_{n_r\times n_y} \end{bmatrix} \begin{bmatrix} Ip \\ d \end{bmatrix}$$

Input to System
State Measurement Noise Input

$$\mathbf{C}_{cl} = \begin{bmatrix} \mathbf{C}_y & \mathbf{0}_{n_y\times n_a} & \mathbf{0}_{n_y\times n_c} & \mathbf{0}_{n_y\times n_m} & \mathbf{0}_{n_y\times n_o} & \mathbf{0}_{n_y\times n_h} & \mathbf{0}_{n_y\times n_r} \\ \mathbf{0}_{n_{uc}\times n} & \mathbf{0}_{n_{uc}\times n_a} & \mathbf{K}_b\mathbf{C}_c & \mathbf{0}_{n_{uc}\times n_m} & -\mathbf{K}_b\mathbf{D}_c\mathbf{C}_o & -\mathbf{K}_b\mathbf{D}_c\mathbf{C}_h & \mathbf{K}_b\mathbf{D}_c\mathbf{C}_r \end{bmatrix} \begin{bmatrix} x \\ x_a \\ x_c \\ x_m \\ x_o \\ x_h \\ x_r \end{bmatrix} \quad y = \begin{bmatrix} y \\ u_c \end{bmatrix}$$

State Output
Control Signal

$$\mathbf{D}_{cl} = \begin{bmatrix} \mathbf{D}_y & \mathbf{0}_{n_y\times n_d} \\ \mathbf{K}_b\mathbf{D}_c\mathbf{D}_r & \mathbf{0}_{n_d\times n_d} \end{bmatrix} \begin{bmatrix} Ip \\ d \end{bmatrix}$$

While non-linear effects like rate limiting, position limiting, and saturation elements could not be modeled, it was found that the results of non-linear simulation using Simulink® and the results from a single large state space model were virtually identical under nominal and even most failed conditions Using the closed loop model in shown in Fig. 3-4 the nominal system was run using the nonlinear Simulink® model and the state space model, a section of the results for the two runs is shown in Fig. 3-5

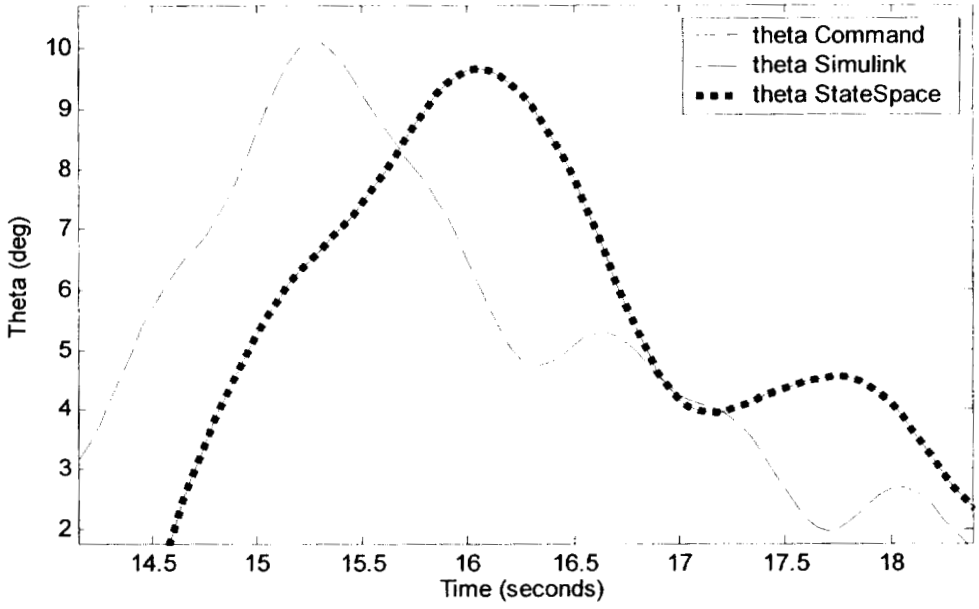

Figure 3-5: Magnified response to input of both SS and Simulink® models. Nominal Case. FSAVro

3.3 Multiple Observers

3.3.1 Rationale For Multiple Observers

One of the features of feedback linearization on a square system is decoupling of the control variables. In this design, the SMC controller is performing the feedback linearization, however any controller type which performs the linearization may benefit from multiple observers. In a standard setup, one observer has the task of reconstructing

all of the states. This has multiple drawbacks from both a practical and theoretical standpoint.

Because of frequency tailoring, noise sensitivity, cross-coupling, as well as robustness issues that will be discussed later, choosing an ideal speed in a single observer becomes quite difficult and acceptable performance is often impossible to achieve, particularly when measurement noise is included. These issues lead one to investigate using an independent observer for each channel.

3.3.1.1 Independent Frequency Tailoring

In any model where multiple decoupled loops run at different speeds, a single observer will expose each variable to every eigenvalue in the observer. The desire to tailor the convergence rates of the observers on each channel independently suggests that the observers should be decoupled and then tune each one to the desired eigenvalues.

3.3.1.2 Noise Reduction for low Frequency Variables

A further suggestion that each channel should use its own observer is found when one considers the transfer function between an additive disturbance, an observer, an output. Consider the system shown in Fig. 3-6

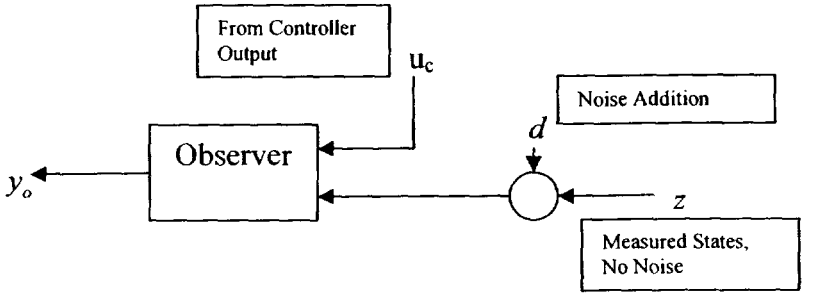

Figure 3-6: Observer Layout for Noise TF

The equation which describe the general observer system are shown in Eq. (3.5)

$$\begin{aligned} &\dot{x}_o = Ax_o + Bu_c + G((z+d) - Cx_o) \\ &\textit{Can be written as}: \\ &\dot{x}_o = (A - GC)x_o + Bu_c + G(z+d) \\ &y_o = C_o x_o \end{aligned} \qquad (3.5)$$

This shows that a disturbance has the same effect on the system as the feedback variable. This can be seen by the fact that any gains or dynamics which operate on z also operate on d. While this is clearly not ideal, it suggests that a slow observer will suppress noise compared to a faster one. This may be desired if the bandwidth of the desired loop is small.

3.3.1.3 Cross-Coupling

There are strong cross-coupling effects in situations where single observers are used to construct multiple states. While this is sometimes desired, it can be extremely detrimental.

Further evidence from a noise standpoint can be seen if there is some degree of coupling between the states in the plant model. Using the FSAV and a single observer with poles at λ=-21,-22,-23,-24, the magnitude of the cross-coupling term can be as higher than -20db from airspeed noise to q_o. Thus a 1 m/s noise in airspeed will be a 0.1 rad/sec noise in pitch rate. Initially this seems acceptable until the realization that the RMS value of the noise in the airspeed loop is 25 m/s. This corresponds to a q_o noise contribution of 2.5 rad/sec. However, the magnitude of q and q_o peaks around 0.25 rad/sec. Thus, the cross-coupled noise is one order of magnitude higher than the feedback variable! This is clearly not tolerable in almost any system.

While the drawbacks of certain types of cross-coupling in a single observer were outlined in the above paragraph, multiple observers present an interesting ability to implement the exact cross-coupling a design engineer desires. The design engineer could, use the multiple observer structure to construct any amount of feedback cross-coupling by proper selection of the 'plants' defined in the individual observers. For this project, this design flexibility is not investigated.

3.3.1.4 Multiple Observer Architecture

A multiple observer architecture is shown in the block diagram in Fig. 3-7.

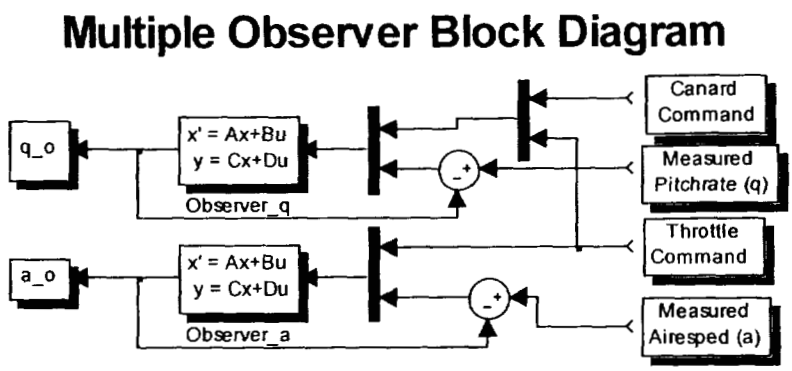

Figure 3-7: Block diagram of Observer

Consider in this formulation, what the 'plant' should be in the individual observers? Perhaps instead of putting in a full plant, a reduced order model of the particular variable's transfer function should be used. For example, in Fig. 3-7 there is a path for coupling from a throttle command to q_o. Missing from Fig. 3-7 is a path which predicts airspeed changes due to canard command inputs. It is not included in this construction because the magnitude is negligible. As a result, the 'plant' used in the airspeed observer is not a full, nominal plant. It is, in fact, a state space representation of the plant airspeed transfer function assuming the pitch rate loop is already closed. The

result is a simpler, more noise friendly observer. The coupling term could have been included, but the construction is slightly more complex.

The multiple observer methodology has many features such as noise reduction, increased design freedom, and tailored loop control. Drawbacks to the multiple observer method are few. The models can be simply two identical plant models running at different speeds, or they can be highly tailored plant approximations with the precise cross-coupling desired. This improvement was instrumental in achieving the performance and robustness presented later.

3.4 Robustness and Observer speed selection

Intuitively, the observer speed should have a strong effect on model performance and robustness. As observer poles go to infinity, the observer is identical to pure output feedback. Thus, as the observer poles become faster, the observer puts increasing weight on the feedback variable relative to the observer's internal calculation of the feedback variable based on the control input and the observer's model of the plant. This begins to explain why faster observers are more robust to plant changes, and less robust to actuator damage. Decreasing observer speed increases the weight placed on the internal model which reduces phase lag in the reconstructed state that is present in the output feedback path. This is because the feedback path goes through the real, 2^{nd} order actuators, while the control path does not, hiding the unmodeled parasitic dynamics. However, this suppression feature is also attenuating variations in the plant parameters, which are potentially matched to the controller, reducing the controller's ability to adapt.

Figure 3-8, taken from Wells[28] shows a classic observer effect on the Innovative Control Effecter, or ICE model. It is a 65° stealthish delta wing with 11 highly coupled actuators. It has significantly different stability and control derivatives, than the models investigated here. However, the plot is identical in shape and behavior. Looking at the phase portion it is seen that, as the observer speed gets higher, the phase rolls off faster as suggested by the above analysis. It is also noted that, for faster observer speeds the magnitude plot shows the extra roll-off associated with the 2nd order unmodeled dynamics present in the feedback path. The phase wrap around also suggests instability for observers which are too fast.

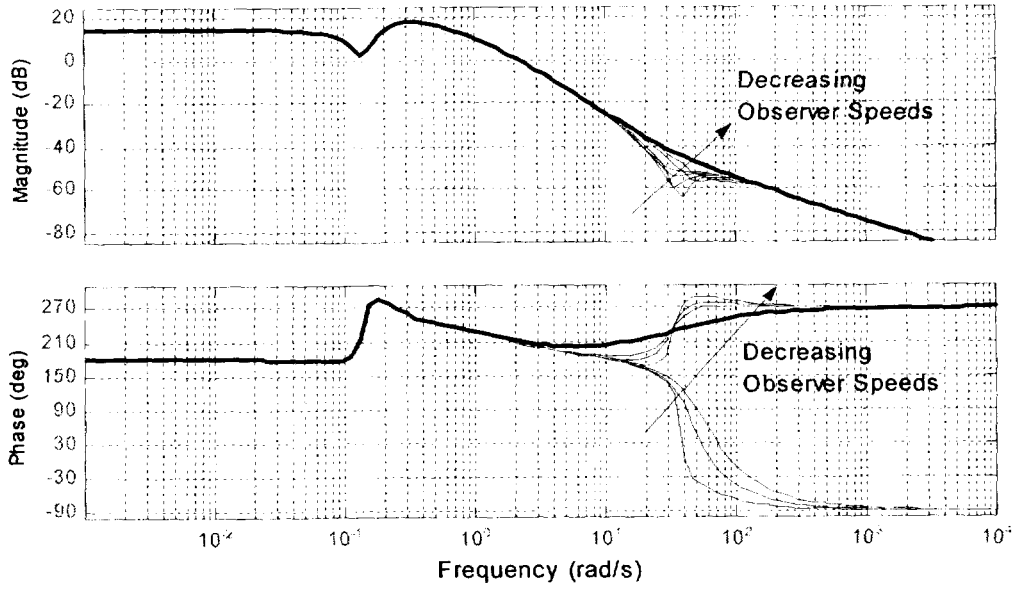

Figure 3-8: Bode Plot of $\frac{\hat{\alpha}}{u_{c\alpha}}$ for ICE model at various observer speeds [28]

Described in another way, the heavy dark line in the magnitude plot represents the design plant which in this case does not include any actuator models. At slower observer speeds, the feedback is nearly identical to the designed system. The true

system, with actuators, rolls off roughly along the fastest observer curve (before it jumps back to the designed curve). Thus, the slower observer is not feeding back the actual behavior of the system but the 'designed' behavior. The faster observers are able to track the effect of the actuators, which leads to instability as the SMC begins to sense a higher relative order than what it was designed for, but also allows the SMC and system to track the effects of plant parameter variation, something they do very well.

From the above analysis a few things can be concluded. First, that observer speed selection has strong implications on robustness, but that the type of robustness desired must be considered. Slower observers improve the capability of the system to deal with reduced bandwidth actuators. The penalty paid is the standard in control system design, reduced tracking performance. Faster observes lead to significantly improved tracking performance, but more importantly allow the SMC to deal with larger plant parameter variation.

3.5 Model Actuators and Observer Effects

Basic SMC design demands that the feedback be of the correct relative order. Thus, in the case where a first order actuator model has been included as part of the plant, those dynamics must be included in the high speed bypass loop, or in $u_c \rightarrow$ observer feedback path. In fact, the designed order of dynamics must be included, lower or higher orders do not return the proper relative order to the SMC controller. There are two apparent options to do this, the first is to create a new 'plant' which contains the actuator model and use that in the observer. The second is to put an independent model of the actuator before the observer, in the u_c path. This is shown as block 'Gm' in Fig. 3-1. Both methods seem feasible although only the second is investigated. It seems

reasonable that the actuator model should be of the same bandwidth as the actual actuator. (Note this is not making a claim about the order of the two models, only their bandwidth) However, perhaps there is a benefit to using a slower model? SMC has shown that if it is stable, then for moderate failures the tracking is not noticeably affected. Thus, if a degree of actuator failure is assumed in the model actuator, is there robustness to gain?

3.6 First Order Vs Reduced Order

3.6.1 Invariance

It seems reasonable that if all the actuator dynamics are included in the definition of the plant many of the parasitic dynamics issues might be solved. Investigation into this concept revealed two important properties of the combined actuator and plant system. The first is that matching conditions depend on the state space selected to represent the system. The second is that matching conditions depend on actuator bandwidth.

The fact that the matching conditions were dependent on the state space realization came as some surprise, except when one considers that the matrices have a drastically different appearance between the combined plant in phase variable form and the actuator-plant state spaces assembled in series. Figure 3-9 shows the two options for constructing the combined plant-actuator model.

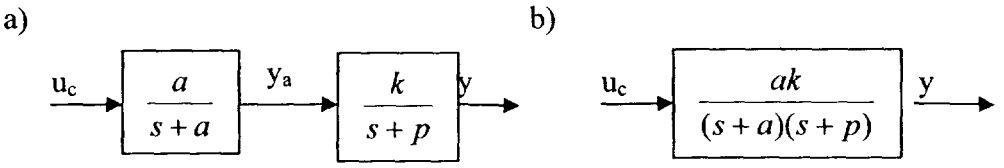

Figure 3-9: Example Plant & Actuator

The differential equation which defines the combined arrangement is:

$$\ddot{y} + (a+p)\dot{y} + (ap)y = (ka)u \tag{3.6}$$

This can be formatted in state space phase variable form as

$$\begin{bmatrix} \dot{x}_1 \\ x_2 \end{bmatrix} = \begin{bmatrix} 0 & 1 \\ -ap & -(a+p) \end{bmatrix} \begin{bmatrix} x_1 \\ x_2 \end{bmatrix} + \begin{bmatrix} 0 \\ k \end{bmatrix} u \tag{3.7}$$

Initial inspections suggest that the system is invariant to both plant and actuator parameters as they both are in the range space of the input. Investigating further, since this is a second order equation, the sliding manifold is one order less and defined as:

$$\sigma = m\dot{y} + y \tag{3.8}$$

Set $\dot{\sigma} = 0$ and solve simultaneously with Eq. (3.6) then solve for u give u_{eq}. As in §2.3

$$u_{eq} = \left(\frac{m(a+p)-1}{mpk} \right) \dot{y} + \left(\frac{p}{k} \right) y \tag{3.9}$$

To find the forced system response, input this equivalent control into Eq. (3.6).

$$\ddot{y} = -\left(\frac{1}{m} \right) \dot{y} \tag{3.10}$$

This shows that the response of the system is invariant to the parameters of both the actuator and the plant!

Reformulating the problem into an actuator and plant in series as in Fig. 3-9a, the state space becomes

$$\begin{bmatrix} \dot{x} \\ \dot{x}_a \end{bmatrix} = \begin{bmatrix} -p & k \\ 0 & -a \end{bmatrix} \begin{bmatrix} x \\ x_a \end{bmatrix} + \begin{bmatrix} 0 \\ a \end{bmatrix} uc$$
$$y = \begin{bmatrix} 1 & 0 \end{bmatrix} \begin{bmatrix} x \\ x_a \end{bmatrix} \tag{3.11}$$

The difference is beginning to show. The plant is partially out of the range space of B. Performing the same analysis as above it is found that that the resulting dynamics are:

$$\begin{bmatrix} \dot{x} \\ \dot{x}_a \end{bmatrix} = \begin{bmatrix} -p & k \\ \frac{p}{m} & -\frac{k}{m} \end{bmatrix} \begin{bmatrix} x \\ x_a \end{bmatrix} \qquad (3.12)$$

The eigenvalues of this matrix are $\lambda = 0, -\left(p + \frac{k}{m}\right)$. It is noted that invariance to p and k has been lost! Additionally, the invariance that does exist is to the actuator! So the state space used to define the sliding surface has a large effect on the invariance of the system. It is this analysis that suggested that x and $\dot{x}$ be used to define the sliding surface in all the models studied. This odd dependence on the chosen state space is perhaps what was described when Young *et.al.* said "some invariance may be lost" with the addition of the actuator.[11]

The second point concerns the degree to which invariance is affected by actuator bandwidth. It has been shown in Eq. (3.10) that if the actuators are included in the design, invariance is observed. There should be additional care in systems where the plant is highly unstable, where at some point the actuators are just too slow for stability. Concern over additional derivatives in the control law prompts the analysis of the effect of neglected actuator dynamics, those not included in the design. In order to use an appropriate sliding surface a second order plant defined in Eq. (3.13) was chosen.

$$\begin{bmatrix} \dot{x}_1 \\ \dot{x}_2 \end{bmatrix} = \begin{bmatrix} 0 & 1 \\ -p_1 & -p_2 \end{bmatrix} \begin{bmatrix} x_1 \\ x_2 \end{bmatrix} + \begin{bmatrix} 0 \\ k \end{bmatrix} uc$$
$$y = \begin{bmatrix} 1 & 0 \end{bmatrix} \begin{bmatrix} x_1 \\ x_2 \end{bmatrix} \qquad (3.13)$$

The sliding surface is designed and the equivalent control is found as:

$$u_{eq} = \frac{1}{k}\left(p_1 x_1 + \left(p_2 - \frac{1}{m} \right) x_2 \right) \tag{3.14}$$

This input yields the desired invariance to p_1, p_2,and k with eigen values of $\lambda = 0, -\frac{k}{m}$.

Putting a first order actuator in series with the plant yields the state space:

$$\begin{bmatrix} \dot{x}_1 \\ \dot{x}_2 \\ \dot{x}_a \end{bmatrix} = \begin{bmatrix} 0 & 1 & 0 \\ -p_1 & -p_2 & k \\ 0 & 0 & -a \end{bmatrix} \begin{bmatrix} x_1 \\ x_2 \\ x_a \end{bmatrix} + \begin{bmatrix} 0 \\ 0 \\ a \end{bmatrix} uc$$
$$y = \begin{bmatrix} 1 & 0 & 0 \end{bmatrix} \begin{bmatrix} x_1 \\ x_2 \\ x_a \end{bmatrix} \tag{3.15}$$

Instead of redesigning the sliding surface and recalculating the equivalent control the control given in Eq. (3.14) is applied again. However, because of the improperly designed sliding surface, the sliding mode cannot be maintained without including a way to deal with deviation from the sliding surface. This can be found in the standard signum function.

$$u = \frac{1}{k}\left(p_1 x_1 + \left(p_2 - \frac{1}{m} \right) x_2 \right) - \rho\, sign(\sigma) \tag{3.16}$$

The symbolic calculations using this nonlinear function are difficult at best. Since the sign function will be replaced by a boundary layer in the actual design and since the controller will operate entirely within the linear boundary layer, replace the sign function with the linear approximation such that Eq. (3.16) becomes:

$$u_{approx} = \frac{1}{k}\left(p_1 x_1 + \left(p_2 - \frac{1}{m} \right) x_2 \right) - \frac{\rho}{\varepsilon}(\sigma) \qquad (3.17)$$

$$where: \quad \sigma = m x_2 + x_1$$

This leads to the following system response:

$$\begin{bmatrix} \dot{x}_1 \\ \dot{x}_2 \\ \dot{x}_a \end{bmatrix} = \begin{bmatrix} 0 & 1 & 0 \\ -p_1 & -p_2 & k \\ \frac{a}{k}p_1 - \frac{a\rho}{\varepsilon} & \frac{a}{k}\left(p_2 - \frac{1}{m} \right) - \frac{a\rho k}{\varepsilon} & -a \end{bmatrix} \begin{bmatrix} x_1 \\ x_2 \\ x_a \end{bmatrix} \qquad (3.18)$$

$$Characteristic\ Equation: \det(SI - A)$$

$$s^3 + (p_2 + a)s^2 + \left(\frac{a}{m} + \frac{a\rho mk}{\varepsilon} + p_1 \right) s + \frac{a\rho k}{\varepsilon} = 0$$

The first bit of bad news is that the system response is invariant to nothing! In addition some values of p_1, p_2, k, a, ρ, ε, m can lead to unstable and or oscillatory behavior. The symbolic analysis of the roots of the third order system is not a trivial process, but since the point of interest is only what happens to the roots of the system as 'a' goes to infinity, some analysis can be performed.[31]

$$s^3 + (p_2 + a)s^2 + \left(\frac{a}{m} + \frac{a\rho mk}{\varepsilon} + p_1 \right) s + \frac{a\rho k}{\varepsilon} = 0$$

let t=1/s, multiply by t^3, and divide by 'a' results in:

$$\frac{1}{a} + \left(\frac{p_2}{a} + 1 \right) t + \left(\frac{1}{m} + \frac{\rho mk}{\varepsilon} + p_1 \right) t^2 + \frac{\rho k}{\varepsilon} t^3 = 0$$

let $a \to \infty$ leaves:

$$t + \left(\frac{1}{m} + \frac{\rho mk}{\varepsilon} + p_1 \right) t^2 + \frac{\rho k}{\varepsilon} t^3 = 0$$

or equivelently

$$t\left(1 + \left(\frac{1}{m} + \frac{\rho mk}{\varepsilon} + p_1 \right) t + \frac{\rho k}{\varepsilon} t^2 \right) = 0$$

This shows that as a→∞ one root, in 't', approaches zero. Converting to the 's' space results in $s = \frac{1}{t} \Rightarrow \lambda_1 \to -\infty \; as \; a \to \infty$. Now solve the internal quadratic and substitute in 's' for the other roots to get $\lambda_2 = \frac{-\rho km}{\varepsilon}$ and $\lambda_3 = \frac{1}{-m}$!

The root at -∞ and $\frac{1}{-m}$ are good but the last one should be at zero to be identical to pure sliding behavior! λ_2 is a function of the boundary layer. It would be tempting to let ε go to zero and claim that this would approach the eigenvalue of the signum function. The linearized formulation used to get to this stage prohibits this analysis as the nonlinear features quickly play a role as ε decreases. It can be said that as ρ increases and/or ε decreases that, as long as the model stays in the linear region, the last eigenvalue decays faster and faster.

One assumption which has been made in the above analysis is that the only parameter changes being considered are ones which do not change the order of the system. While this encompasses a huge class of failures, it could be important to increase the system robustness to system order changes. Changes in order could result from damaged linkages, and other sources. However, it must be pointed out that in all systems investigated the actual order of the actuator-plant systems is larger than the modeled order. The neglected dynamics are either too fast or too small to be of concern; this may not be the case in some failure scenarios.

From the above analysis it can be seen that the invariance of a system is heavily dependent on the space chosen for the sliding surface. Furthermore, it has been shown

that unmodeled dynamics reduce the invariance arbitrarily and can lead to instability. As those dynamics speed up, invariance can be returned in the limit.

3.6.2 Noise

The effect of noise on system performance is the chief concern in the decision to include some or all of the actuator dynamics in the designed plant. The relative order of the system with actuators included increases by the relative order of the actuator model used. If a first order model of the actuator is included in the plant definition, the order of the sliding manifold must be increased by one. This requires taking the derivative of the observed plant states. These states are quite noisy and taking a very high frequency derivative can result in an extremely noisy command to the actuators. Including second order actuators would require taking a second derivative and leads to extremely active control signals, a condition to which much of this research is dedicated to avoiding. Noisy control signals result in excess actuator wear and increased likelihood of failure. While little attempt was made in this project to construct filters or other noise suppression systems, beyond observer tailoring, it is generally noted that this must be done with extreme care. Any phase lag inserted into the system can have large effects on the resulting performance and robustness. Noise remains one of the largest issues in using higher-order sliding surfaces.

Chapter 4

Example Designs

4.1 The Model Setup

4.1.1 Unstable Vehicle

Continued research into the applicability of SMC for robust flight control and the zero adaptation time features of SMC prompt us to investigate its application to unstable aircraft where adaptation delay could lead to departure. In highly unstable vehicles, the reconfiguration time of reconfigurable control architectures becomes a paramount concern. The aircraft may depart well before the adaptation algorithm has a chance to determine the necessary parameters. The forward swept wing aero elastic vehicle (FSAV) provides us with just such a model.[13] Fig. 4-1 shows a sketch with sign conventions.

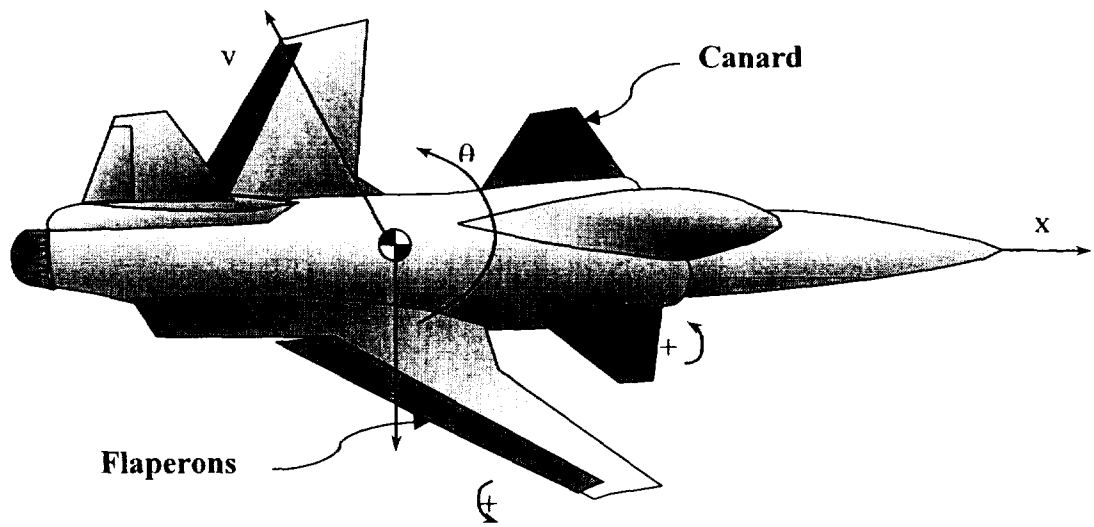

Figure 4-1: Simple Picture of FSAV with Sign Conventions.

The model contains the state space representation for three different C.G. positions, aft, center, and forward, denoted in Eq. (4.1) as 'a', 'c', and 'f' respectively. The model also includes two wing deflection modes.

C

D $X = \begin{bmatrix} a \\ \alpha \\ \theta \\ q \\ \eta_1 \\ \dot{\eta}_1 \\ \eta_2 \\ \dot{\eta}_2 \end{bmatrix}$ *Airspeed*, *Angle of Attack*, *Stability Pitch Angle*, *Pitch Rate*, *Wing Bending*, *Wing Bending Rate*, *Wing Torsion*, *Wing Torsion Rate*

$U = \begin{bmatrix} \delta_c \\ \delta_t \\ \delta_f \end{bmatrix}$ *Delta Canard*, *Delta Throttle*, *Delta Flap*

E (4.1)

$$A_a = \begin{bmatrix} 6.6355E-4 & 10.19 & -32.2 & -16.24 & -0.2674 & 2.890E-3 & 5.261 & 3.806E-5 \\ -6.438e-5 & -2.881 & -5.2316E-4 & 1.010 & 7.627E-2 & -8.182E-4 & -1.489 & -1.077E-5 \\ 0 & 0 & 0 & 1 & 0 & 0 & 0 & 0 \\ 2.534e-6 & 119.9 & 2.053E-5 & -1.086 & -2.122 & 2.907E-2 & 45.85 & 1.609E-3 \\ 0 & 0 & 0 & 0 & 0 & 1 & 0 & 0 \\ -1.122 & -31800 & -8.45E5 & 103.8 & -3624 & -20.64 & -28050 & 3.852E-2 \\ 0 & 0 & 0 & 0 & 0 & 0 & 0 & 1 \\ 1.039e-2 & 75.20 & -1.95E-5 & -0.7286 & -7.574E-2 & -8.238E-4 & -45240 & -3.6E-2 \end{bmatrix} \quad B_a = \begin{bmatrix} 1.804 & 0.002 & 6.654 \\ -0.5108 & 0 & -0.4627 \\ 0 & 0 & 0 \\ 68.48 & 0 & 12.97 \\ 0 & 0 & 0 \\ 281.6 & 0 & -6200 \\ 0 & 0 & 0 \\ 64.93 & 0 & 1.337 \end{bmatrix}$$

$$A_c = \begin{bmatrix} 5.266E-4 & 5.315 & -32.2 & -14.53 & -0.1405 & 1.507E-3 & 2.743 & 1.984E-5 \\ -6.438e-5 & -2.881 & -4.672E-4 & 1.006 & 7.627E-2 & -8.182E-4 & -1.489 & -1.077E-5 \\ 0 & 0 & 0 & 1 & 0 & 0 & 0 & 0 \\ 2.033e-6 & 79.56 & 1.457E-5 & -0.8311 & -1.055 & 1.762E-2 & 25.01 & 1.458E-3 \\ 0 & 0 & 0 & 0 & 0 & 1 & 0 & 0 \\ -0.9439 & -31160 & -6.779E-5 & 66.40 & -3624 & -20.64 & -28050 & 3.855E-2 \\ 0 & 0 & 0 & 0 & 0 & 0 & 0 & 1 \\ 3.363e-3 & 75.09 & -1.564E-5 & -0.645 & -7.6254E-2 & -8.13E-4 & -45240 & -3.6E-2 \end{bmatrix} \quad B_c = \begin{bmatrix} 0.9407 & 0.002 & 5.871 \\ -0.5108 & 0 & -0.4627 \\ 0 & 0 & 0 \\ 61.33 & 0 & 19.44 \\ 0 & 0 & 0 \\ 281.7 & 0 & -6200 \\ 0 & 0 & 0 \\ 64.99 & 0 & 1.338 \end{bmatrix}$$

$$A_f = \begin{bmatrix} 3.633E-4 & -1.995 & -32.2 & -11.98 & -5.614E-2 & -5.801E-4 & -1.035 & 3.886E-7 \\ -6.439e-5 & -2.881 & -3.856E-4 & 1.001 & 8.079E-2 & -8.349E-4 & -1.490 & -5.592E-7 \\ 0 & 0 & 0 & 1 & 0 & 0 & 0 & 0 \\ 1.385e-6 & 19.11 & 8.292E-6 & -0.6335 & 0.5061 & 1.776E-3 & -6.272 & 1.198E-3 \\ 0 & 0 & 0 & 0 & 0 & 1 & 0 & 0 \\ -0.7488 & -31010 & -1.273E-4 & 6.26 & -3510 & -20.88 & -2.836E4 & 1.760E-2 \\ 0 & 0 & 0 & 0 & 0 & 0 & 0 & 1 \\ -5.798e-3 & 124.5 & -1.3204E-5 & -0.5188 & -8.535E-1 & -2.955E-3 & -4.52E4 & -3.646E-2 \end{bmatrix} \quad B_f = \begin{bmatrix} -0.355 & 0.002 & 4.698 \\ -0.5108 & 0 & -0.4628 \\ 0 & 0 & 0 \\ 50.61 & 0 & 29.16 \\ 0 & 0 & 0 \\ 776.7 & 0 & -6275 \\ 0 & 0 & 0 \\ 80.51 & 0 & 7.888 \end{bmatrix}$$

While all C.G. cases presented above are investigated, the design procedure focuses on the nominal, center C.G., *without* the structural modes system. All performance plots and failures are then run on the aft C.G. model with the structural modes included, demonstrating the extreme flexibility and robustness of the presented control system. All cases are flight conditions corresponding to level flight at 1000ft/sec at sea level and no compressibility effects (M=0). While this is quite fast to ignore compressibility effects, the model was calculated at this 'speed' to obtain suitably high dynamic pressures (1189.0psf)[13] to drive the bending modes.

The nominal plant is daunting to any control engineer. It contains a pole at +7 rad/sec and a zero at +0.0004078 in the pitch rate transfer function. This makes the system non-minimum phase. The model is a full longitudinal model with both short period and phugoid modes. The SMC design was performed on a non-structural mode model of the FSAV. Again, this allowed the later addition of these modes to test the robustness and tolerance of the SMC design.

4.1.2 Structural modes

"The results of Fig. 4-2 indicate that the canard has significant control influence over the wing bending mode throughout the entire flight range. This means, for instance, that the use of the canard to alter the aircraft attitude dynamics will also affect the wing bending dynamics." In addition, the flaperons will "primarily affect the wing bending modes" below 1500ft/sec.[13]

The FSAV's forward swept wings, and resulting aero elastic effects, present many difficult challenges to the control engineer and system. While many dynamic models in the literature include fuselage bending, this model has a rigid fuselage and flexible

wings. The wings are allowed to deform in pure spanwise bending and torsional deflection. Interestingly the phugoid mode and the torsional mode are speed independent with the later very near the *jw* axis at a frequency of 212 rad/sec. Gilbert goes to extended lengths to show the effects of each actuator upon each state and the methods used to produce the controllability plots.[13] There are some critical points which will be reiterated here. The canard is the primary pitch control device. However, from Fig. 4-2, taken directly from Gilbert,[13] it is seen that at the flight speed investigated, 1000 ft/sec, the modal controllability of the wing bending mode from the canard is almost half as strong as the attitude modes! Thus, the coupling is quite pronounced.

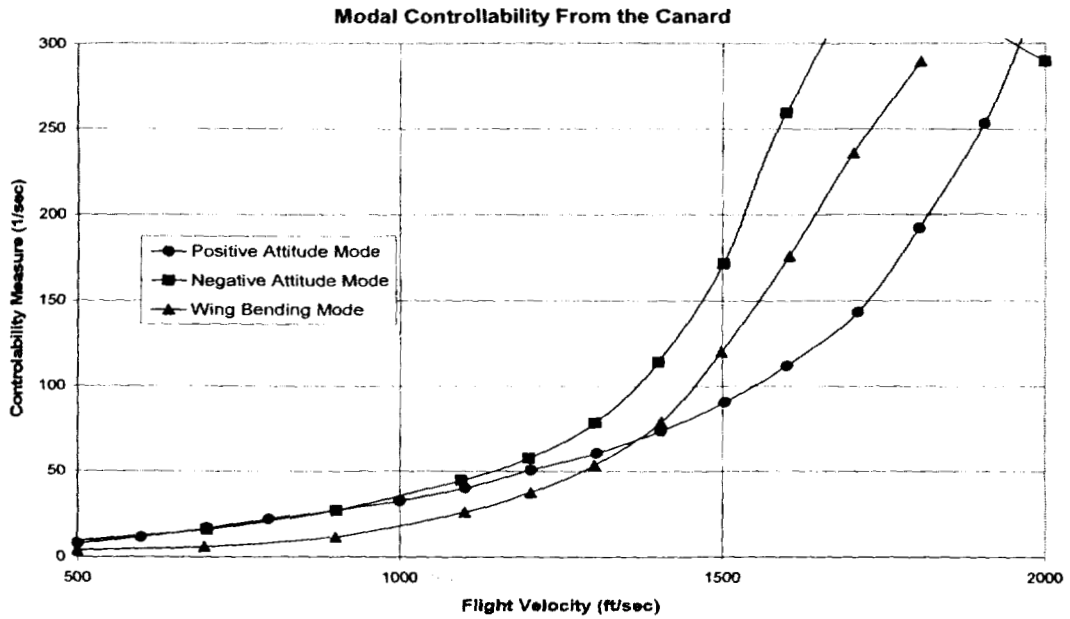

Figure 4-2: Modal Controllability From the Canard. FSAV[13]

Figure 4-3 has even worse news. It shows that the effect of the flaperons on the attitude of the aircraft is a small effect relative to its power over the bending mode of the wing. It is shown that the effect of the flaperons at speeds below 1500 ft/sec is almost entirely the deformation of the wing and only secondarily the control of pitch rate.

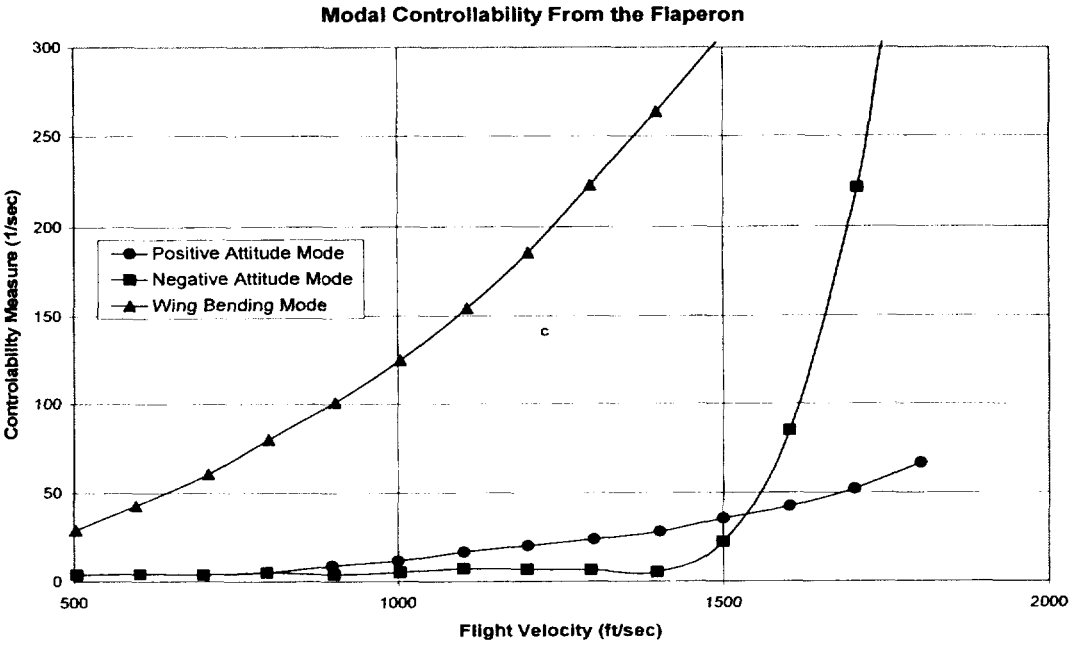

Figure 4-3: Modal Controllability From the Flaperon FSAV[13]

The 'modal controllability' measure is discussed in detail by Gilbert, without explanation here, it is a measure of the ability of an actuator to affect a particular mode of the system.[13] Gilbert, when discussing higher velocities above 1500ft/sec, states,

"...the pitch rate $\dot{\theta}$ and wing tip bending rate $\dot{z}_T$ responses, which were dominated by a single mode at low flight velocities, are actually a combination of several modes at higher velocities. For these reasons, the terms 'wing bending mode' and 'attitude or short period mode' must be used carefully when discussing [the planes] dynamics."[13]

While this investigation is not dealing with the highest velocities he was referring to, his analysis is valid at our speed, but to a lesser degree.

Despite all the evidence which suggests the structural modes cannot be ignored, throughout the analysis and design procedures here, they have been totally omitted. The addition of these modes into the finalized model is meant to test the ability of the SMC system to compensate for the unmodeled dynamics. It is shown later that the SMC controller can compensate for the structural modes during most types of failures.

4.1.3 Actuators

The highly unstable nature of the airframe places abnormally large demands on the actuators. The close-coupled canard is the primary and most effective pitch control device. As stated earlier, in order to stabilize the system, an outer airspeed loop is used, and thus an engine model must be assumed. In addition, for the last design example, the inclusion of the flaperons adds a redundant, though less effective pitch control device. The actuators models were selected as shown in Table 4-1.

	Dynamics	Position Limits	Rate Limits
Canard	$\frac{70}{s^2 + 2 \cdot 0.7 \cdot 70 \cdot s + 70^2}$	±15 deg	100 deg/s
Engine	$\frac{1}{s+1}$	n/a	n/a
Flaperons	$\frac{35}{s^2 + 2 \cdot 0.7 \cdot 35 \cdot s + 35^2}$	±35 deg	60 deg/s

Table 4-1: Nominal Actuator Properties FSAV.

4.1.4 Noise Model

Since any aircraft flight control system must measure such variables as airspeed, pitch rate, and alpha through sensors, the system's ability to reject measurement noise must be tested. This is particularly true of high bandwidth systems like SMC where the controller is capable of 'tracking' and passing the noise to the actuators. The high bandwidth of the controller is one of its benefits, however, passing amplified noise to actuators leads to excessive wear and tear as well as increased likelihood of failure. While this author considers a detailed design of noise control to be beyond the scope of this project, an initial analysis was made to confirm a nominal amount of noise could be tolerated. The model for the noise used is shown in Fig. 4-4. The output RMS value of the two signals is 0.25 deg and 25 ft/sec respectively. The band limited white noise

requires a seed number, this number is set to a different integer in the two blocks to prevent identical noise from entering the system.

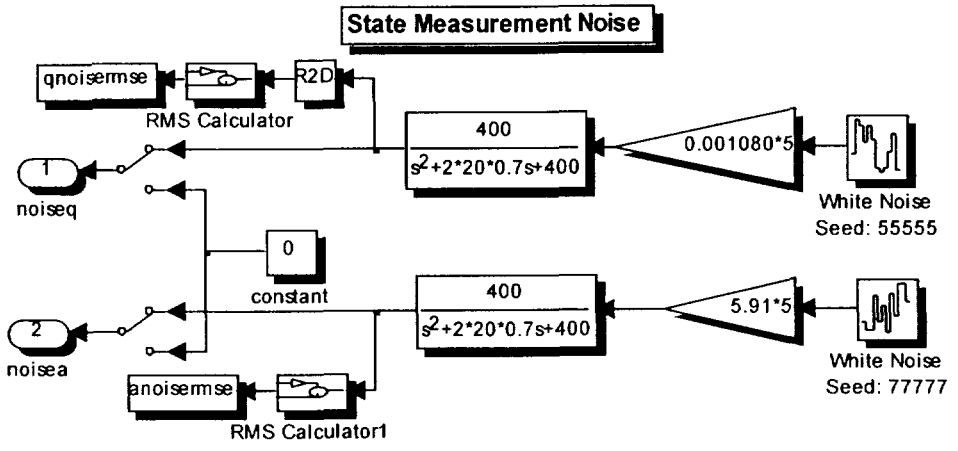

Figure 4-4: Block Diagram of Noise Generator. FSAV

4.1.5 Flight Control System

The short period mode is controlled with an inner loop pitch rate (q) feedback using a SMC to the canard actuators. In the first two designs the flaperons were not used, they are added to a final design to investigate limiting and robustness effects of redundant actuators.

A slower, airspeed loop is closed using a linear gain controller through a simple engine model to stabilize the slowly divergent phugoid mode. The reduced model seen by the airspeed loop is very simple and does not require a SMC controller. (See Fig. 4-19) In addition, SMC's rapid response times and robustness are of little benefit to the slow turbine control and would contribute unnecessarily to model complexity.

A pilot is assumed to close an outer loop where the system output is the Euler pitch angle theta (θ). This is found by integrating the pitch rate q or measuring the θ state.

4.1.6 Failure/Damage models

Clearly there are an infinite number of possible failures which such an aircraft could experience. While no airframe failure or damage is precisely modeled, attempts to challenge the control system by 'failing' the system into configurations which are significantly more difficult to control than the nominal case are performed. The failures investigated are slightly different from example to example but each case can contain any or all of the following: the plant model is made more unstable, the actuators are slowed down and can be amplitude and rate limited, a pure time delay is added to the actuators, and the control power matrix is reduced. All of these failures are based on the aft C.G. model, which is less stable than the designed center C.G. model. In each case studied, an SMC controller is designed and simulated. In addition, a second controller is designed using "classical" loop-shaping techniques for the nominal case. The classical design provides a comparison to the SMC design.

To model a plant failure, the A matrix was multiplied by 1.20. This has the effect of multiplying the eigenvalues by a factor of 1.2. Thus, the unstable pole at ~+7 moves farther into the right half plane. Care must be exercised to keep the proper kinematical relations. The theta state is a pure integration of the q state and should not be multiplied in a failed case. This is true in some of the structural mode states as well. The states which are related to the airframe are multiplied, while the integration terms are left at unity.

At the same time that the A matrix is modified, the control power was reduced by multiplication of the input matrix by 0.75. Again, kinematical modes as well as the inputs to the structural excitations were not scaled. This will model a worst case damage

to the model, where the divergent poles are sped up and the control power is decreased but structural excitation is unchanged. These changes were accomplished as in Eq. **Error! Reference source not found.**.

$$A_{failed} = \begin{bmatrix} A(Row1)*1.2 \\ A(Row2)*1.2 \\ A(Row3) \\ A(Row4)*1.2 \\ A(Row5) \\ A(Row6)*1.2 \\ A(Row7) \\ A(Row8)*1.2 \end{bmatrix} \quad B_{failed} = \begin{bmatrix} B(Row1)*0.75 \\ B(Row2)*0.75 \\ B(Row3)*0.75 \\ B(Row4)*0.75 \\ B(Row5) \\ B(Row6) \\ B(Row7) \\ B(Row8) \end{bmatrix} \tag{4.2}$$

In addition to modification of the plant, severe damage to the actuators was modeled as indicated in **Table 4-2** below. The severity of these failures is remarkable, and combined with the failure of plant correspond to 'large and unknown' failure as required in the stated definition of reconfigurable control. Time delays and decreases in dampening, and bandwidth attempt to show robustness to higher order actuators, actuator failures, as well as tolerance to the inherent delays in all digital systems.

	I Actuator Properties:	J Nominal	K Failed RO	L Failed FO	M Failed FOF
N Canard	O ω (rad/sec)	P 70	Q 40	R 35	S 30
	T Delay(ms)	U ~0	V 10	W 15	X 20
	Y Damp(ζ)	Z 0.7	AA 0.5	BB 0.5	CC 0.5
	DD Rate Limit(deg /sec)	EE ±100	FF Nominal	GG Nominal	HH Nominal
	II Pos. Limit(deg)	JJ ±30	KK Nominal	LL Nominal	MMNominal
NN Flaperons	OO ω (rad/sec)	PP 30	QQ N/A	RR N/A	SS Nominal
	TT Delay(ms)	UU ~0	VV N/A	WW N/A	XX 10
	YY Damp(ζ)	ZZ 0.7	AAA N/A	BBB N/A	CCC 0.5
	DDD Rate Limit(deg /sec)	EEE ±60	FFF N/A	GGG N/A	HHH Nominal
	III Pos. Limit(deg)	JJJ ±30	KKK N/A	LLL N/A	MMM Nominal

NNN Table 4-2 Comparison of Nominal and Failed Actuators

4.2 Pilot model and Task

While the investigated benefits of SMC could easily be applied to both piloted and autonomous flight, the more difficult piloted condition will be investigated. This has a large impact on the allowable behavior of the model. A pilot, as modeled in Hess[32] was added and tuned to the nominal plant, and did not adapt it to the failed plant. This can severely limit the allowable behavior of any hedging or phase lag allowed into the system. Thus, a worst case pilot/vehicle interaction is presented. The pilot model is shown below in Fig. 4-5. The gains which define the pilot assume that the inner loop SMC tracking is sufficiently close to the model reference that the pilot only 'sees' the reference model.

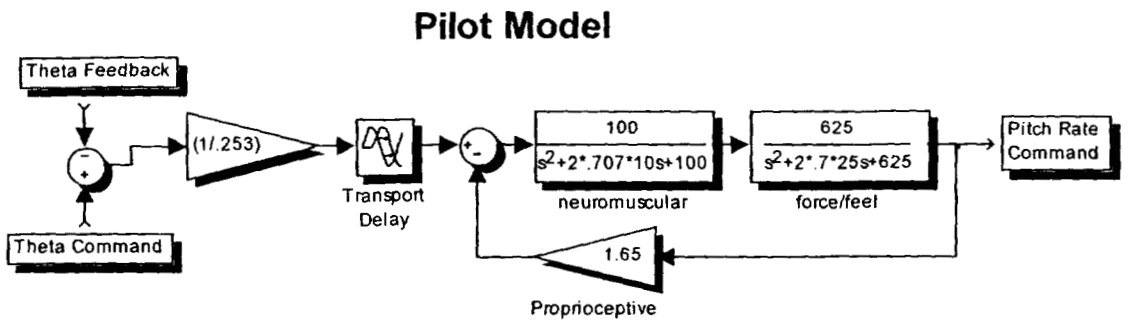

Figure 4-5: Pilot Model Block Diagram.

The task selected is θ (stability axis pitch angle) tracking. The tracking task is a filtered sum of sines.

$$\theta_c(t) = \xi \sum_{i=1}^{7} A_i \sin(\omega_i t) \qquad (4.3)$$

The amplitude gain was set to 5°. The parameters A_i and w_i are taken from Kish[33] and presented in Table 4-3.

i	A_i	ω_i
1	-1.00	0.19947
2	1.00	0.48969
3	1.00	0.89760
4	0.50	1.39626
5	0.20	2.39359
6	-0.20	4.19970
7	-0.08	8.97598

Table 4-3: Sum of Sines Parameters

This input is introduced through a unit step filtered with $\frac{0.8}{s+0.8}$ as shown in Fig. 4-6. After being multiplied by 5 the resulting RMS value is 6.4 deg. The benefit of this method versus a filtered white noise is that this results in a pseudo-random, zero mean, continuous signal with a zero initial condition. It also contains frequencies which properly simulate those found in flight tracking tasks

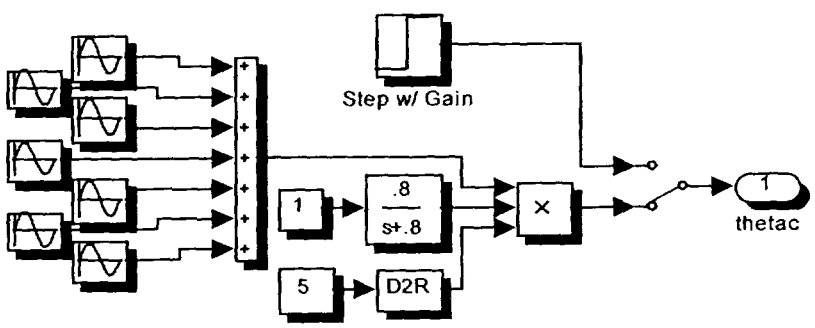

Figure 4-6: Block Diagram of Sum-of-Sines and Step Input.

An unfiltered step can also be applied to test the pilot or bypass the pilot to test the system. Because the step is input into the reference model, the SMC never sees a pure step. This is a feature of the model reference based design.

4.3 Reference Model

All the designs presented use model reference tracking. This attempts to provide a constant feel to the pilot independent of aircraft dynamics. In each design case the same reference model is used. The reference model chosen as:

$$G_r(s) = \frac{q_r}{Ip}(s) = \frac{100}{s^2 + 2 \cdot 0.7 \cdot 10 \cdot s + 100} \qquad (4.4)$$

This provides predicted level 1 handling and no PIO tendencies.[32]

In the airspeed loop the input is a command for zero perturbation velocity and because no variability is involved no reference model is used..

4.4 General Design Procedure

One of the key factors in SMC design is the definition of the sliding surface $\sigma=0$. This can be done by many methods including arbitrary definition. An overview of many design strategies is given in Edwards and Spurgeon.[16] The concepts presented here are based on a loop-shaping, domain approach to MIMO design.[22] Because of the nature of the design, it is limited to square systems, which are feedback linearizable.

(1) Plant Definition: A vehicle model is chosen. It may or may not include a first order actuator model per the designer's choice. This decision will be highlighted later in this chapter. A 'limit frequency' is defined above which parasitic dynamics, and unstructured uncertainties become a concern.

(2) Reference Model: A reference model is chosen. Since this study is directed toward achieving piloted flight, a reference model which will produce a Cooper-Harper rating of Level 1 with no PIO tendencies should be selected.[32] Consult Hess[32] for examples and selection procedure.

(3) Sliding Surface Definition: The desired feedback structure is determined. In this example a pitch rate command system is desired. Pitch rate (q_r) is the output of the reference model. Estimated pitch rate q_o is fed back to the SMC from the observer and a hedge signal q_h is also subtracted. System error is now defined as, $e(t) = q_r(t) - q_o(t) - q_h(t)$. A feedback variable not used during design is set to zero. If there are multiple actuators per channel then a control distribution matrix must be created by any number of methods. The sliding manifold can then be created using the following rules:

a. σ is derived from a tracking error expression in Eq. (4.5) where p is the relative order of the system. Note that the $(p-1)^{st}$ derivative of the error signal is in the definition of σ. The benefits and ramifications of this will be discussed in §5.4. Also note that contrary to the ideal sliding mode, an integral term is also included compensating for the addition of the boundary layer.

$$\sigma = e(t)^{p-1} + K_{p-2}e(t)^{p-2} + \ldots + K_0 e(t) + K_{-1}\int e(t)dt \qquad (4.5)$$

b. Since a continuous boundary layer will be added to the controller use the linear control law defined earlier and shown in Eq. (4.6)

$$. \; u(s) = \frac{\rho}{\varepsilon}\sigma = K_\rho\left(s^{p-1} + K_{p-2}s^{p-2} + \ldots + K_0 + \frac{K_{-1}}{s}\right)e(s) \qquad (4.6)$$

In the frequency domain the K_i are chosen to produce broad K/s properties around crossover in the loop transmission. This will always be possible to achieve because enough derivatives are included in Eq. (4.5) to produce the desired shape at frequencies at least as high as the limit

frequency. K_ρ is also obtained in this step to set the crossover frequency. If one looks at the Simulink® formulation used, as in Fig. 4-8 one can potentially see a problem at this step. Since the linear version of sigma is bounded at $\pm$ 1 and ε is divided before the $\pm$ 1 limiter, ρ is the largest possible control output of the SMC. Thus, to use the entire range of the actuator, the minimum ρ must be equal or greater than the position limit of the actuator. In a multiple actuator per SMC channel it would be set to the largest actuator downstream. The crossover frequency obtained in this step can be significantly higher than any allowable loop shape bandwidth and probably well beyond the limit frequency. This is of no concern and will be addressed later.

(4) Sliding Behavior: The existence of the sliding mode must now be confirmed. Use the ideal signum function and no boundary layer. A reaching phase followed by infinite switching should be observed in addition to an identically zeros $\sigma(t)$ for $t>t_s$ where t_s is at the first crossing of $\sigma=0$. Depending on the numerical program used, some care must be taken since plotting and numerical interpretations can be deceiving. Note that an observer, additional actuator orders, reference models, and hedging have not yet been added and there are no outer loop closures. If sliding behavior is observed, then move to step (5). If sliding behavior (infinite switching) is not observed, then increase ρ until it is. There exist many analytical methods to choosing ρ but the quickness and simplicity -keeping in mind the above warning- of computer simulation lends itself to this analysis.

(5) Boundary Layer: Replace the ideal control law of Eq. (4.5) with the linearized control law of Eq. (4.6). Modifying K_ρ can be important in this step. Do not decrease K_ρ, particularly if it was limited by actuator position limits. If ε increases above 1 then increase K_ρ to maintain a constant $\rho/\varepsilon=K_\rho$. ε is increased until no infinite switching is observed while maintaining near perfect tracking as seen in $\sigma\approx 0$. This should be possible with large variations in plant dynamics.

(6) Parasitic Dynamics: The real - full order, actuator should now be added to the system. This will almost surely cause the system to be unstable.

(7) Observers: The observer's design is of critical importance to the tracking performance and robustness of the entire system. In a SISO case, this is a simple Luenberger observer. The poles of this observer should be chosen to lie between the limit frequency and the bandwidth of the reference model. The lower limit can be stretched a bit, but care must be taken. Eigenvalues which are too high defeat the observer and decrease stability. Eigenvalues which are too small decrease robustness. In the MIMO case, an independent observer on each feedback channel often dramatically improves tracking and robustness and can help control noise. If there are multiple channels, choose each observer speed and/or define each observer plant and choose speeds as shown in §5.2.

(8) Hedging: The model reference hedging is designed as in §2.5.4.2.

(9) Model Actuators: Model actuators which were added as per §3.5 can now be analyzed to determine an optimal case. The bandwidth of the model observers should usual range between 50% and 75% of the actual bandwidth. This provides great tracking with improved robustness. Be careful to minimize the

interaction between the model actuators and the observer. In some sense the model actuator becomes the definer of the observers limit frequency.

(10) Finalize design parameters. This may require some iteration, particularly in steps 7-9.

4.5 Application Example: Reduced Order Model

The first design of interest shall be called the "reduced order model" or FSAVro. It follows very closely the design procedure above. The plant is defined as above. Pitch rate tracking is desired, so q is the feedback variable. The system, shown in Fig. 4-7 has non-minimum phase and requires an additional outer feedback loop of the airspeed. The system is now square and an assumption of feedback linearizable has been made.

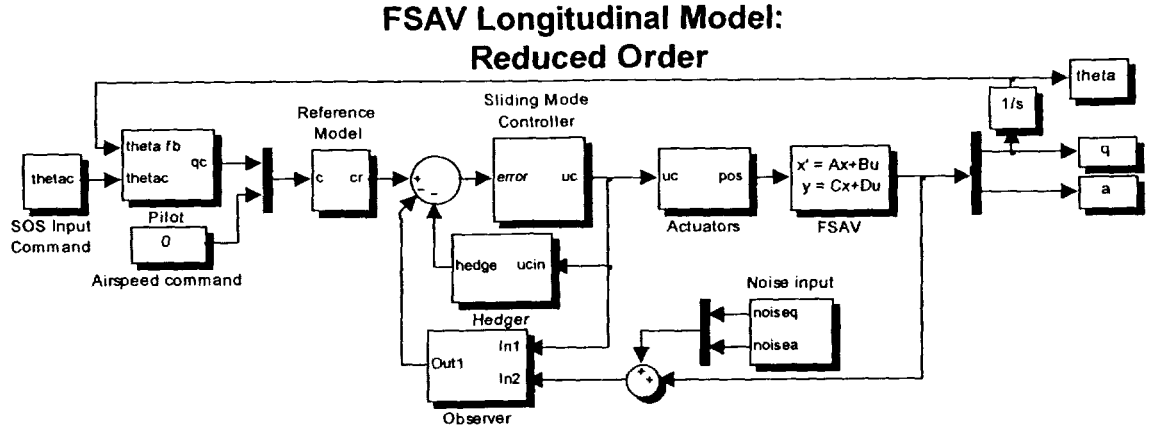

Figure 4-7: Block diagram of Reduced Order Model

An outer, pilot loop as defined in §4.2 controlling θ will generate the q command. This will be fed through a reference model defined in §4.3. The SMC will control q and a linear gain controller will regulate the perturbation airspeed.

In the q (pitch rate) loop, since no actuators are assumed in this model, it is of relative order 1. Thus, the sliding manifold is defined as:

$$\sigma = K_0 e(t) + K_{-1} \int e(t)\partial t \qquad (4.7)$$
$$e(t) = q_r - q_o$$

The corresponding Simulink® diagram of the SMC is shown in Fig. 4-8.

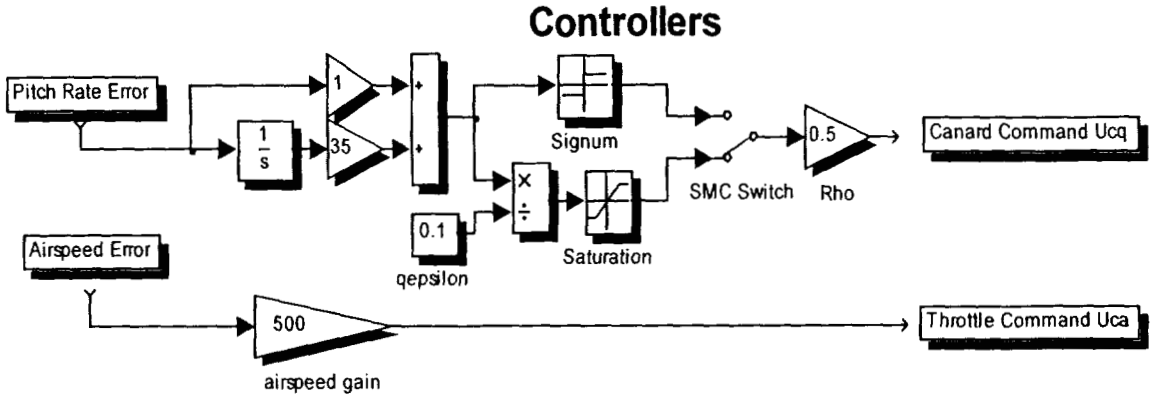

Figure 4-8: Block Diagram of SMC and Gain Controller used in FSAVro design

This leads to a control law in the frequency domain of :

$$u_c(s) = K_\rho \left(\frac{K_0 s + K_{-1}}{s} \right) \qquad (4.8)$$

The values selected are K_ρ=0.5, K_0=1, K_{-1}=35, which leads to the desired $\frac{K}{s}$ shape (-20 dB/dec) around the crossover frequency of 300 rad/s.

The compensated loop transmission is shown in Fig. 4-9. The -20 dB/dec area extends to lower bandwidths than was finally used, however, in this case, the minimum K_ρ was dictated by position limits of the canard actuator.

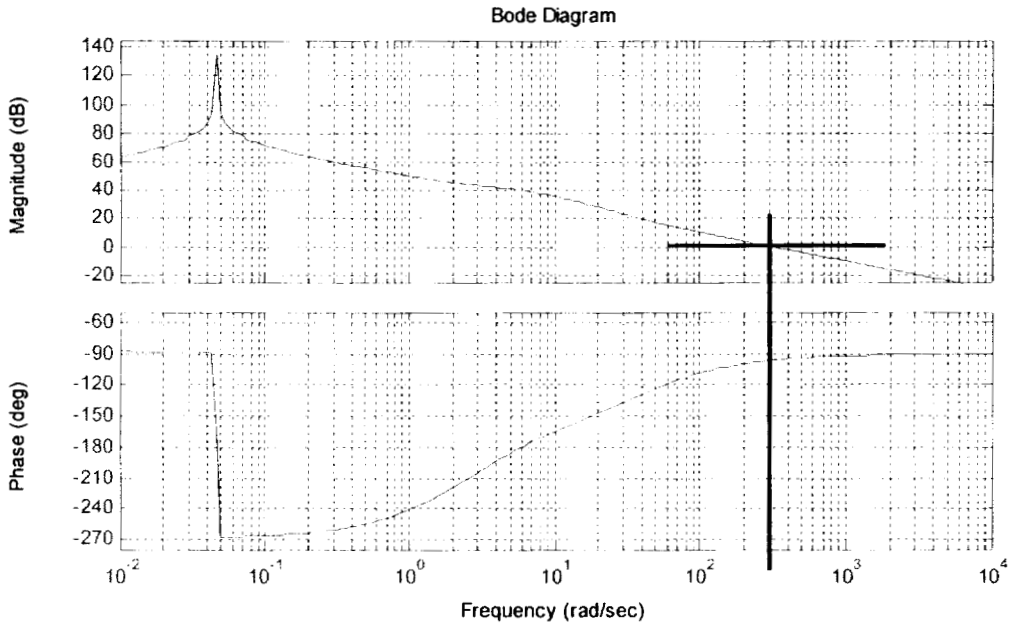

Figure 4-9: Pitch rate (q) Loop Transmission of Compensator* Plant. FSAVro

(end of page)

This next step is not part of the SMC design, but is critical to this non-minimum phase system. If the resulting system is analyzed, it is found to be still unstable. This is not a fault of the SMC design or theory, but a function instead of the non-minimum phase nature of the plant. After completing the ideal SMC design the outer loop airspeed feedback can be designed. Because this feedback loop is very slow, quite simple, and not controlled by a sliding mode controller, a classical loop shape design is performed. In this system, only a proportional control is required.

With the pitch rate (q) loop closed, the airspeed loop bode diagram, excluding the engine model, is shown in Fig. 4-10. Choosing a crossover frequency of one rad/sec, the desired controller is found to be a pure gain of 500.

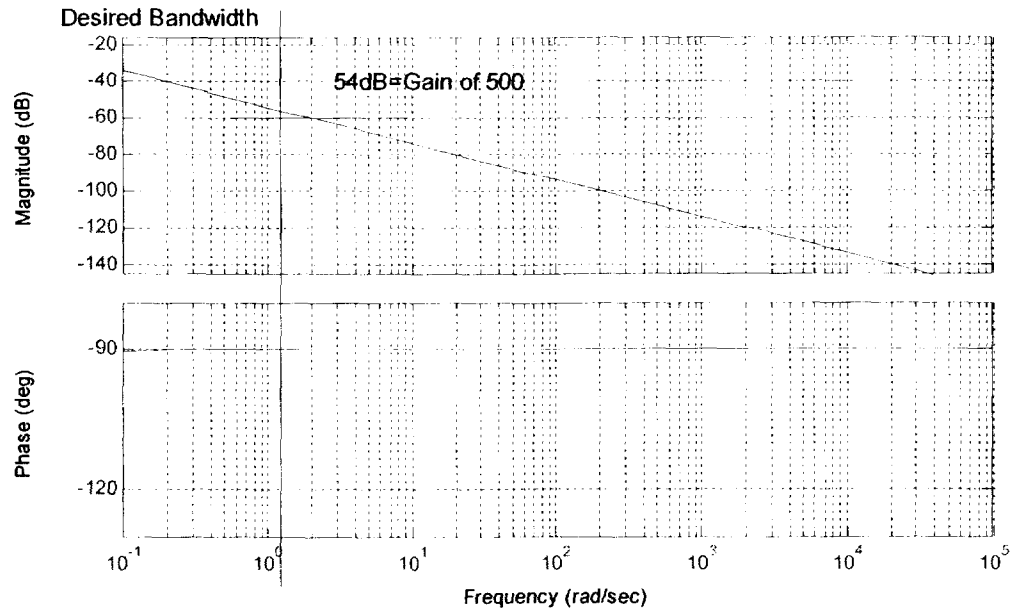

Figure 4-10: Loop transmission of airspeed with q loop closed. FSAVro

Next, sliding behavior should be shown. Setting the switch "SMC Switch" in Fig. 4-8 to use the signum function in the upper path, creates an ideal, nonlinear, sliding mode controller. Using Simulink® with the solver set to ODE2 and Δt=0.0001 ideal sliding is demonstrated by the high frequency switching seen in Fig. 4-11, and the invariance to the failure at time t=10 sec.

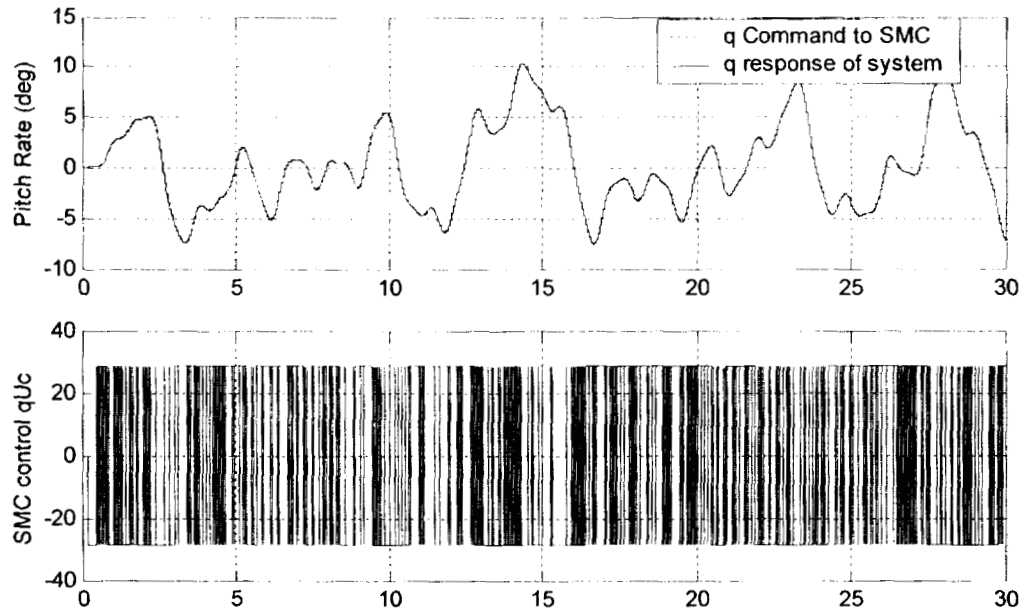

Figure 4-11: Pure SMC, Failure at 10 sec. FSAVro

-End of Page-

Moving to the next step, the boundary layer is added and increased until the controller outputs a continuous control signal. Setting the switch "SMC Switch" in Fig. 4-8 to use the saturation function, this changes the model from 'ideal' to a linear approximation utilizing a sliding surface boundary layer mode. Starting with a ε=0.00001, a very good approximation of the signum function, the boundary layer is increased and finally set to 0.1 when a continuous output is realized.

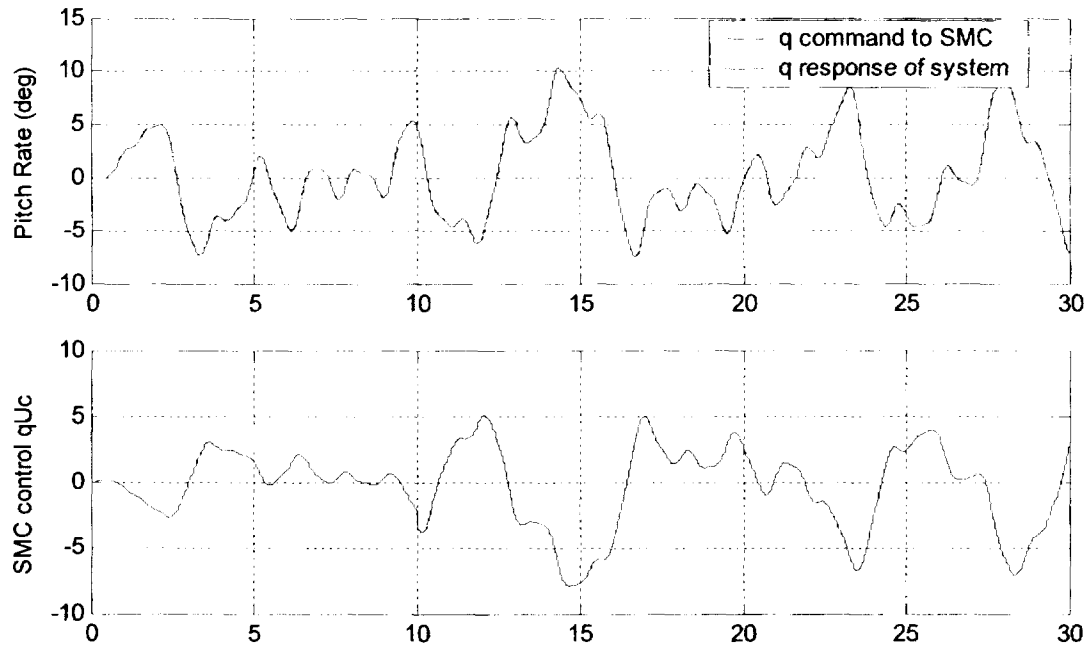

Figure 4-12: Inner loop Tracking and Control, Failure at 10 sec. FSAVro

While some tracking degradation is present, it is very difficult to see on almost any scale. This plot also includes a massive failure at 10 sec. The reader will note that, as per the caveat in this stage of the general design, $\frac{\rho}{\varepsilon} = K_\rho$ was not kept constant because ε was below unity. Reducing ρ would result in an inability to command to position limits.

The result of the above design is excellent tracking and robustness, near that of ideal SMC. The actuators are now included the large ramifications are addressed. When the actuators are added the system instantly becomes unstable; the controller cannot deal with the phase lag imposed by real actuators. The observer and then hedge models must be added to compensate.

Because of the benefits of using independent observers, a pitch rate and an airspeed observer are constructed instead of using a single observer. The standard, single, strongly coupled observer is replaced by multiple decoupled observers. The decoupling is clearly evidenced by the transfer function matrix shown in Table 4-4 below which represents the entire dual observer assembly.

Observer Input	Observer Output q_o	Observer output a_o
Canard Command	$\frac{61.33s(s+2.218)(s-0.0004078)}{(s+15)(s+16)(s+17)(s+18)}$	0
Throttle Command	~0 peak magnitude= -180 dB	$\frac{0.002}{(s+0.5)}$
Measured Pitch rate (q)	$\frac{62.29(s+11.18)(s^2+16.25s+105.5)}{(s+15)(s+16)(s+17)(s+18)}$	0
Measured Airspeed (a)	0	$\frac{0.5}{(s+0.5)}$

Table 4-4: Observer system transfer functions. FSAVro λ_q=-15,-16,-17,-18 λ_a=-0.5

The design of the combined observer system allows any amount of coupling to be arbitrarily chosen by including and tailoring cross terms. This would be seen in non-zero transfer functions in Table 4-4 for the crossed terms. These investigations choose to use no coupling for simplicity and noise issues.

In the model investigated, a nominal plant in the airspeed (a) observer was *not* used. Using state space algebra, after the q loop has been closed, the a transfer function,

from airspeed perturbation command to airspeed output, could be found. Eliminating nearby pole zero cancellations resulted in a simplified model. This model was used as the airspeed 'plant'. In this case it has a positive effect on the noise rejection with little to no model tracking degradation.

As explained in step (6) of §(4.7), the $\left(\frac{q_o}{u_c}\right)$ bode plot is analyzed and/or simulations are run at varying observer speeds. It has been suggested that at slower observer speeds, the tracking performance suffers and that at higher observer speeds, the system becomes unstable due to the parasitic dynamics of the actuator being passed to the SMC. While many more conventional plants can show very good performance using only an observer and no hedging, all of the research into this system realized only moderate performance in the absence of hedging. Thus, no optimization in this step is performed as it is merely used as a starting point to select the final, hedged, observer speed. An observer speed is selected which is slower, but near to, perhaps 10% lower, to the highest observer speed which is stable. In this model that was selected at $\lambda_q = -8,-9,-10,-11$. This is equivalent to the statement Pq1=8. Also note that this is below the reference model bandwidth.

As stated above, improved performance and increased robustness can be realized with increased observer speed. The negative interaction with the SMC can be minimized by inclusion of hedging into the model. Thus, the observer speed is pseudo-arbitrarily increased by approximately 25% leading to an unstable system. The hedge system is then designed using the methods shown in §2.5.4.2. For this system, that results in an

observer speed of $\lambda = -15,-16,-17,-18$, or Pq1=15, and a hedge model of $y_h = 85\left(\frac{70s}{s+70}\right)\left(\frac{1}{(s+20)(s+20)}\right)$. The resulting bode diagram is shown in Fig. 4-13.

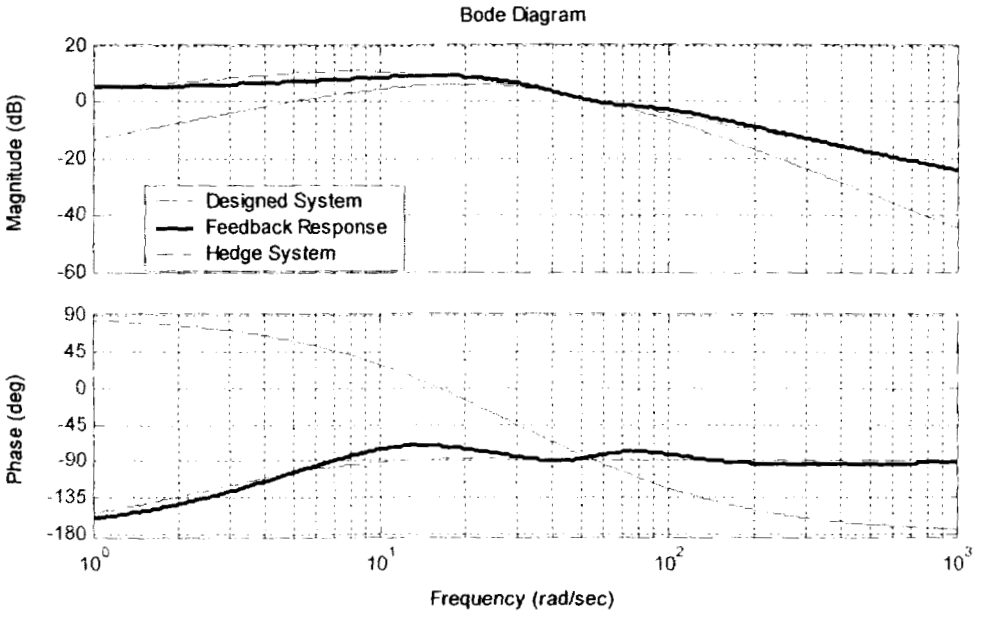

Figure 4-13: Bode plot of hedged observed feedback. FSAVro

Note in the Fig. 4-13 that the poles which define the upper end of the -20 dB/dec section are as low as possible while still retaining the effect of 'pushing up' the high frequency response. But also note that the poles which define the beginning of the -20 db/dec region extend as low as possible, risking pushing the hedged plot above the designed response. Keep in mind that any actuator failure or introduced time delay will shift the observer notch and actuator roll-off to lower frequencies, and thus will require higher, low frequency gain from the hedge system. It should be noted that this is a trade-off and many simulation runs are executed before a good feel for this parameter is obtained. The narrower and more defined the -20 dB/dec hedge band, the better the

tracking. The cost, as one might expect, is decreased robustness. These choices are the result of iteration between the observer and hedge models.

Figures 4-13 through 4-23 show the tracking performance, inner loop tracking, actuator tracking and commands as well as handling qualities and PIO tendency for both the nominal and failed case. All the model responses presented include the structural modes which were not included in the design.

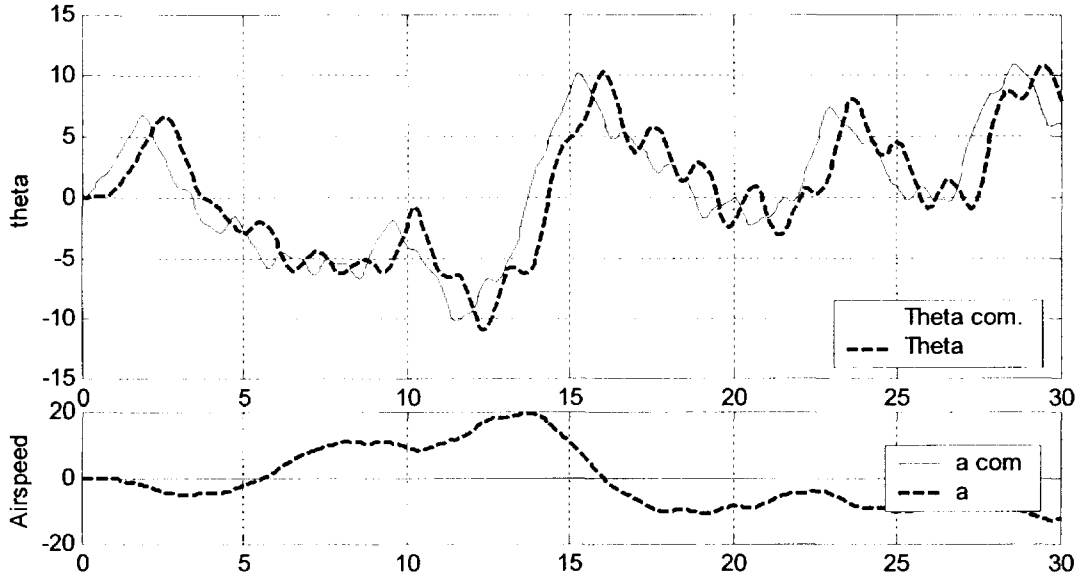

Figure 4-14: Plot of Tracking, Failure at 10 sec. Pilot/ Noise/ Observer/ Hedge/ Actuators all on. FSAVro

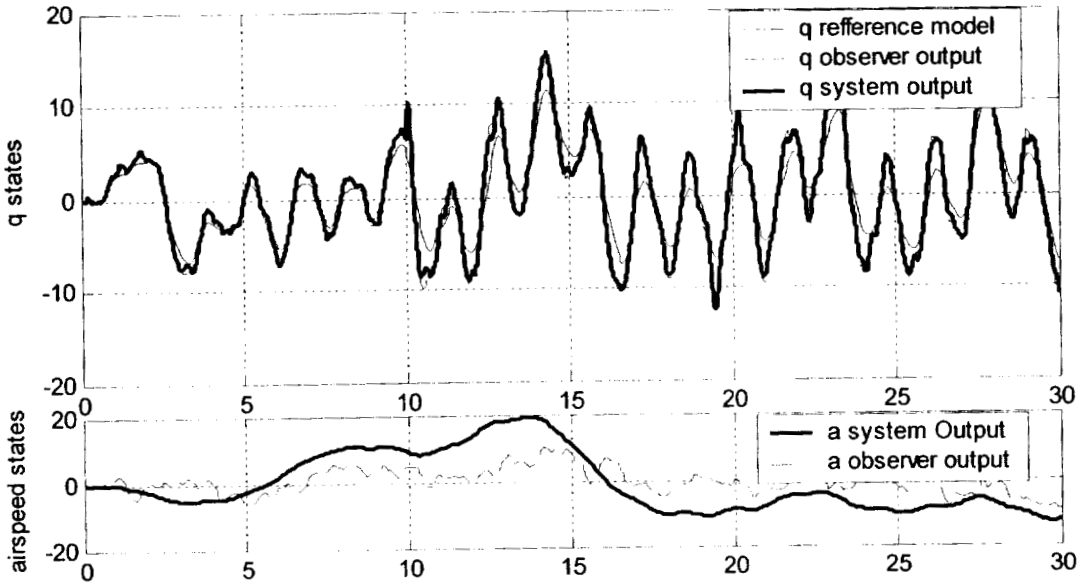

Figure 4-15: Plot of pitch rate and airspeed states. Failure at 10 sec. FSAVro

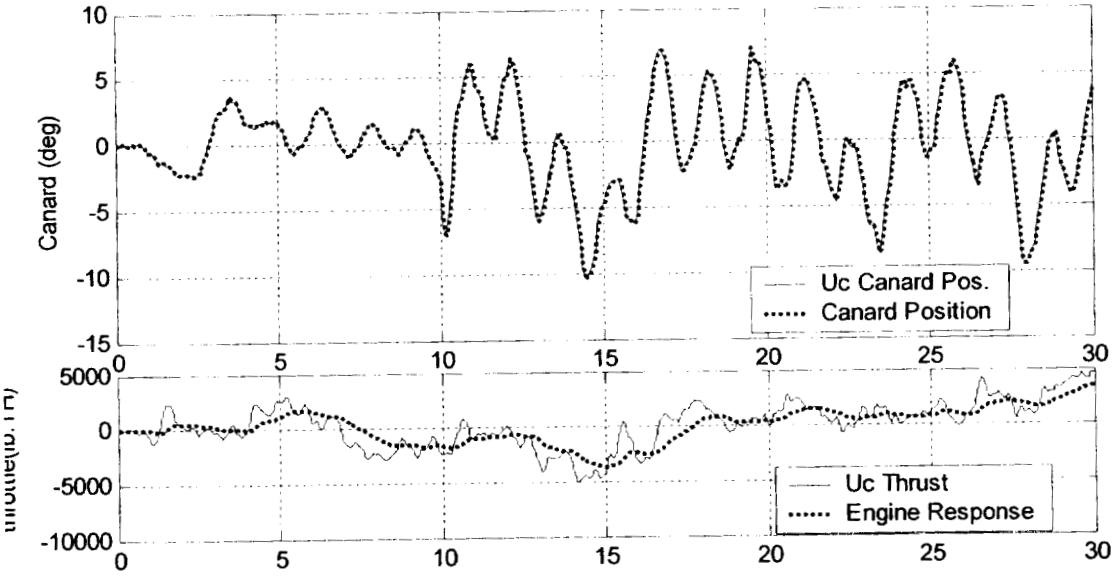

Figure 4-16: Plot of actuator command and response: Failure at 10 sec. FSAVro

Figure 4-17 shows how well the controllers are tracking their inputs. This makes no claim on the error of the system, only on the error the SMC system sees. The plot is the error which the SMC and airspeed controllers are attempting to drive to zero. It is

seen that this number is very small when compared to the system outputs. The airspeed outputs seem like they could be better, but this is only around 1% of the input magnitude. While the error is only 1%, the reconstructed state also contains an error which accounts for more actual airspeed deviation.

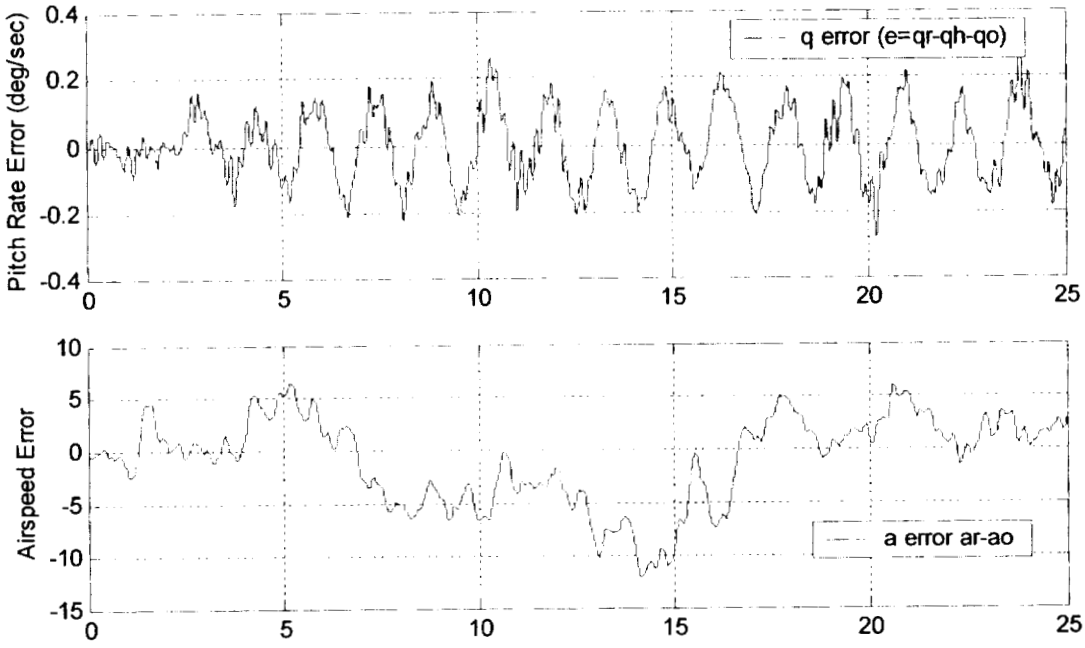

Figure 4-17: Plot of how well the controllers are tracking. FSAVro

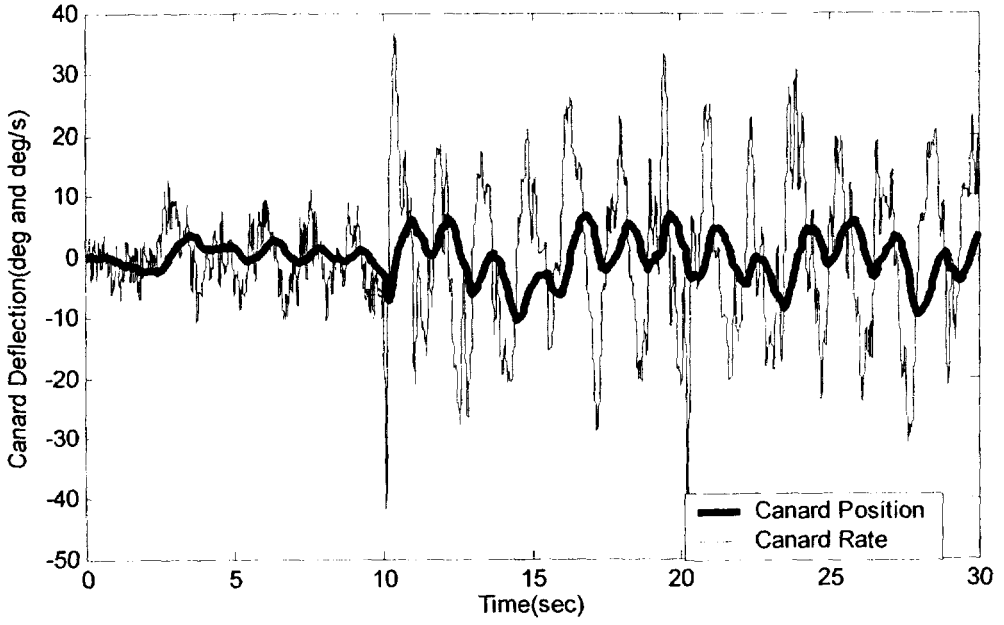

Figure 4-18: Plot of Canard actuator position and rate. Failure at 10 sec. FSAVro.

Figure 4-18 shows that the actuators are being commanded harder after the failure, but that now position or rate limits are encountered. This model is very sensitive to any nonlinear limiting. When one considers the unstable nature of the aircraft, and only one control effector, this seems reasonable. If a position limit is encountered, the craft no longer has enough control power to perform the stabilizing task and the unstable nature of the airplane quickly takes over. While one could imagine some rate limit tolerance, any rate limiting which lasts longer than around 0.1 seconds will cause instability. Again, given the time to double amplitude of the aircraft's unstable mode (approximately 0.1 sec), this doesn't seem unreasonable. The failure used includes a pure time delay of 10 ms. If this delay is reduced, then more rate limiting can be tolerated. The 10 ms delay is intended to show the systems robustness to pure phase lag, the nemesis of previous SMC designs as well as other types of control.

For comparison a standard loop shape model was also designed. The nominal case runs quite well. The pitch rate loop compensator chosen is $u_c = \frac{0.5(s+10)(s+10)(s+0.1)}{s^2(s+2.2)} * StateError$ and the open loop compensated transfer function is shown in Fig. 4-19. In the final design the airspeed loop is closed identically to the SMC design.

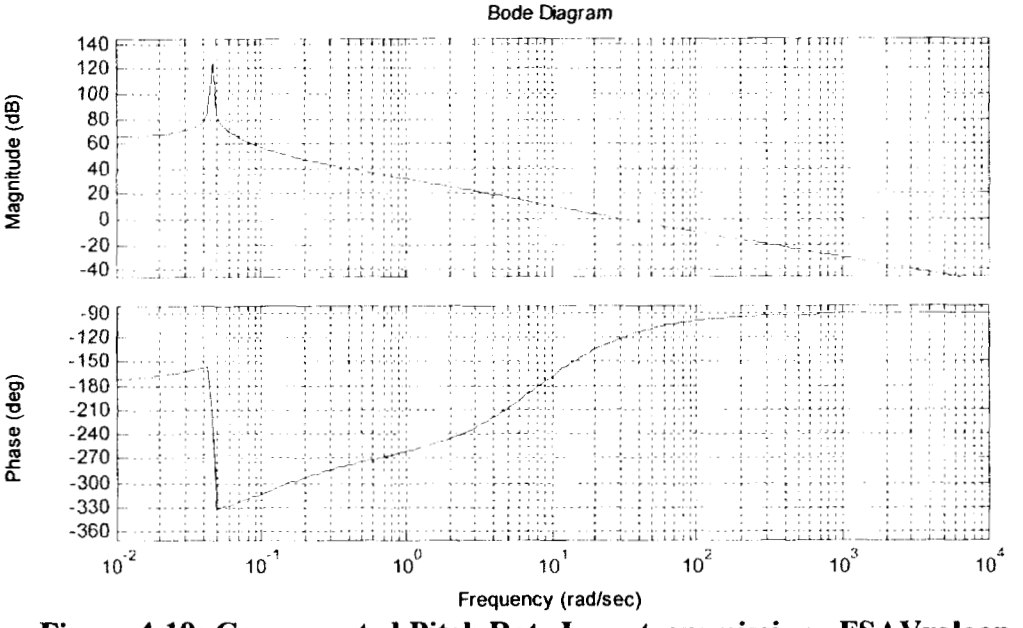

Figure 4-19: Compensated Pitch Rate Loop transmission. FSAVroloop

It is seen that the system is not able to remain stable during this failure, as shown in Fig. 4-20. While certain types of failures are stable with the loop shape design, the designed SMC system is significantly more robust to most types of failures.

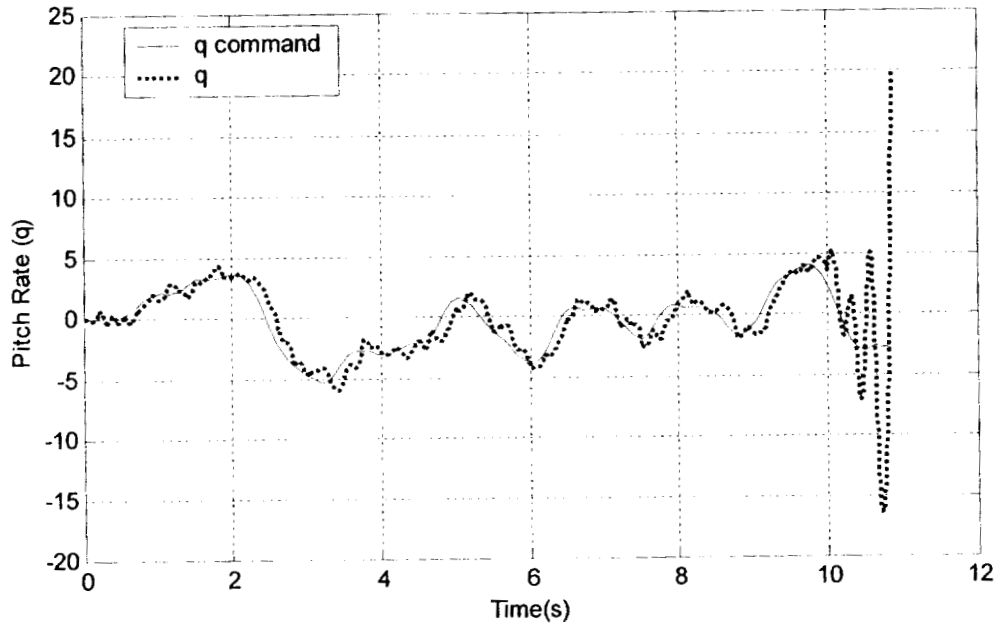

Figure 4-20: Pitch rate tracking of Loop shape model. Failure at 10 sec. FSAVroloop

Piloted flight is the focus of this investigation, and therefore some estimation as to the handling qualities should be performed. Previous work by Hess provide a means of predicting Cooper-Harper ratings of performance and PIO tendency.[32,34,35] The task dependent handling quality plots of the SMC system, in both the nominal and failed case, are shown in Fig. 4-21 through Fig. 4-24.

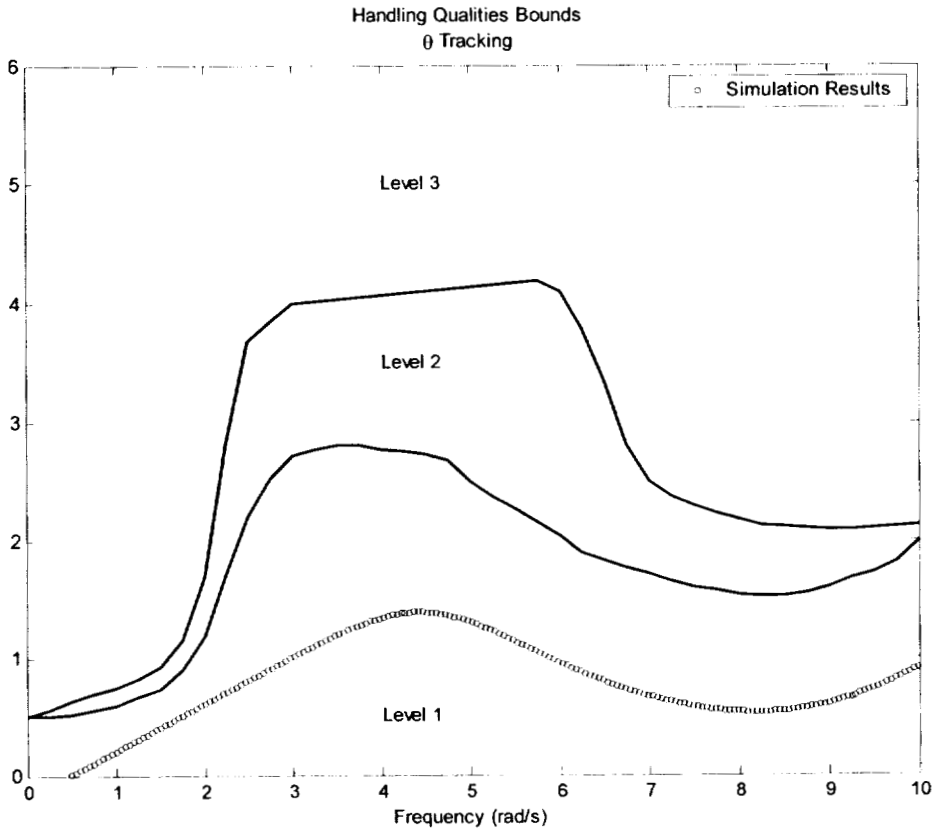

Figure 4-21: Nominal Task Dependent Handling Quality. FSAVro

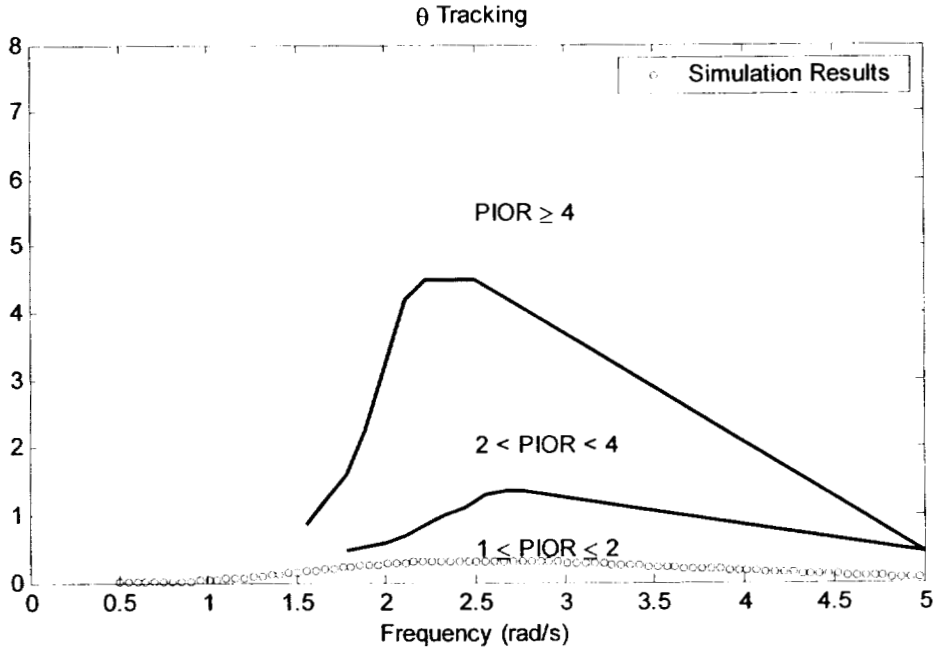

Figure 4-22: Nominal PIO Tendency. FSAVro

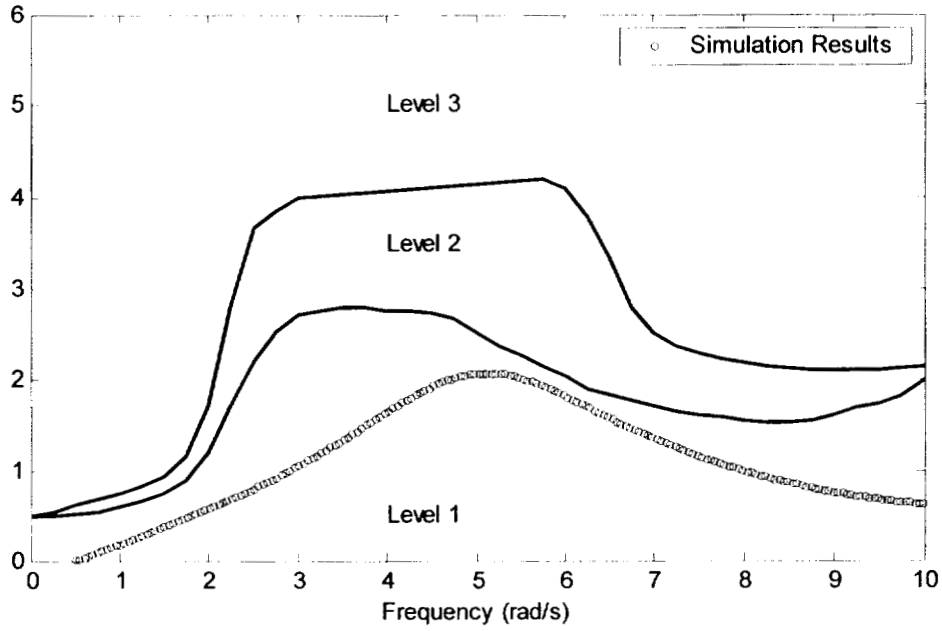

Figure 4-23: Failed Handling Qualities. FSAVro

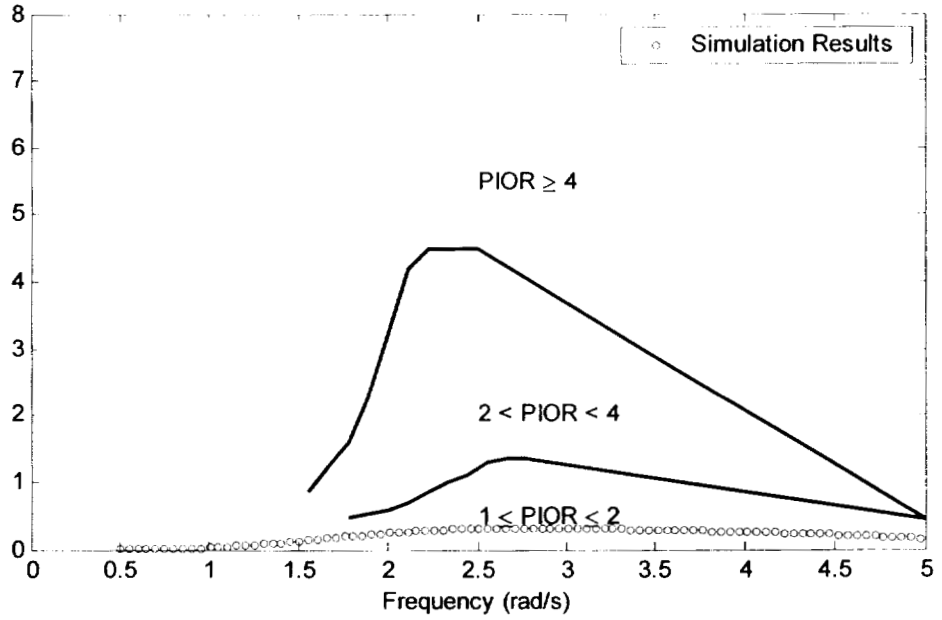

Figure 4-24: Failed PIO tendency estimation. FSAVro

It should be noted that all the failures and nominal runs shown in these plots are actually still off-design. Of the three models given in Gilbert[13] corresponding to three C.G. positions, the system was designed around the center CG position and the structural

modes were not included in the model. These plots were created using the defined failure, as well as the more unstable aft C.G. position with the structural mode included. To achieve Level 1 Handling qualities this far from the design parameters demonstrates the remarkable robustness of this system.

4.6 Application Example: First Order Model

Following a very similar design strategy as in §4.5, a new control structure where first order actuator dynamics are included in the design, will be created. The steps which are similar will not be shown.. This model will be referred to as the 'First Order Model' or FSAVfo. The name derives from the first order actuator dynamics which are included in the plant definition.

The plant model defined in §4.1.1 with the center C.G. position is used. Pitch rate tracking is desired so q is the feedback variable. In this model, included in series, is a first order actuator in the q input, and again no engine model in the airspeed input. The bandwidth of the 'design' actuator will be discussed later, but is initially set to equal the bandwidth of the 'real' or 'actual,' second order actuator. As has been stated, the system has non-minimum phase and requires an additional outer feedback loop of the airspeed. The resulting system is a square system which is feedback linearizable. An outer pilot loop is formed which tracks stability axis pitch angle θ, which is found by integrating pitch rate from t=0. This will be fed through a reference model defined in §4.3. The SMC will control q and a linear gain controller will regulate the perturbation airspeed just as in the FSAVro model. A block diagram is shown in Fig. 4-25.

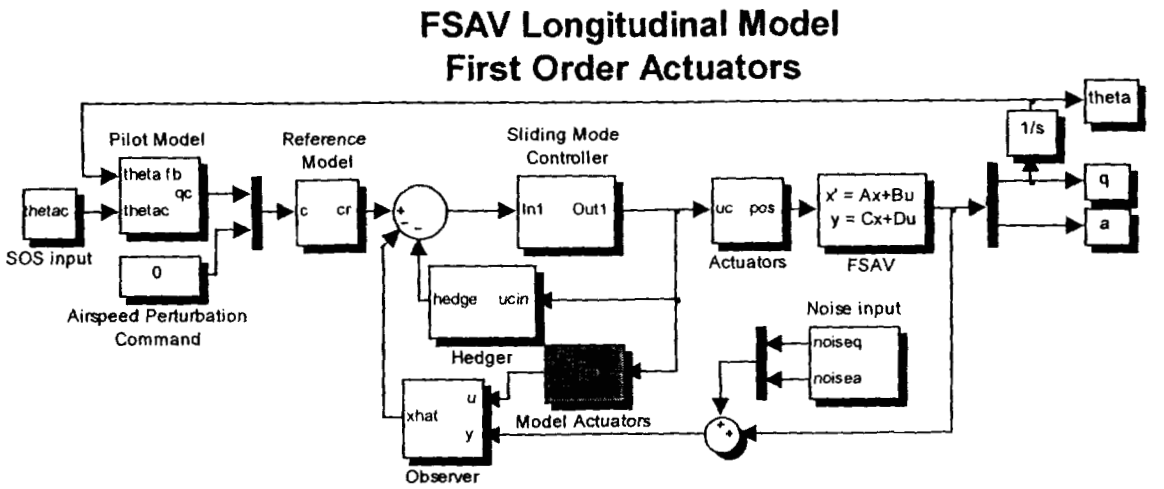

Figure 4-25: FSAV System Block Diagram

In the q (pitch rate) loop, a first order designed actuator is assumed. This increases the relative order of the system and requires the addition of a first derivative to sliding surface. In order to make the feedback the correct relative order, a model actuator is added (marked by the shaded block). Thus, the sliding manifold is defined as:

$$\sigma = K_1\dot{e}(t) + K_0 e(t) + K_{-1}\int e(t)\partial t \qquad (4.9)$$
$$e(t) = q_r - q_o - q_h$$

The corresponding Simulink® diagram of the SMC is shown in Fig. 4-26.

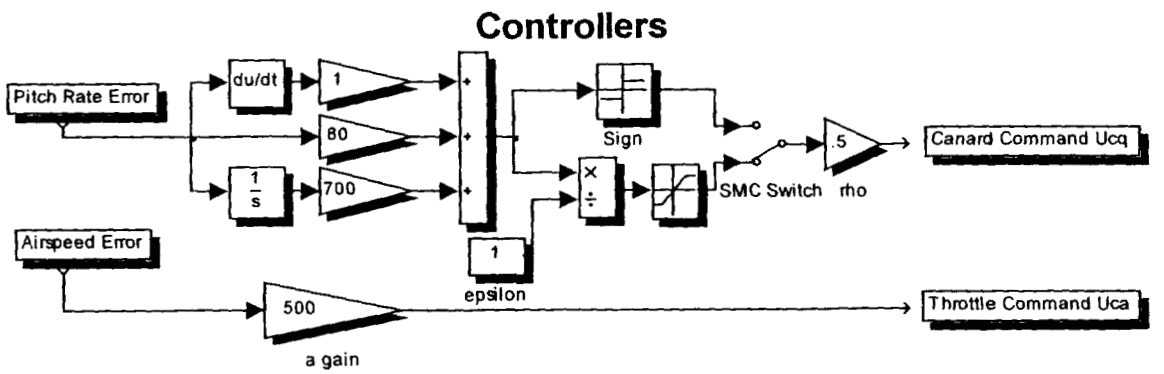

Figure 4-26: Block Diagram of SMC and Gain Controller used in FSAVfo design

This leads to a control law in the frequency domain of :

$$u_c(s) = K_\rho\left(\frac{K_1 s^2 + K_0 s + K_{-1}}{s}\right) \qquad (4.10)$$

The values selected are K_ρ=0.5, K_1=1 K_0=80, K_{-1}=700, which leads to the desired $\frac{K}{s}$ shape (-20 dB/dec) around the crossover frequency of 1000 rad/s. The compensated loop transmission is shown in Fig. 4-27

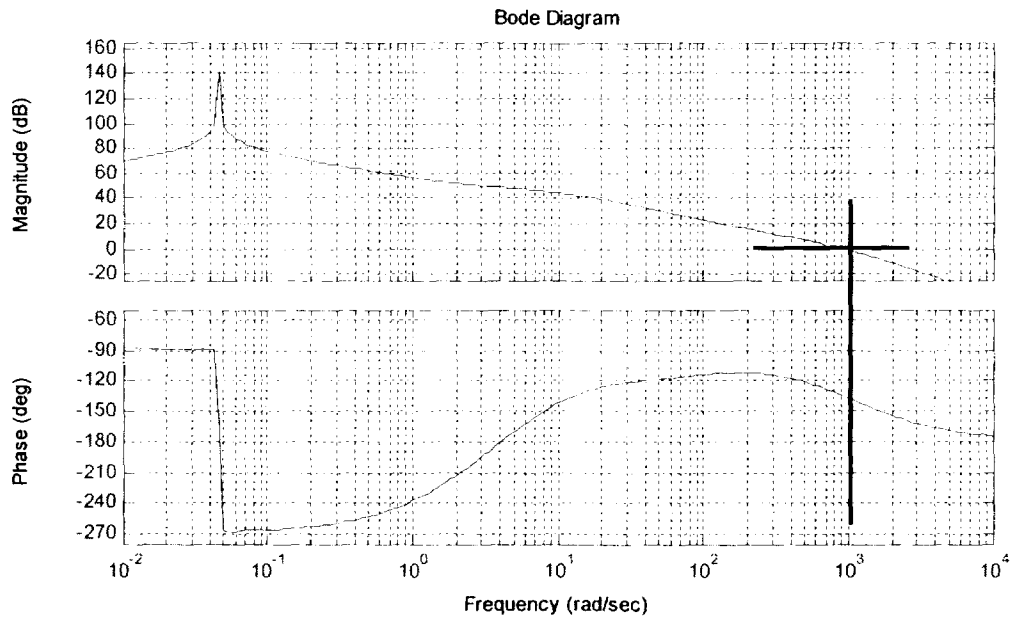

Figure 4-27: Pitch rate (q) Loop Transmission of Compensator* Design Actuator*Plant. FSAVfo

A quick glance reveals that there is additional roll-off just after crossover. This is a result of adding a fast pole at 1000 rad/s to make the compensator proper, a required step in converting to state space. The non-linear Simulink® model does not have this pole, and it was found to have little effect on the results of the state space model and the sysCL transfer function. It might be asked why the gain K_ρ was not decreased to lower the bandwidth into the -20 dB/dec region. Just as in the Reduced Order model, ρ was dictated by the position limits of the actuators. Why not increase the pole speed? Above

1000 rad/sec, the simulations using the state space model became very dependent on using prohibitively small time steps.

Like the FSAVro model, the system is still unstable due to the non minimum phase zero. The design of that loop, however, is not affected by the new sliding surface and is not shown here.

Next in our design procedure, sliding behavior is shown. Setting the switch "SMC Switch" in Fig. 4-27 to use the signum function in the upper path creates an ideal, nonlinear, SMC. Using Simulink® with the solver set to ODE2 and Δt=0.0001, ideal sliding is demonstrated by the high frequency switching seen in Fig. 4-28 and the invariance to the failure at time t=10 sec.

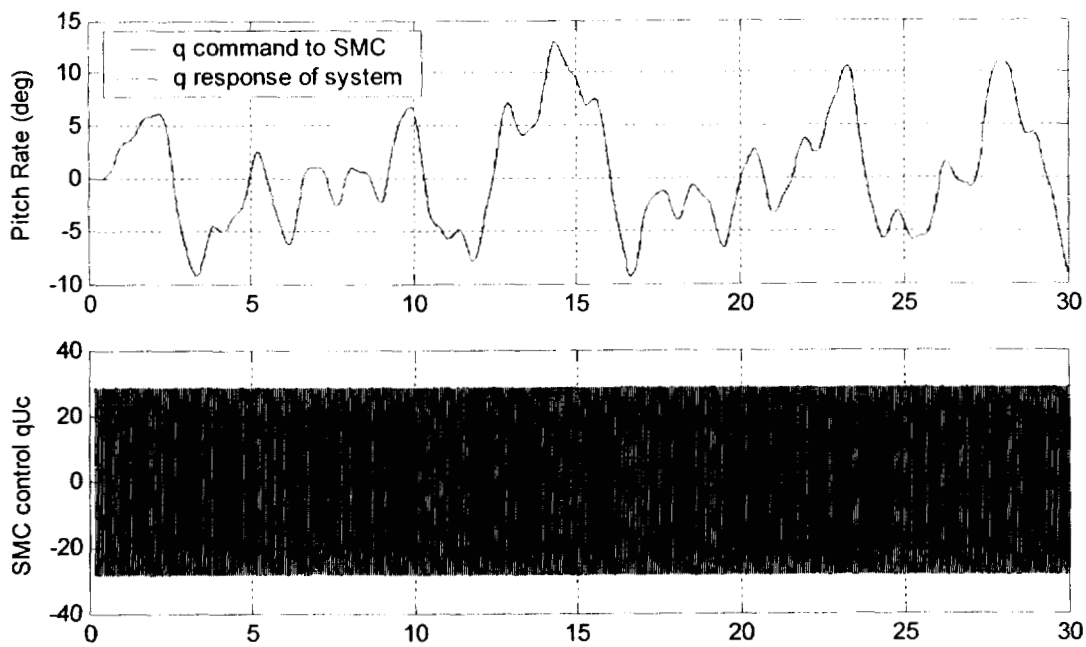

Figure 4-28: Pure SMC, Failure at 10 sec. FSAVfo

Moving to the next step, a boundary layer is added until the controller outputs a continuous control signal. Set the switch "SMC Switch" in Fig. 4-26 to use the saturation function.. Starting with a ε=0.00001, a very good approximation of the

signum function, the boundary layer is increased and finally set to unity when a continuous output is realized.

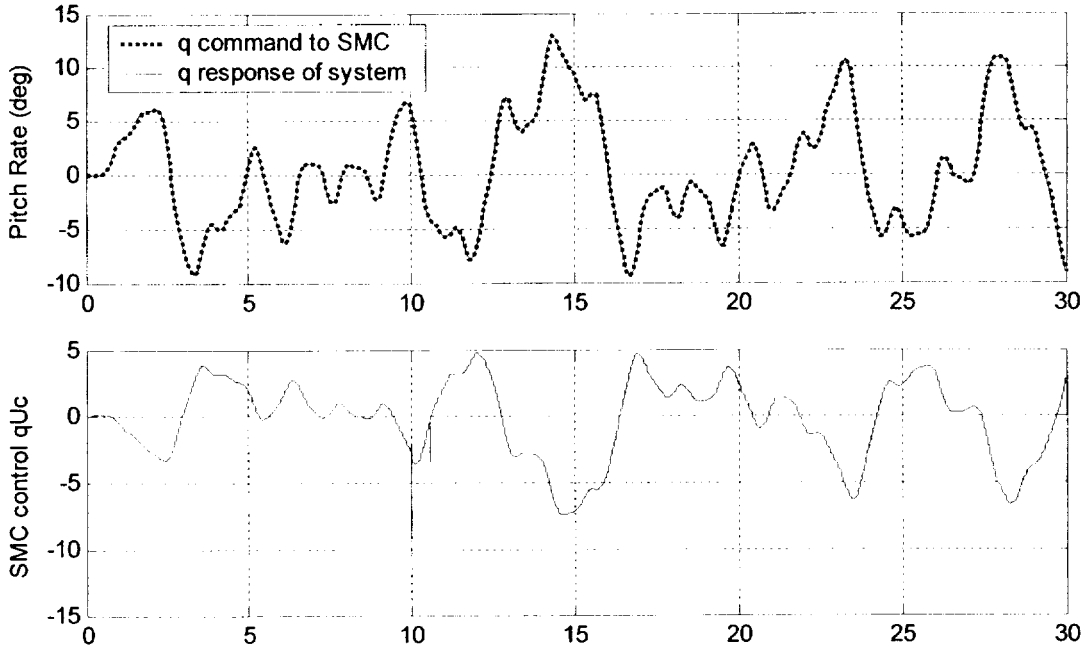

Figure 4-29: Inner loop Tracking and Control, Failure at 10 sec. FSAVfo

While very high magnification shows some tracking degradation, it is very difficult to see on almost any scale. Because ε was set to unity, no $\frac{\rho}{\varepsilon} = K_\rho$ scaling was required. The spikes in the control signal are a common feature at the moment of failure. The model fails in a single time step, and this spike is of little effect or concern.

While actuators were included in the design, they were only first order. The full actuator model, which is second order, is now added to the system, replacing the first order model. The model actuators are not changed. When the additional actuator dynamics are added, the system instantly becomes unstable. The controller cannot deal with the phase lag, and improper relative order is imposed by the additional parasitic dynamics. Now the observer and then hedge models are designed.

Like the FSAVro model, an independent observer is used for each channel. The successful decoupling is clearly indicated by the transfer function matrix shown in Table 4-4 below which represents the entire dual observer assembly.

Observer Input	Observer Output q_o	Observer output a_o
Canard Command	$\frac{61.33s(s+2.218)(s-0.0004078)}{(s+23)(s+22)(s+21)(s+20)}$	0
Throttle Command	~0 peak magnitude= -190 dB	$\frac{0.002}{(s+0.5)}$
Measured Pitch rate (q)	$\frac{82.3(s+12.69)(s^2+21.93s+203.5)}{(s+23)(s+22)(s+21)(s+20)}$	0
Measured Airspeed (a)	0	$\frac{0.5}{(s+0.5)}$

Table 4-5: Observer system transfer functions. FSAVfo λ_q=-20,-21,-22,-23 λ_a=-0.5

The design of the combined observer system allows any amount of coupling to be arbitrarily chosen by including and tailoring cross terms. This would be seen in non-zero transfer functions in Table 4-5 for the crossed terms. These investigations choose to use no coupling for simplicity and noise issues. Comparison of Table 4-5 to Table 4-4 shows the similarity of this observer to the observer used in the reduced order design. The only significant difference, besides the different roots, is the change in the transfer function from the pitch rate input to the $\hat{q}$ output. A bode plot reveals that they have almost identical frequency responses, with the FSAVro having a slightly lower bandwidth. It is also pointed out that the effect of the model actuator is not observed because those dynamics are added before the observer.

As in the FSAVro model, the full plant model was not used in the airspeed (a) observer. A reduced order plant was constructed based on the apparent system with q loop closed.

As explained in step (6) of §(4.7), the $\left(\frac{q_o}{u_c}\right)$ bode plot is analyzed and/or simulations are run at varying observer speeds. Like the FSAVro model, the research into this system realized only moderate performance in the absence of hedging. Thus, no optimization in this step is performed as it is merely used as a starting point to select the final, hedged, observer speed. An observer speed is selected which is slower but near, say 10% below, the highest observer speed which is stable. In this model that was selected at $\lambda_q = -14,-15,-16,-17$, Pq1=14.

Since increased robustness can be realized with increased observer speed, pseudo-arbitrarily increase Pq1 by 25% leading to an unstable system. The negative interaction with the SMC can be minimized by inclusion of hedging into the model. The hedge system is then designed using the methods shown in §2.5.4.2. For this system, that results in an observer speed of $\lambda = -20,-21,-22,-23$ and a hedge model of $y_h = 9000\left(\frac{80s}{s+80}\right)\left(\frac{1}{(s+40)(s+45)(s+45)}\right)$. The resulting bode diagram is shown in Fig. 4-30

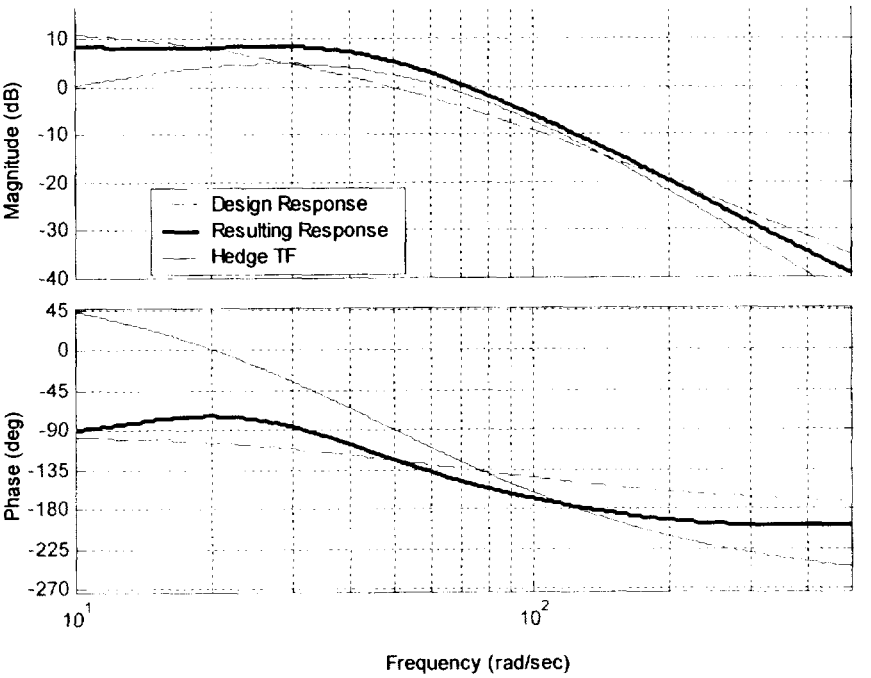

Figure 4-30: Bode plot of hedged observed feedback. FSAVfo

In this model it was desirable to use significantly more hedging than in the FSAVro model. The phase response of this hedge system is not ideal, but as stated before, while the basic hedge shape is well defined, the exact shape is a bit of trial and error. Ideally the phase would stay closer to the designed model, and in many cases the hedge shape introduces lag at low frequencies in exchange for lead at high frequencies. However, this hedger provides leads at low frequency and lag at high frequency. While this seems to be undesirable, it is important to realize that the phase lag experienced by the system is not the designed phase lag. The actual system without hedging would have considerably more phase lag than found here. Thus, this hedger is doing a good job of removing phase lag and magnitude effects of the actuators and observer.

Figures 4-31 through 4-23 show the tracking performance, inner loop tracking, actuator tracking and commands as well as handling qualities and PIO tendency for both the nominal and failed case.

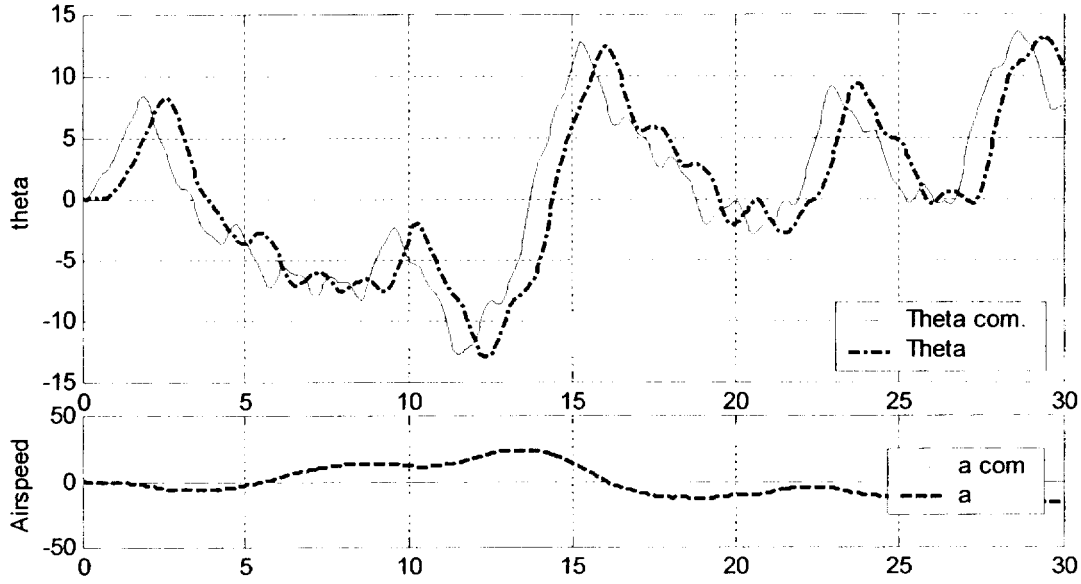

Figure 4-31: Plot of Tracking, Failure at 10 sec. Pilot/ Noise/ Observer/ Hedge/ Actuators all on. FSAVfo

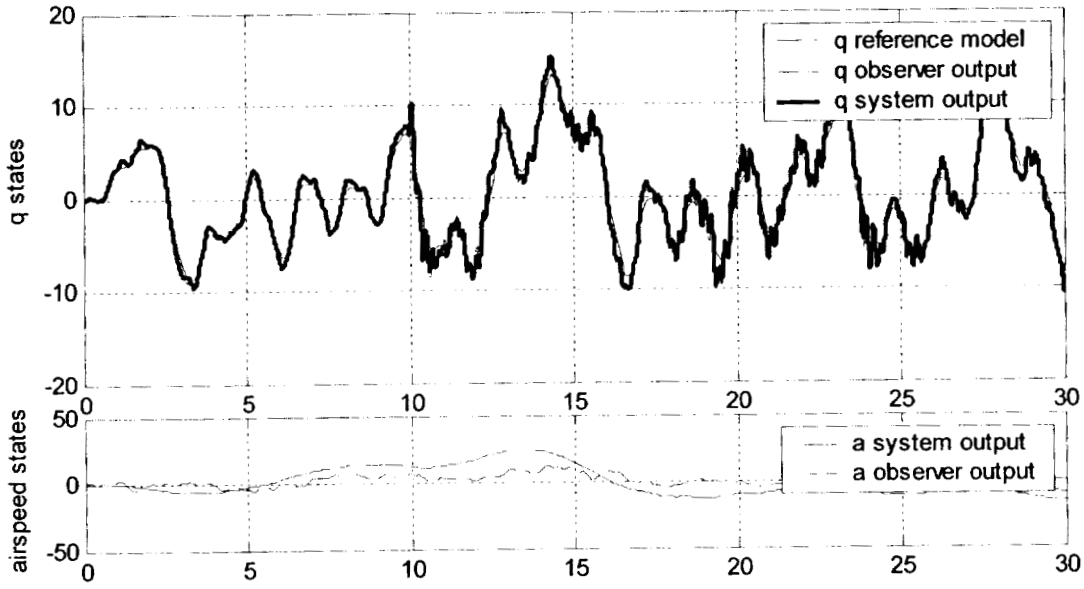

Figure 4-32: Plot of pitch rate and airspeed states. Failure at 10 sec. FSAVfo

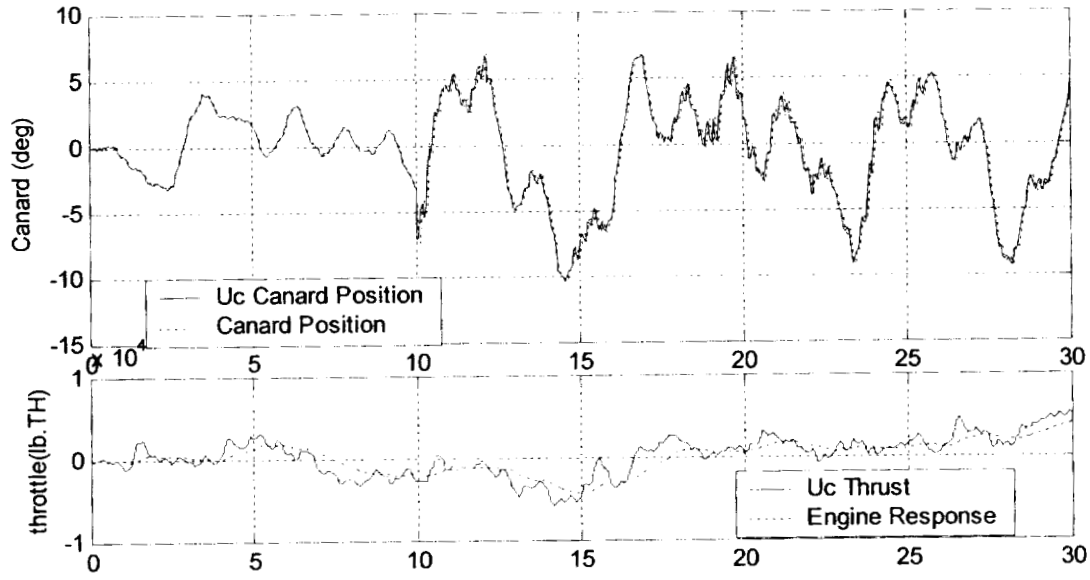

Figure 4-33: Plot of actuator command and response: Failure at 10 sec. FSAVfo

the SMC can track.

Figure 4-34 shows how well the SMC is tracking its input. The signal SMC is being passed is the difference between the hedged reference model and the output of the

observer, q_o. Since proximity of these plots to zero shows that the SMC is doing a very good job of matching its input. Any path or tracking error is elsewhere in the system. However, it would be incorrect to assume that other errors could be optimized at will. Much of the purpose of hedging and observers it to purposely degrade or modify the signal to a type which

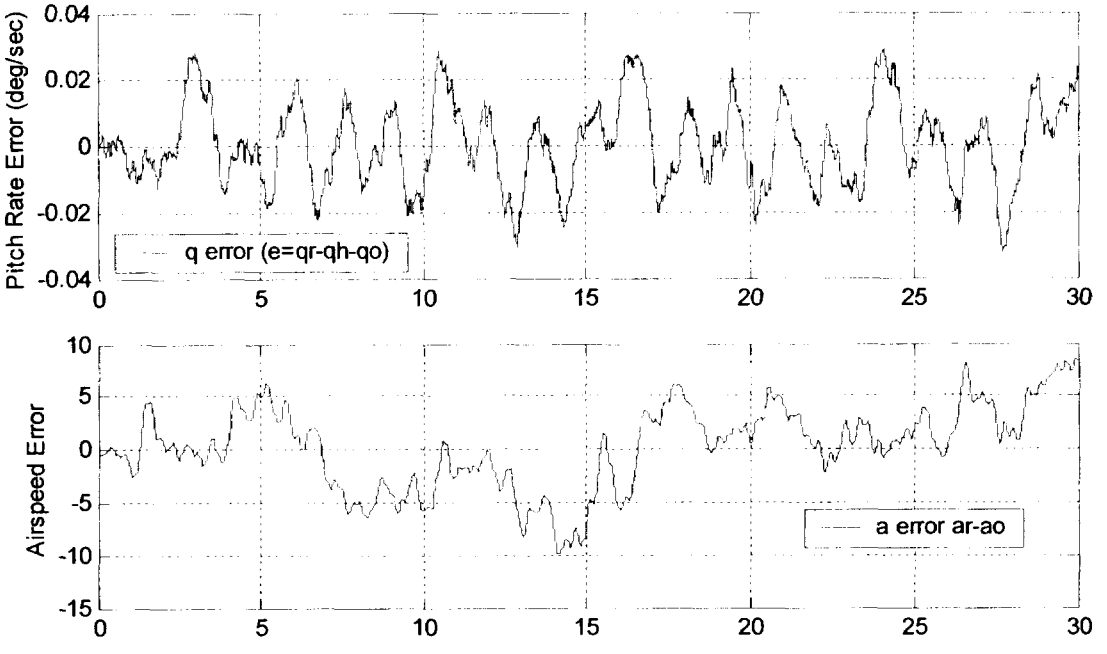

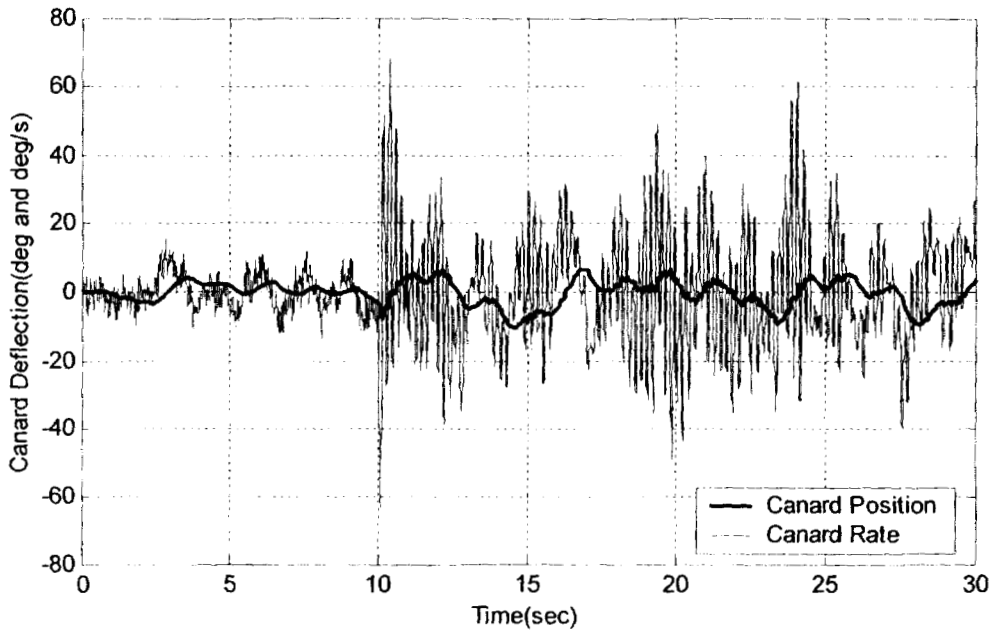

Figure 4-35: Plot of Canard actuator position and rate. Failure at 10 sec. FSAVro.

Figure 4-35 shows the increased actuator activity when compared to Fig. 4-18. While the commanded rates are similar but slightly higher than those for the FSAVro model, this model has a much higher switching frequency. Like the FSAVro model, this model shows very similar sensitivity to any position or rate limiting. The 15 ms delay shows its ability to tolerate larger delay when compared to the FSAVro model (10 ms).

It would be fair to compare the results above to a loop shape model where there was a first order design actuator. However, this actuator is outside the open loop bandwidth and the gain and phase margins do not require that it be dealt with. Thus, the resulting design is identical to the one described previously which was unable to stabilize the system.

Piloted flight is the focus of this investigation and, as before, the task dependent handling quality plots of the SMC system, in both the nominal and failed case are shown in Fig. 4-36 through Fig. 4-39.

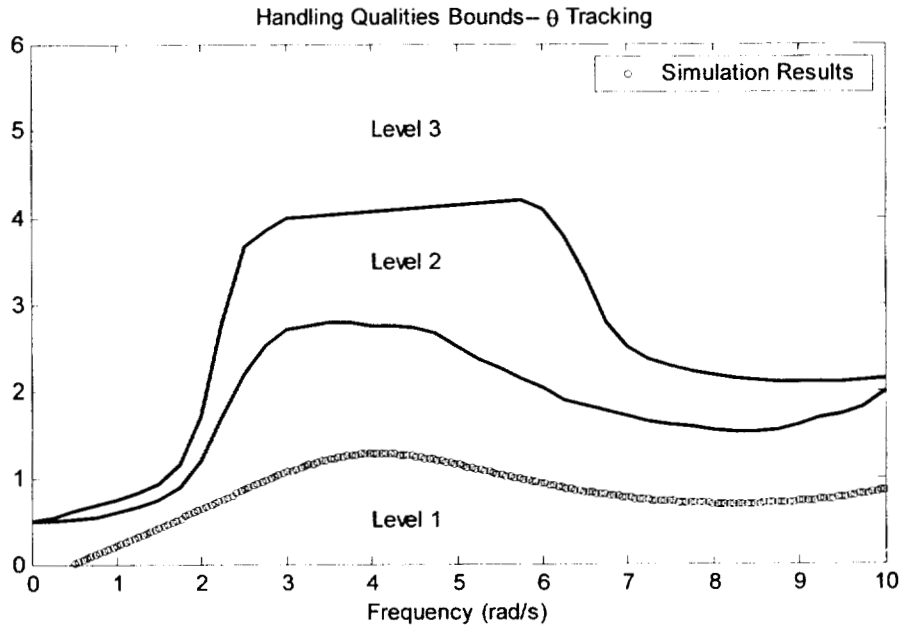

Figure 4-36: Nominal Task Dependent Handling Quality. FSAVfo

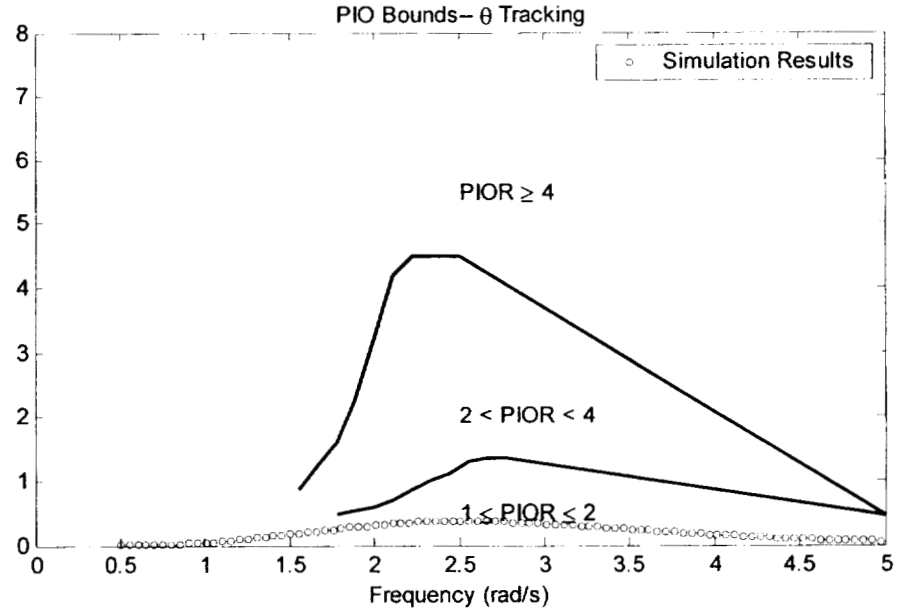

Figure 4-37: Nominal PIO Tendency. FSAVfo

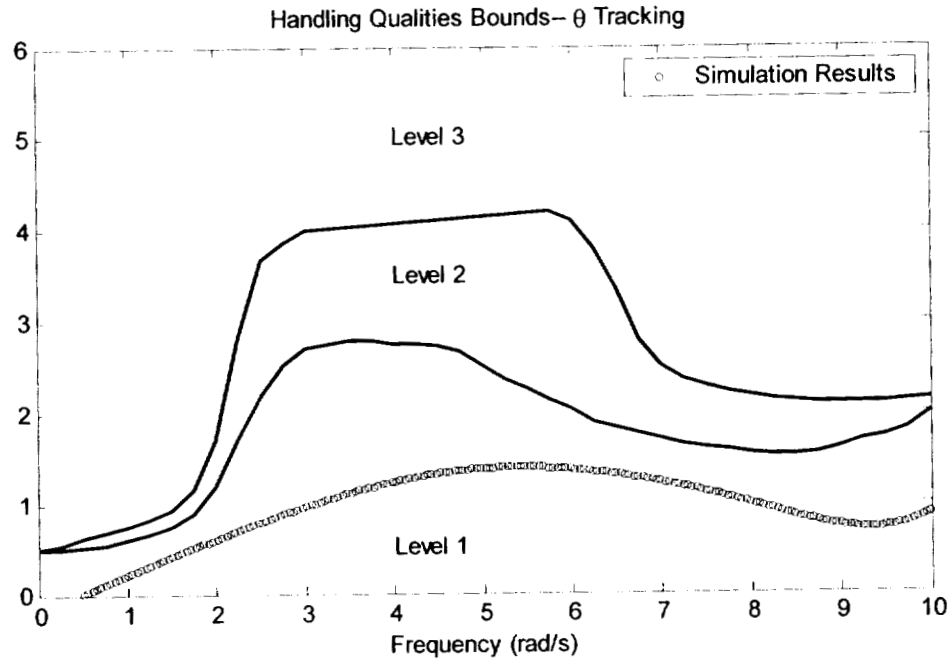

Figure 4-38: Failed Handling Qualities. FSAVfo

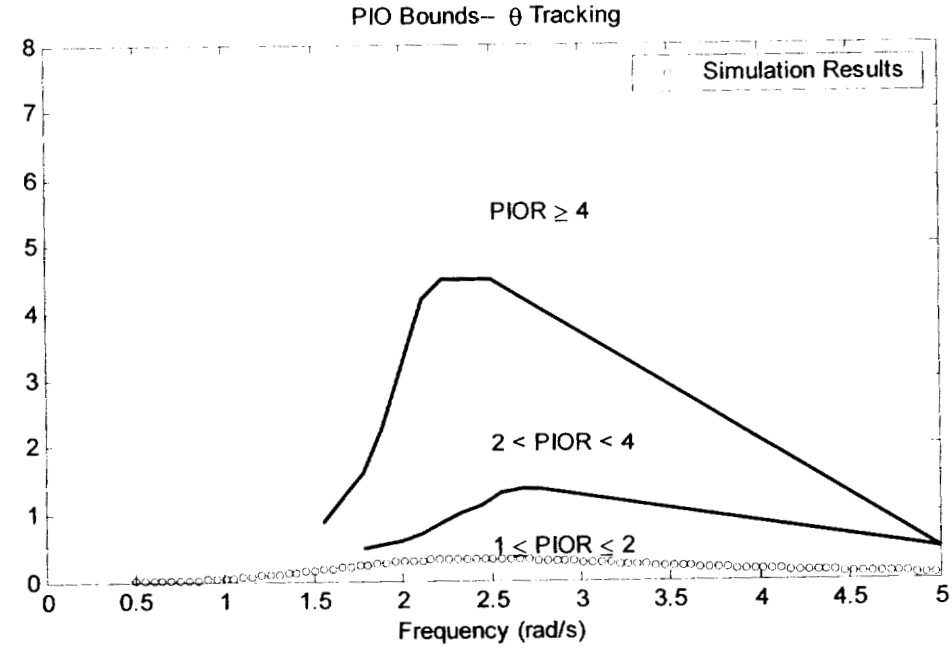

Figure 4-39: Failed PIO Tendency Estimation. FSAVfo

4.7 Application Example: First Order Model with Flaperons

The last design example uses the solution to the FSAVfo model and adapts it to use an additional control surface. It as been shown that the inclusion of multiple actuators can have significant benefits in terms of system robustness to actuator failure.[28] To test whether the flaperons were capable of pitch rate control, a model was constructed which uses only the flaperons. Recalling §4.7 and the controllability issues surrounding the flaperons, the addition of flaperons stresses the ability of SMC to deal with unmodeled dynamics in the plant. The high aeroelastic effects of forward swept wings are amplified when the flaperons are used. In fact, in this flight condition, with a trim air speed of 1000 ft/sec, Gilbert states that the only effective use of the flaperons is wing bending mode control, and that the flaperons only become effective pitch rate control devices above 1500 ft/sec.[13] So this model is attempting to augment the primary control device, the canards, with the slower and less effective flaperons. In addition these flaperons also excite large aeroelastic wing dynamics which are uncontrolled.

Following a very similar design strategy as in §4.5 and §4.6, a similar control structure was created. Initial investigations showed that the addition of flaperons had a dramatic improvement on the reduced order model. However, in §4.6 it was shown that there are benefits to including some actuator dynamics in the design, so to investigate the corners of the design envelope, it was decided to see what additional benefits could be obtained by adding flaperons to the first order model.

Only unique design steps will be shown. This model will be referred to as the 'First Order Model with Flaperons' or FSAVfof.

The plant model is defined in §4.1.1 and the center C.G. position is used during design. All topology is identical to the FSAVfo with the exception that a control distribution matrix is included to split the signal to the flaperons and canard actuators and model actuators. A block diagram is shown in Fig. 4-40.

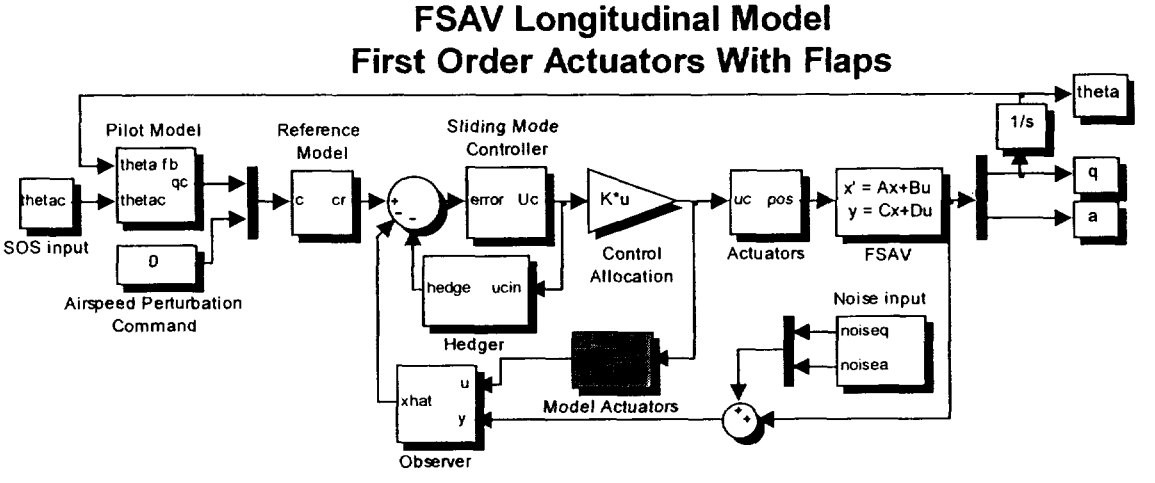

Figure 4-40: FSAV System Block Diagram

In designing the sliding surface, it is found that the same model used in the FSAVfo is appropriate and will not be shown again, see §4.6

The boundary layer is added, and the full second order actuators are added as in the previous example. The system is now unstable. The observer and then hedge models are now designed.

Independent observers for pitch rate and airspeed are constructed. The successful decoupling is evidenced by the transfer function matrix shown in Table 4-6 below which represents the entire dual observer assembly. Note that the architecture here is the same as those previously used, except that the q channel has two command inputs, canard and flaperons.

Observer Input	Observer Output q_o	Observer output a_o
Canard Command	$\frac{61.33s(s+2.218)(s-0.0004078)}{(s+33)(s+32)(s+31)(s+30)}$	0
Throttle Command	~0 peak magnitude= -200 dB	$\frac{0.002}{(s+8)}$
Flaperon Command	$\frac{-19.44s(s+4.774)(s-0.0001313)}{(s+33)(s+32)(s+31)(s+30)}$	0
Measured Pitch rate (q)	$\frac{122.3(s+17.03)(s^2+32.27s+471.5)}{(s+33)(s+32)(s+31)(s+30)}$	0
Measured Airspeed (a)	0	$\frac{8.0004}{(s+8)}$

Table 4-6: Observer system transfer functions. FSAVfof λ_q=-30,-31,-32,-33 λ_a=-8

The negative sign on the flaperons to q_o transfer function seems troublesome at first, except that a trailing edge down deflection of the canard leads to a nose up moment, while a trailing edge down on the flap leads to a nose down moment. In this design, as in the previous one, no cross-coupling was desired. Also, the plant approximation was used as the airspeed observer plant, not a full model just as before. The Pa1 value was increased to -8 rad/sec which does improve the airspeed tracking performance but has almost zero effect on q tracking.

For this system the observer speeds of $\lambda = -30,-31,-32,-33$ were selected. The hedge model is extremely sensitive in this model because, while the shape of the unhedged signal is similar to the previous models, there are more dynamics involved from the second actuator and the model actuators. The additional dynamics from the model actuators are exactly in the area which the hedge system modifies. This often leads to unpredictable shapes at certain hedge pole/zero locations. These interactions can lead to unanticipated results in the hedge performance. However, patience and testing can produce results which are highly desirable. In addition to using the hedge

shaping techniques outlined in §2.5.4.2, the FSAVfo hedge model was used as a starting point. A hedge model of $y_h = 6500\left(\frac{80s}{s+80}\right)\left(\frac{1}{(s+20)(s+45)(s+45)}\right)$ was finally selected. The resulting bode diagram is shown in Fig. 4-41.

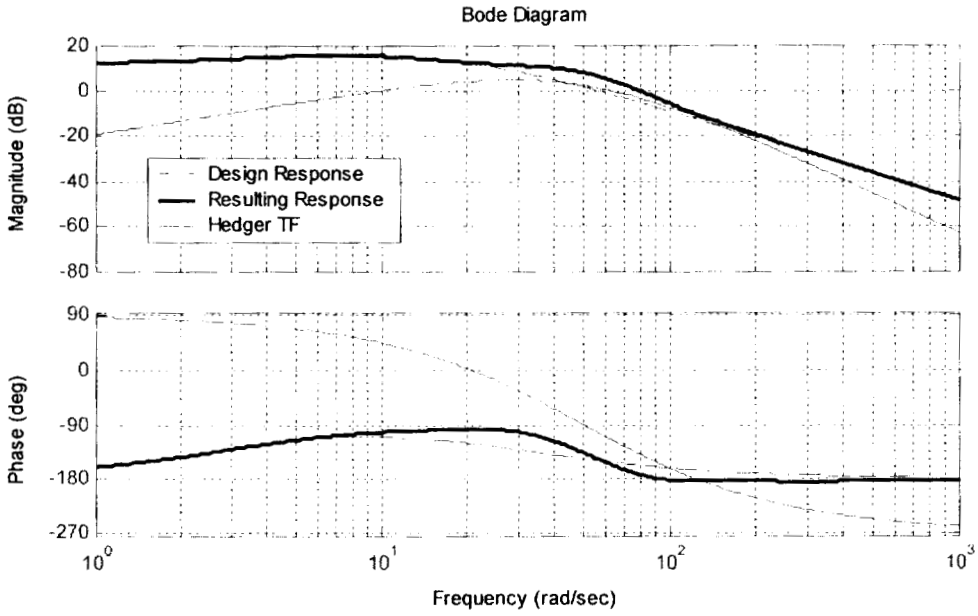

Figure 4-41: Bode plot of hedged observed feedback. FSAVfof

Figures 4-42 through 4-53 show the tracking performance, inner loop tracking, actuator tracking and commands as well as handling qualities and PIO tendency for both the nominal and failed case.

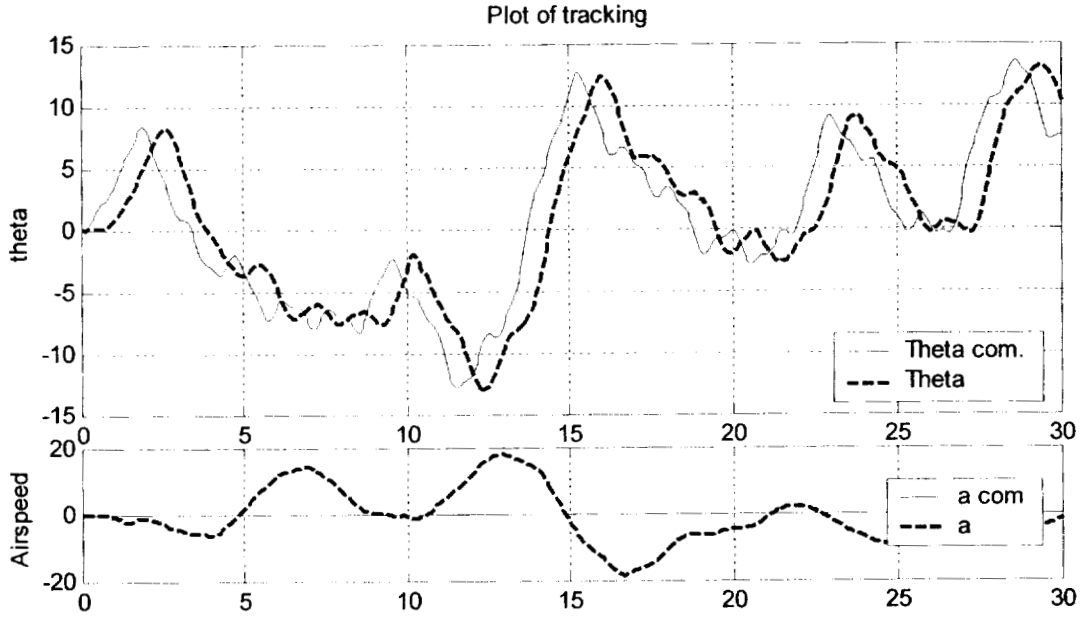

Figure 4-42: Plot of Tracking, Failure at 10 sec. Pilot/ Noise/ Observer/ Hedge/ Actuators all on. FSAVfof

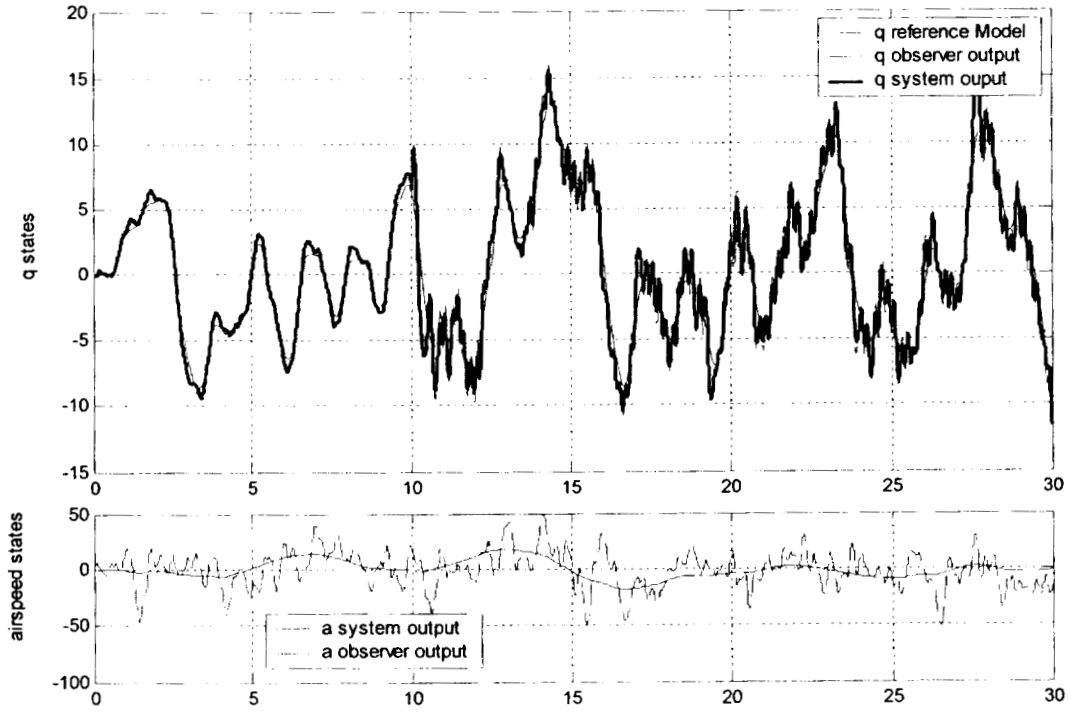

Figure 4-43: Plot of pitch rate and airspeed states. Failure at 10 sec. FSAVfof

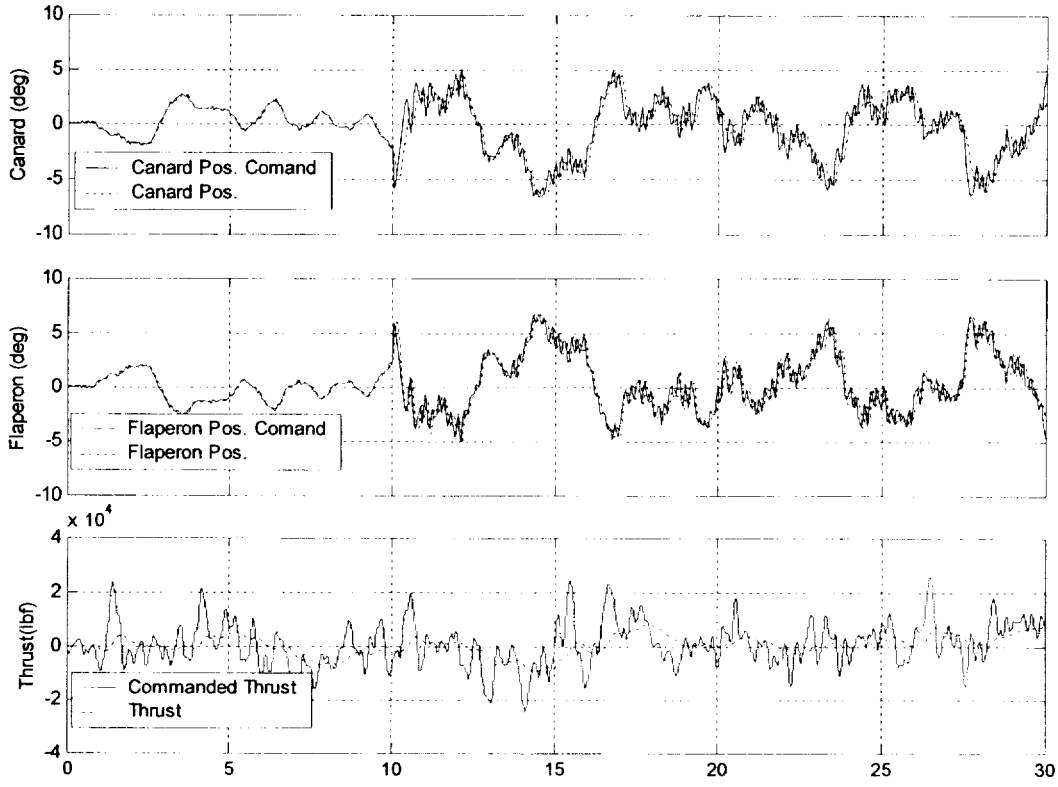

Figure 4-44: Plot of actuator command and response: Failure at 10 sec. FSAVfof

Figure 4-45 shows how well the SMC is tracking its input. The signal SMC being passed is the difference between the reference model and the output of the observer, q_o. Since these plots are so close to zero, the SMC is doing a very good job of matching its input.

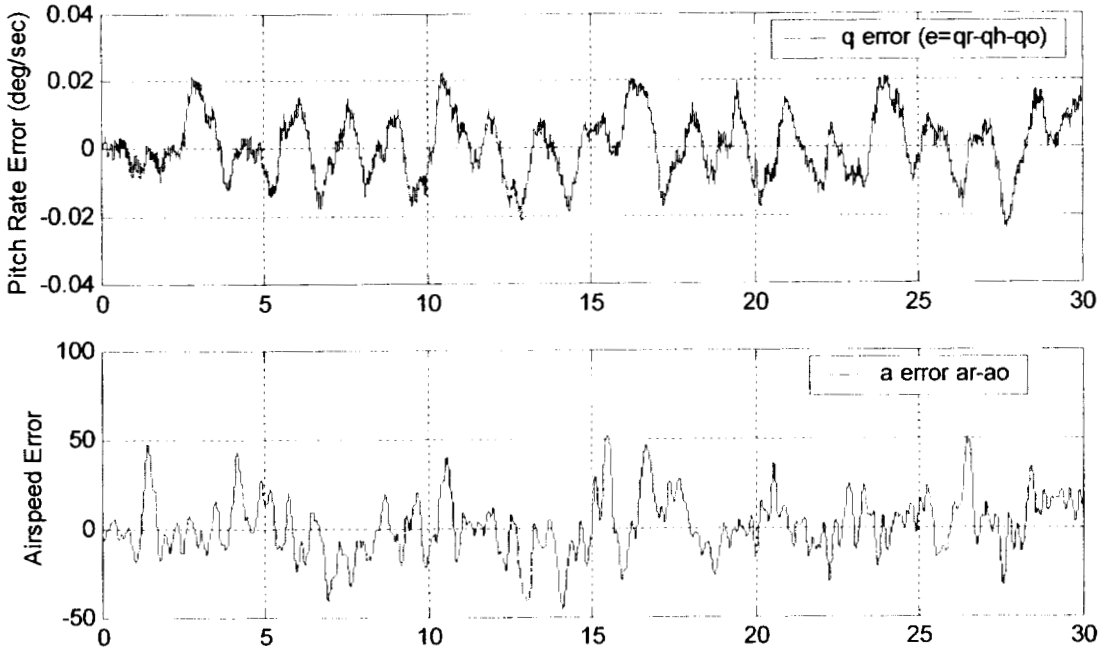

Figure 4-45: Plot of how well the SMC controller is tracking its input. FSAVro

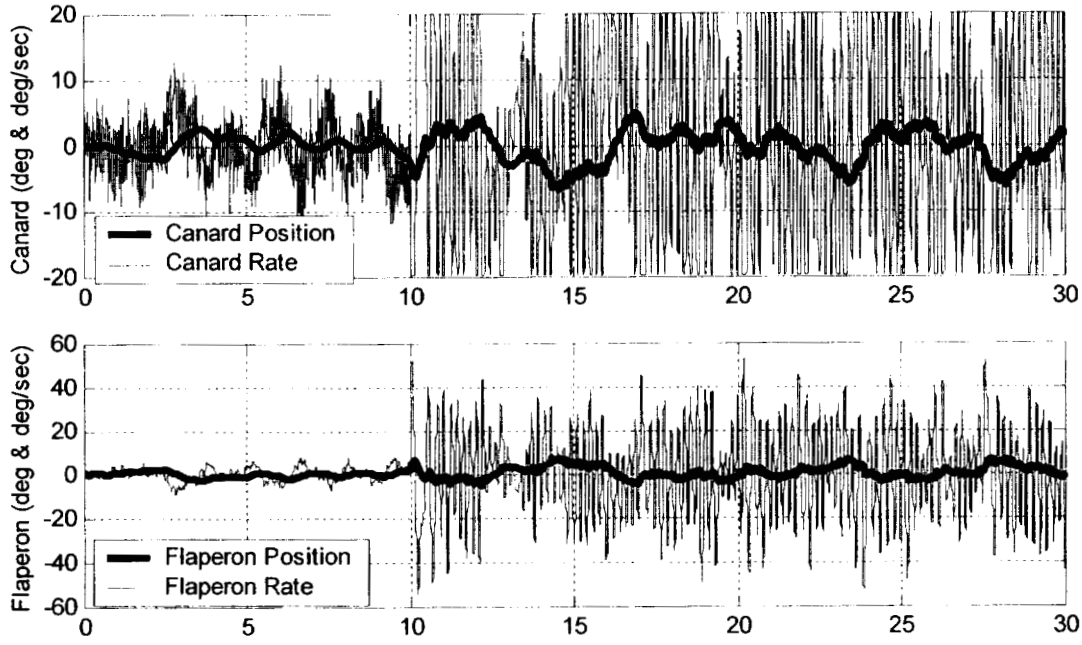

Figure 4-46: Plot of actuator positions and rates. Failure at 10 sec. FSAVfof.

Figure 4-46 shows that the increased actuator activity found in the FSAVfo model are still present when flaperons are included. This is entirely expected. It also shows this model is more robust to failures than the previous models. The time delay of 20 ms

is quite large relative to the bandwidth and divergent speed of this system. This model is able to tolerate larger delays compared to the FSAVro and FSAVfo models (10 and 15 ms respectively).

We can again compare the results above to a loop shape model where the flaperons are included. The compensator designed for the loop shape model is $uc = \frac{4(s+35)(s+10)(s+10)(s+0.1)}{s^2(s+2.2)(s+500)} * StateError$. The resulting bode diagram is shown Fig. 4-47.

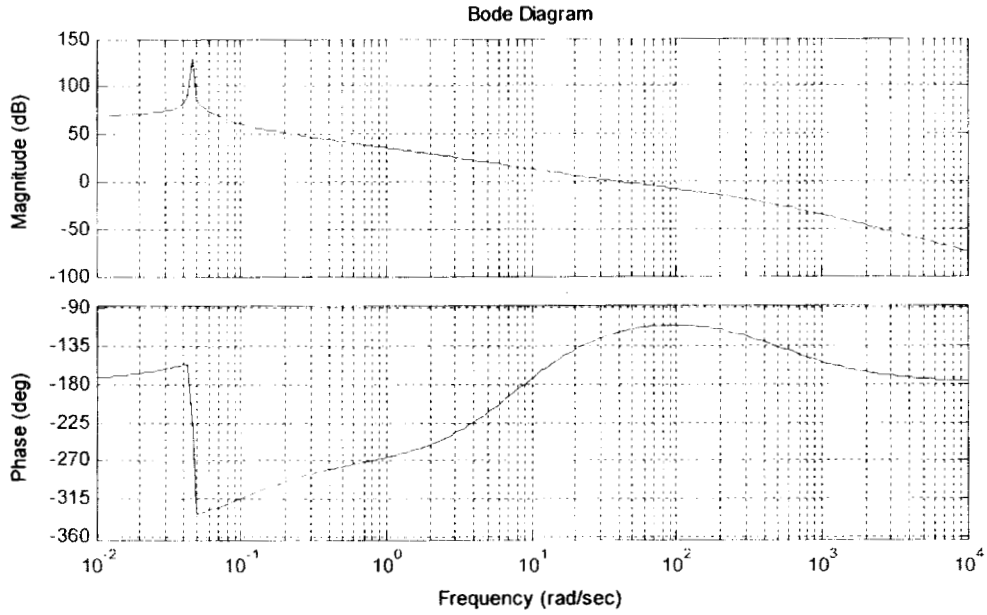

Figure 4-47: Compensated open loop pitch rate bode diagram. FSAVfofloop

The resulting tracking performance is shown in Fig. 4-48, but again, do you really have to look? The actuator inputs and responses are shown below in Fig. 4-49.

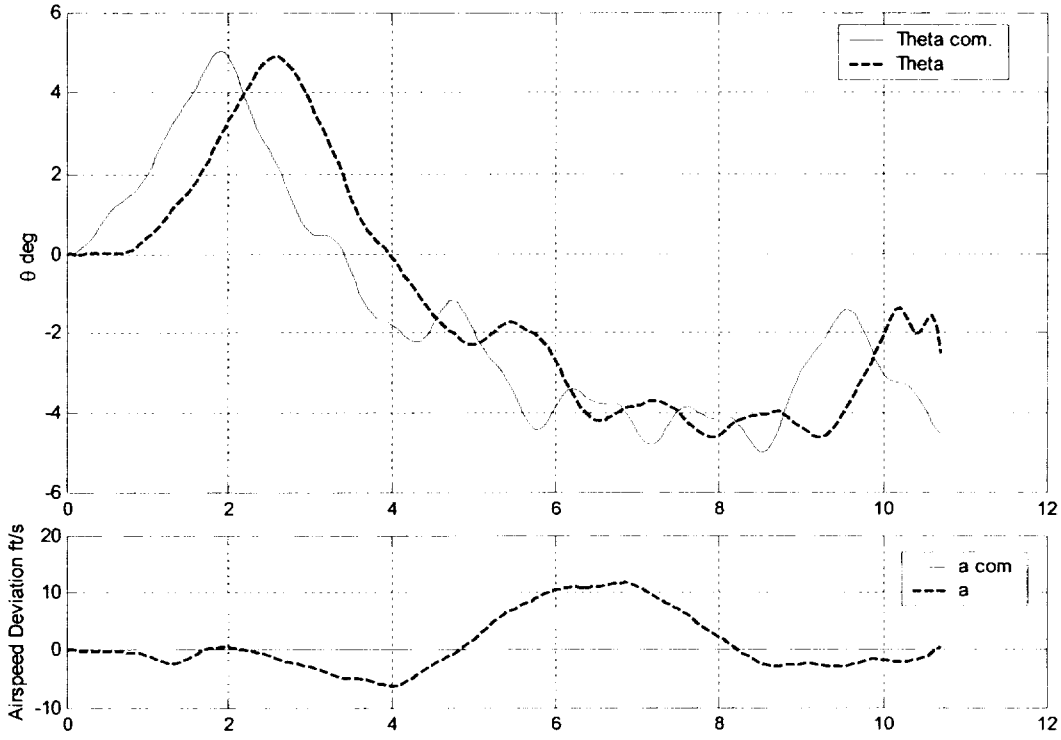

Figure 4-48: Theta Tracking. Failure at 10 sec. FSAVfof_Loop shape.

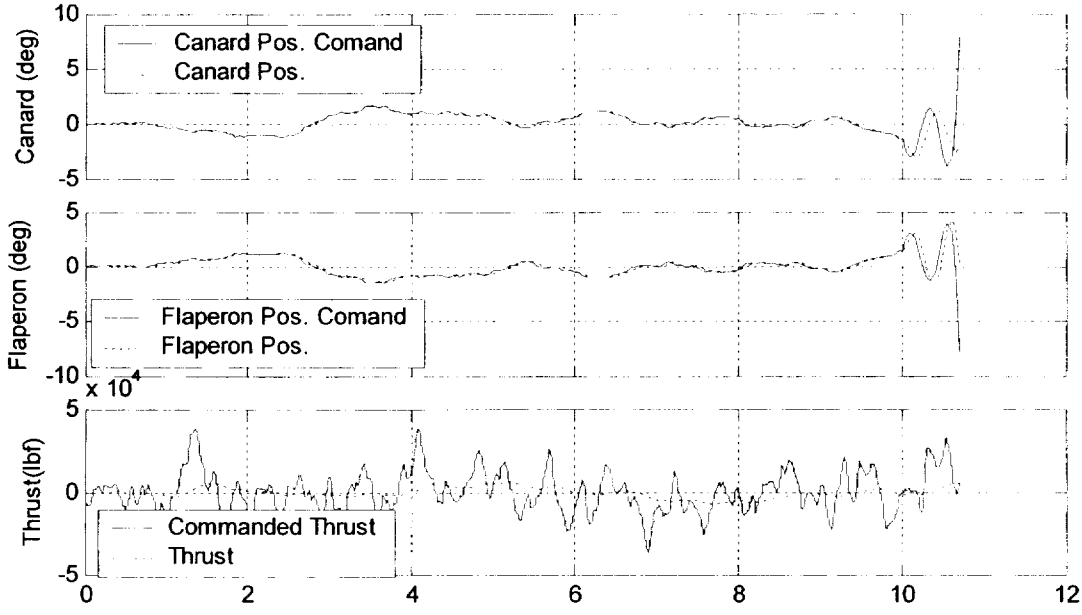

Figure 4-49: Plot of actuator command and response. FSAVfofloop

You knew that would happen, didn't you?

Again, the handling qualities and PIO tendency will be assessed for the nominal and failed models. These are shown in Fig. 4-50 through Fig. 4-53.

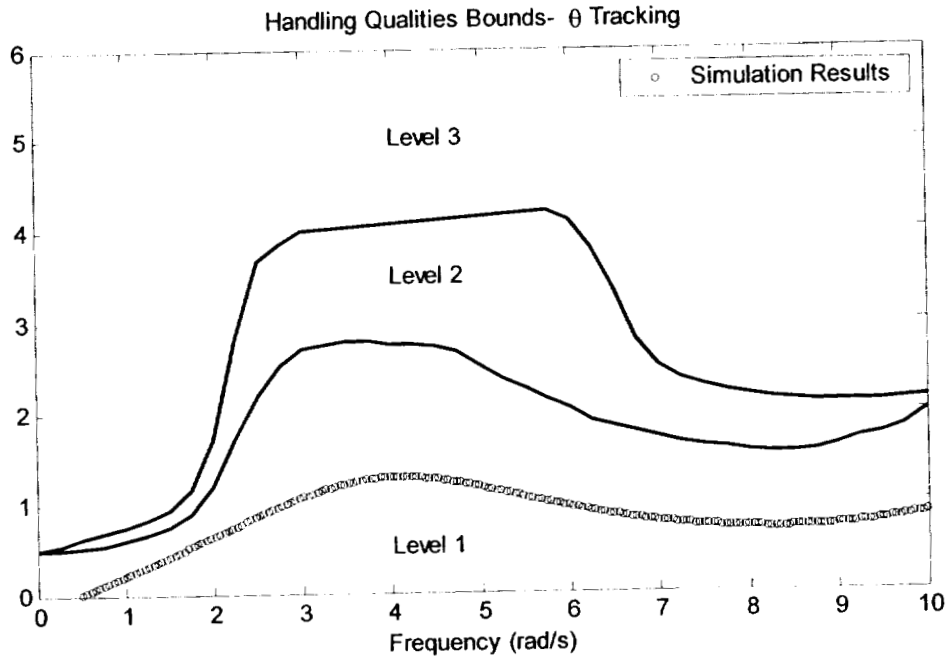

Figure 4-50: Nominal Task Dependent Handling Quality. FSAVfof

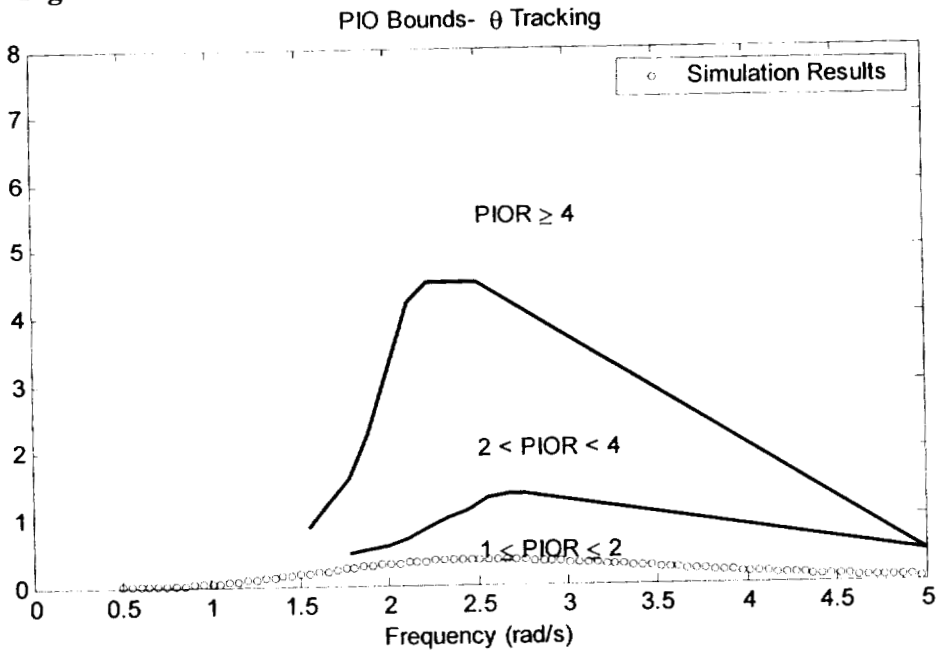

Figure 4-51: Nominal PIO Tendency. FSAVfof

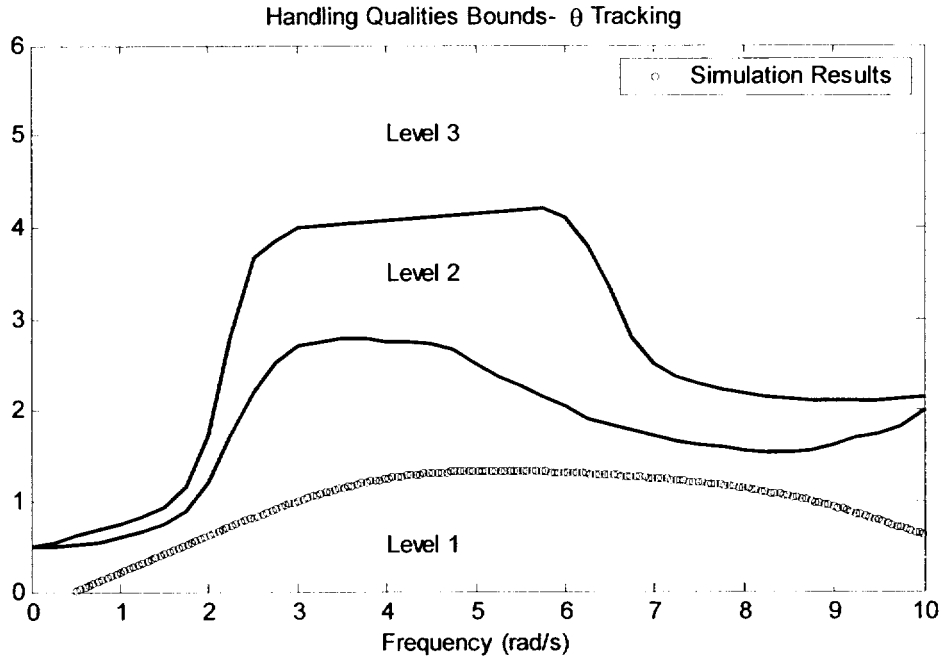

Figure 4-52: Failed Handling Qualities. FSAVfof

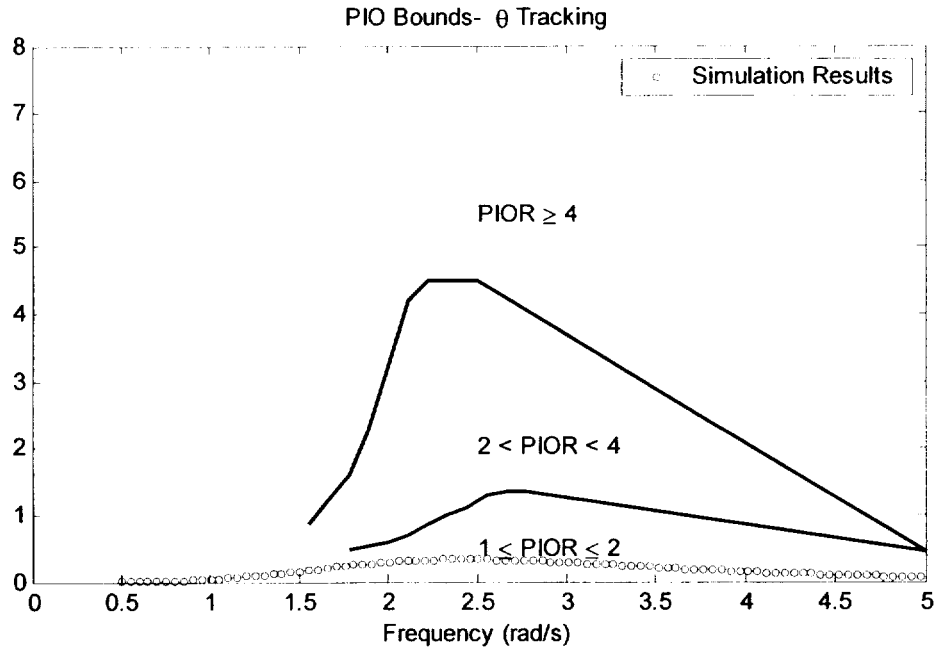

Figure 4-53: Failed PIO Tendency Estimation. FSAVfof

Chapter 5

Discussion

5.1 Effective Adapted Linear Controller

SMC presents a bit of a conundrum; It is considered an adaptive control law, and yet the gains and structure of the control don't change! In fact, it is found that if the 'effective' controller is calculated in the failed and nominal conditions, it can be seen that it does 'adapt' to system parameter variation. For this analysis the sysCL state space will be used as defined in §3.2. Using this formulation the effective compensator, can be back calculated assuming unity feedback. From the entire system the pitch rate transfer function is obtained, the open loop transfer function is calculated assuming unity feedback. Then, the effective compensator is obtained by dividing by the plant and actuator dynamics. This is summarized in Eq. (5.1).

$$GCLq = sysCL(1\{qout\},1\{qcommand\})$$

$$Lq = \frac{GCLq}{1 - GCLq} \qquad (5.1)$$

$$Gc_{eq} = \frac{Lq}{PlantTF * ActuatorTF}$$

Looking at how the resulting transfer function Gc_{eq} changes between the failed and nominal cases is a good indication of the effective adaptation of the control architecture. The first step is to look at the FSAVro model when only the actuators have failed. The resulting nominal and failed *PlantTF*ActuatorTF* are shown in Fig. 5-1.

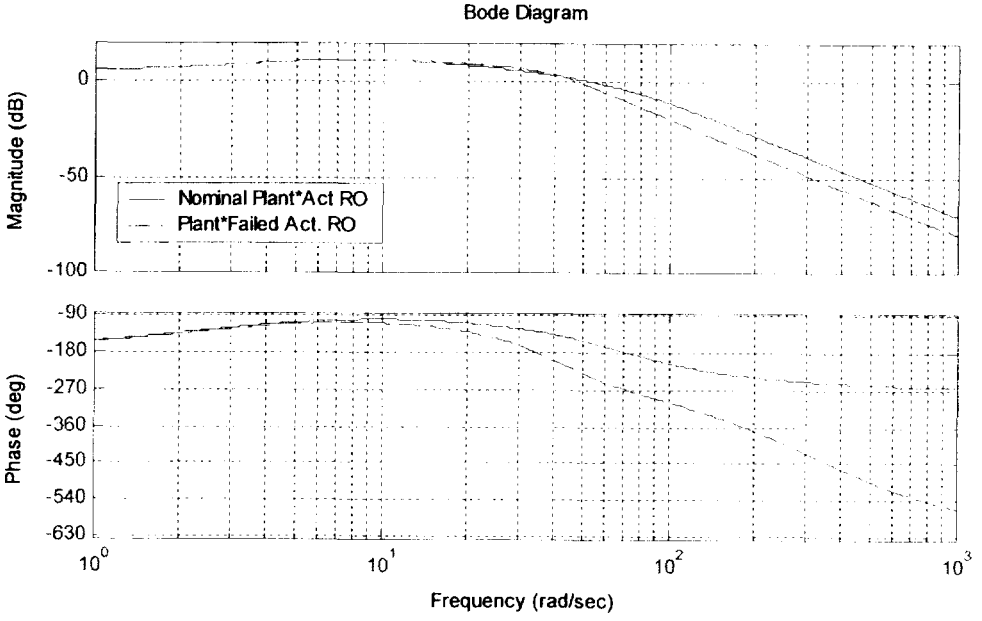

Figure 5-1: Bode Plot of Nominal and Failed Actuator FSAVro Plant*Actuator.

It is easy to see the magnitude roll-off occurring earlier but the more drastic effect is found in the phase roll off. This is expected in an actuator failure.

(end of page)

Gc_{eq} are shown in Fig. 5-2 below. Notice how the controller modifies the shape of the magnitude plot to drive the actuators very hard near their decreased bandwidth of 40 rad/sec, and most importantly, adds large amounts of phase lead.

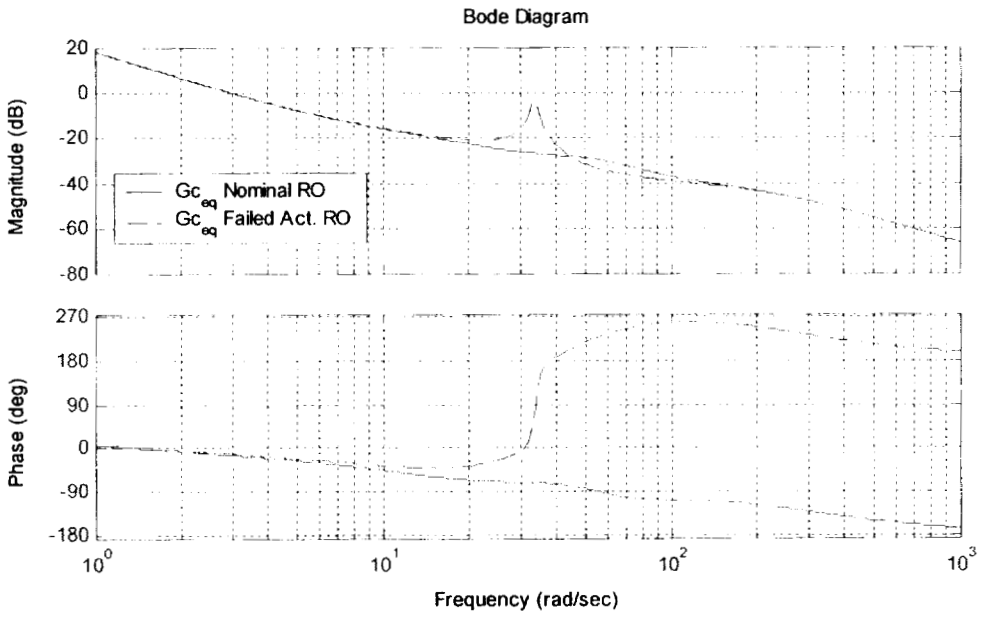

Figure 5-2: Gc_{eq} Nominal and Failed Actuator Showing Control Adaptation. FSAVro.

(end of page)

The other type of failure that was investigated was plant parameter variation. The failure method consisted of multiplying 'A' by 1.2 (except for kinematic terms) and 'B' by 0.75 and this shows up primarily as a change in gain in the bode diagram. This is confirmed in Fig. 5-3 comparing the nominal case to the failed plant case. There is a small phase effect and bandwidth, but the main change is an increase in gain of ~5db.

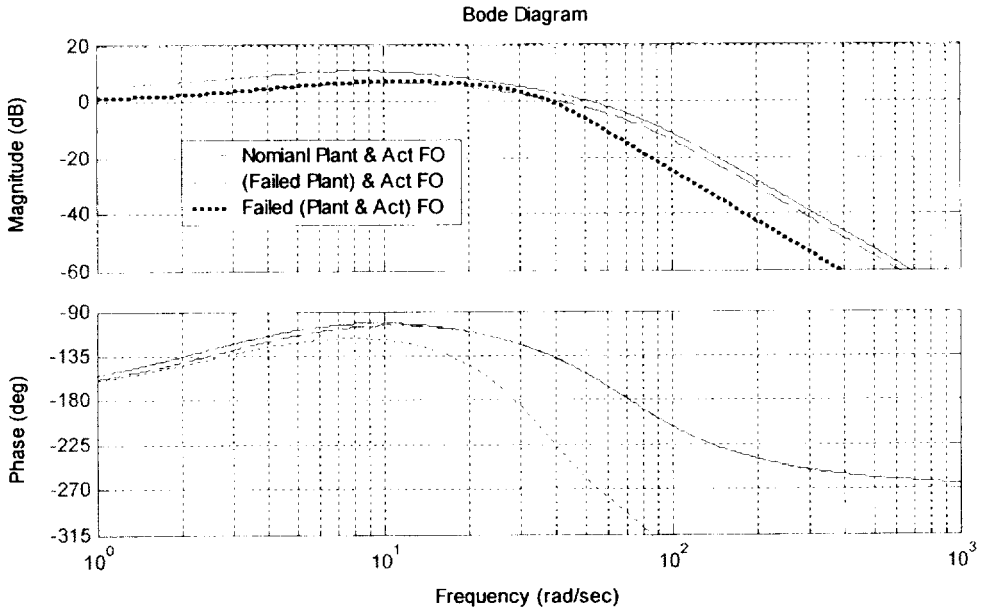

Figure 5-3: Bode Plot of Nominal and Failed Plant FSAVfo, Plant*Actuator.

The resulting effective controller after failure is shown in Fig. 5-4. Note the increased gain of Gc_{eq} (failed plant) plot of almost exactly the gain lost for that failure in Fig. 5-3. There is a bit of additional phase lag in the controller when the plant is failed, but it is very difficult to determine the effect this has on the model, whether it is good adaptation or just a result of gain adaptation.

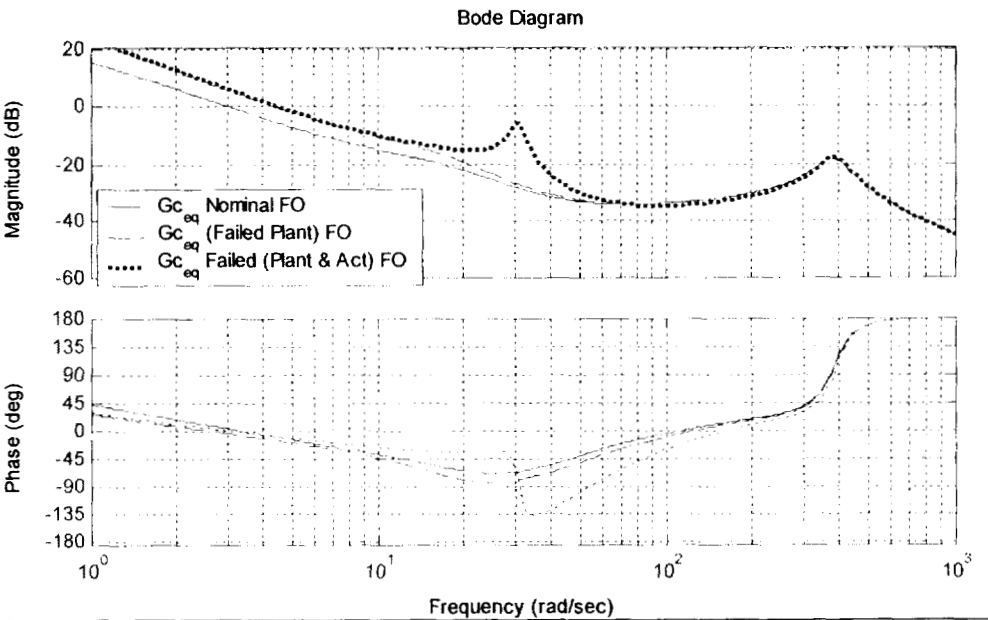

Figure 5-4: Gc_{eq} Nominal and Failed Plant Showing Control Adaptation. FSAVfo

The last failure examined here is the combination of both failures just examined. This is plotted along with the previous case in Fig. 5-3 and Fig. 5-4. It is seen that failing both the actuators and the plant results in a magnitude deficient frequency response with large phase roll-off. The controller is able to adjust for these effects successfully. There is helpful lead at low frequency and the poles to help with the failed actuators undamped natural frequency. Of interest is that the added pole is just below the *failed* actuator speed. A value which is unmeasured! The lag seen at high frequency is beyond the actuator bandwidth and less crucial than the lead before crossover. In addition it is well above the open loop bandwidth of 10 rad/sec.

Whatever the failure tested, investigation shows that in both models the controller is adapting to the failure. It should be restated that this adaptation is *instantaneous*, and *continuous*. This demonstrates the power of the SMC system when designed by the methods presented in this paper.

5.2 Multiple Observers

Throughout this project, the task of state estimation and the high frequency bypass loop was accomplished with observers. The independent observer structure provides huge benefits and significant design flexibility. The ability to compress the entire multiple channel assembly into a single state space is also beneficial to modeling as all of the internal states are available. This enhances the ability to tailor each input-output transfer function to some desired shape. This model had very little cross-coupling from airspeed to pitch rate and vice versa. If the model had been a lateral directional model, there could be large coupling between β(side slip angle) and yaw rate (r) which would require large cross-coupling terms. This could be done in either a plant style observer or a desired reduced order transfer function could be constructed, similar to the airspeed transfer function in this model, and then included in a constructed observer.

The benefits realized by the multiple observer architecture were critical to the success of this investigation and show great promise in any system where convergence needs to be controlled on independent loops.

5.3 Robustness and Observer Speed Selection

In §3.3 the ideas behind observer speed selection were discussed. While the above approach seems reasonable, it is necessary to verify that the models exhibit this behavior. Table 5-1 shows the results from simulations using the linear state space solution with no hedging on the FSAVfo model with model actuators at 30 rad/s and 2nd order actuators at 70 rad/s with no limiting.

Pq1	Wamin	RMS	Kamax
8	24	0.004483	2.35
11	28.5	0.003868	3.15
15	34	0.003649	4.4

Table 5-1: Table of Observer speed effects on Wa, RMS, and Ka max (FOwm30wa70, No Hedging)

The 'Pq1' term is defined in §2.5 but is the lowest observer eigenvalue. 'Wamin' is the minimum bandwidth of the actual 2nd order actuator required for stability of the system. It is a measure of the entire system's ability to tolerate parasitic dynamics, whether they take the form of pure time delay, limited bandwidth, or rate limiting. 'RMS' is the root-mean-square of the path error to a step input, compared to the response of the reference model. In an ideal system this error would be zero, indicating that the controller has forced the system to behave exactly like the reference model. It is, therefore, a measure of tracking performance. 'Ka_{max}' is the maximum plant multiplier, (kinematics excluded) for which the system will remain stable; it is a measure of the robustness to plant variation. Each of these factors is intended to show relative robustness and performance and no two are varied simultaneously.

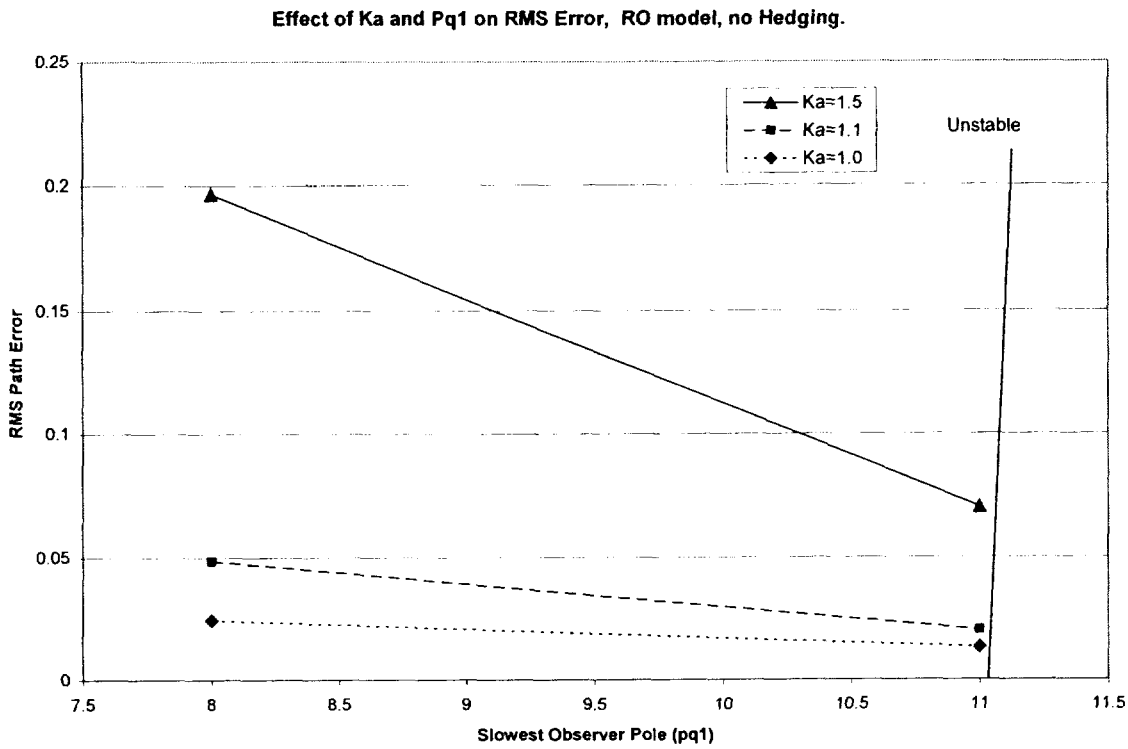

Figure 5-5: Effect of Ka and Pq1 on RMS error. FSAVro, No Hedging, Wa=70r/s

From the above definitions, Table 5-1 shows the following trends which are accurate for a very broad range of setups. Looking at Table 5-1 and Fig. 5-5, it is seen that as the observer speed is increased, the RMS path error decreases showing the improved tracking of the system. However, also notice that the minimum actuator bandwidth (Wamin) required for stability increases, demonstrating increased sensitivity to parasitic dynamics with increasing observer speed. Looking at Fig. 5-5, it is seen that in the case of the FSAVro model, the system is actually unstable at an observer speed of Pq1=15! This is of great interest as it shows the difference between the RO and FO models ability to handle the actuator dynamics. As stated, the parameter Ka_{max} relates to robustness to plant changes. The higher observer speeds are able to stabilize the system with twice as much parameter variation. Note here that multiplying the plant 'A' matrix

by 4.4 moves the plant's unstable eigenvalue from ~7 to ~31! This is only a linear ability, non-linear effects such as rate and position limits quickly reduce this margin. Figure(5-8 further supports this statement by showing that not only can the system tolerate larger plant parameter variation with increased observer speed, but there is significantly less path error sensitivity to small plant changes as revealed by the decreased slope of the faster observers.

5.4 Model Actuator Design and Observer Effects.

In §3.5 an alternative design, the FSAVfo was considered in which first order actuator dynamics are included in the SMC designed plant. This has many effects on the design. It mandates that a second order sliding manifold be used as was discussed, but it also suggests the use of a 'model actuator' in the control feedback path to the observer.

When the first order model was initially tried it was extremely sensitive to observer speed and actuator bandwidth. It was realized that the observer, which is intended to recreate the 'designed' plant, was not performing this action because the 'designed' plant from an SMC standpoint had first order actuators included. Thus, the high frequency bypass loop (§2.5.3) was not of the correct relative order. This suggests the inclusion of these dynamics in the bypass loop is appropriate. One might think to use the output of the actuators as the input to the observer, however, this requires measurement of those actuators with corresponding noise and failure detection issues and will likely be the incorrect relative order. Thus, a 1^{st} order model actuator is the next logical choice: It has the correct relative order and a dynamic response that is expected by the system and controller. Because the model actuators directly affect the input to the observer, this suggests and indeed it is found, that there are very large coupling effects

between them. The inclusion of the model actuator in the control loop greatly increases the robustness of the system and its tolerance to slow actuators. However, it was quickly realized that setting the bandwidth of this model actuators had a large effect on overall system performance. Perhaps if a slow model actuator is used the system will be more tolerant of actuator failure?

In order to answer the question, the state space representation of the entire model was used, including the reference model and SMC controller but not the pilot. To reduce the number of variables, the hedge gain is set to zero, removing it from the model. In Fig. 5-6 the effect of model actuator bandwidth on the ability to tolerate reduced actuator bandwidth is shown.

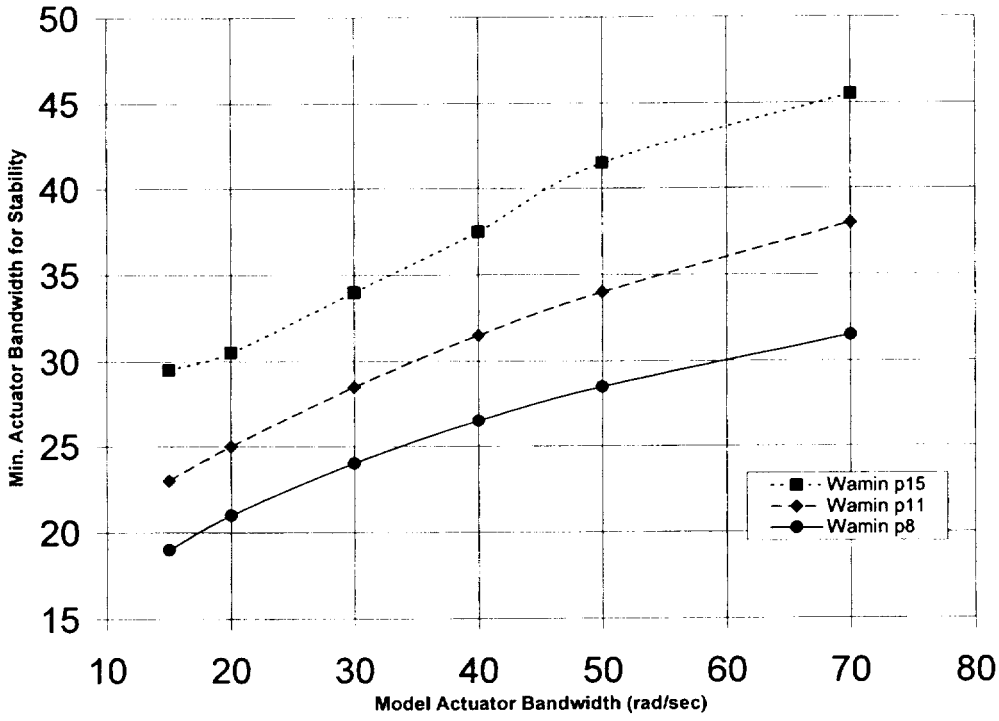

Figure 5-6: Plot of Min. Actuator Bandwidth vs. Model Actuator Bandwidth. FSAVfo

Multiple observer speeds are included in the plot as well, which shows two important points. First, it reiterates what was demonstrated in §3.4, that faster observers are less tolerant of slower actuators. Secondly, it shows that the trend in model actuator effect is not particular to a single observer speed. The system can now be made significantly more robust to some types of actuator failures by slowing down the model which the observer "sees".

In Fig. 5-7 it is shown that there are even some plant robustness benefits to a slower model actuator. The idea here is that the model actuators are adding in phase lag which the actual system doesn't possess. In addition, the added lag forces the system to drive the plant less aggressively, which leads to larger allowable plant variation.

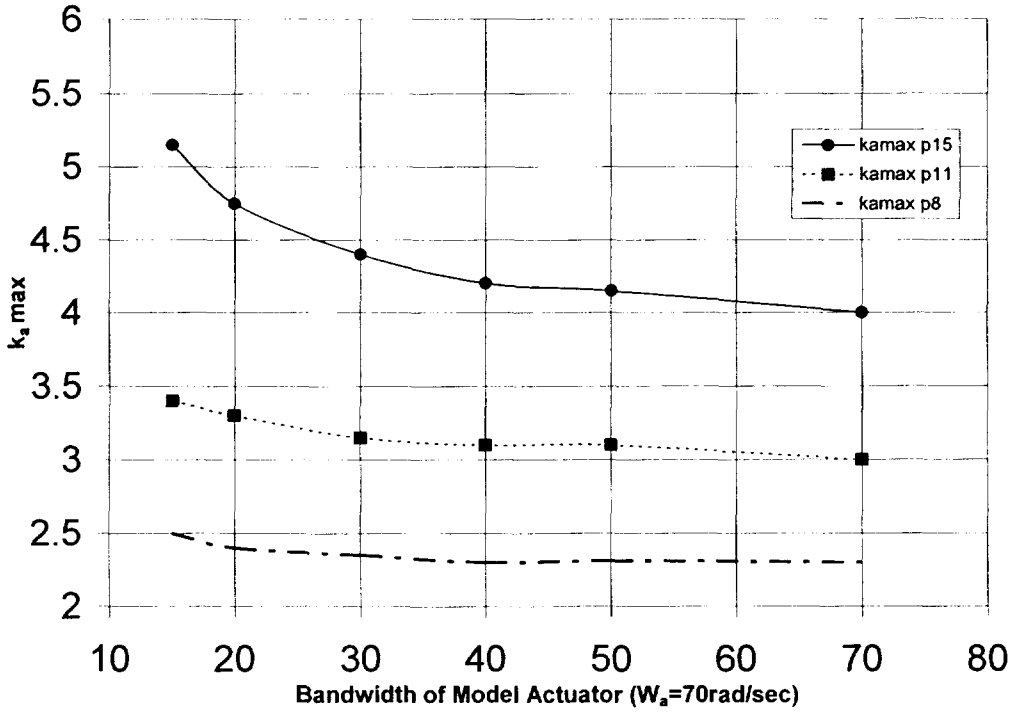

Figure 5-7: Allowable $K_a$max vs. Model Actuator Bandwidth. FSAVfo

It seems too good to be true; slow down the model actuators and obtain stability for some very large and dramatic actuator failures as well as some extra plant robustness. As the above paragraph suggested and as might be expected, there can be a price to pay in tracking performance.

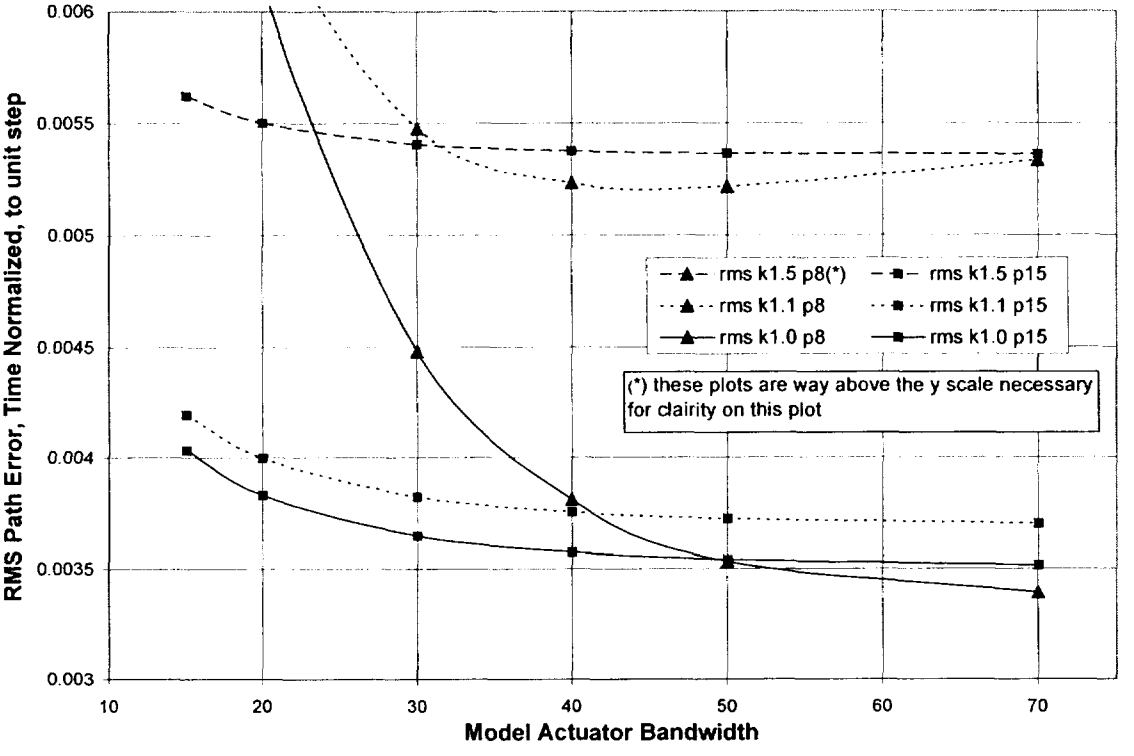

Figure 5-8: Path error as a function of K_a Pq1, and Model Act. bandwidth. FSAVfo

In Fig. 5-8 the RMS path error with varied plant failure parameter K_a, observer speed Pq1, and model actuator bandwidth is shown. This is a fairly complicated graph so detailed discussion is warranted. First, by comparing two lines with the same observer speed (constant symbols are used, like square or triangle data point markers) and a given model actuator bandwidth, it is seen that a slower observer has less ability to minimize error with plant parameter variation, except for a small area above W_a=50

rad/sec. (This will be discussed later.) However, more importantly for a given plant failure, the tracking error is flatter when the model actuators are slowed down. In other words, the model actuator bandwidth has a smaller effect on RMS path error for faster observers. Furthermore, path error changes due to plant changes are reduced for faster observers and faster model actuators. They are flatter as the observer speed increases, indicating that they are also less affected by a slower model actuator.

In all the models studied, there was a point, roughly 30% below the designed actuator bandwidth, where there is a high level of invariance with observer speed, and a decreased RMS path error for slower observer speeds. This behavior is quite contrary to the expected and perceived behavior of the nonlinear system. The details of this are not entirely understood.

The result of this analysis to the design engineer is that he/she must select the trade-off between performance and robustness. A recommendation at this step would be to favor robustness and then use hedging and any other method to increase observer speed. The observer design is rarely adapted to the actuator model, but the actuator model design is affected by the observer speed selected. If an initial design parameter must be selected, a value approximately 60% of the nominal actuator bandwidth would be appropriate, remembering that model actuator design must be optimized on a system level. The results of this effort is greater robustness to actuator bandwidth, and as long as the observer speed is increased with hedging, little, if any, tracking performance is lost.

5.5 First Order Vs Reduced Order and Noise

One of the primary investigations of the research was to examine the costs and benefits of including some of the actuator dynamics in the designed plant model. Analysis of the matching conditions in §3.6.1 suggests that perhaps including the actuator in the model could be beneficial. While it is tempting to believe all orders of the actuator dynamics should be included, the increasing order of the derivatives in the controller combined with state measurement noise will be disastrous to stability and the actuator command signal. The noise penalty of higher derivatives prompted the concept of including some, but not all of the actuator dynamics in the plant model.

Given the noise and actuator command issues, with all the actuator dynamics, only the first order dynamics were included. Thus, a first order actuator is assumed as part of the plant, and only one derivative needs to be taken in the controller. The results were mixed. In systems with little noise, or with actuators which do not object to noise, the inclusion of the first order dynamics increased robustness and off design performance. Comparison of the tracking response in this system showed noticeable improvement. Under the nominal case shown in Fig. 5-9 there is small difference with the FSAVro system being negligibly bouncier.

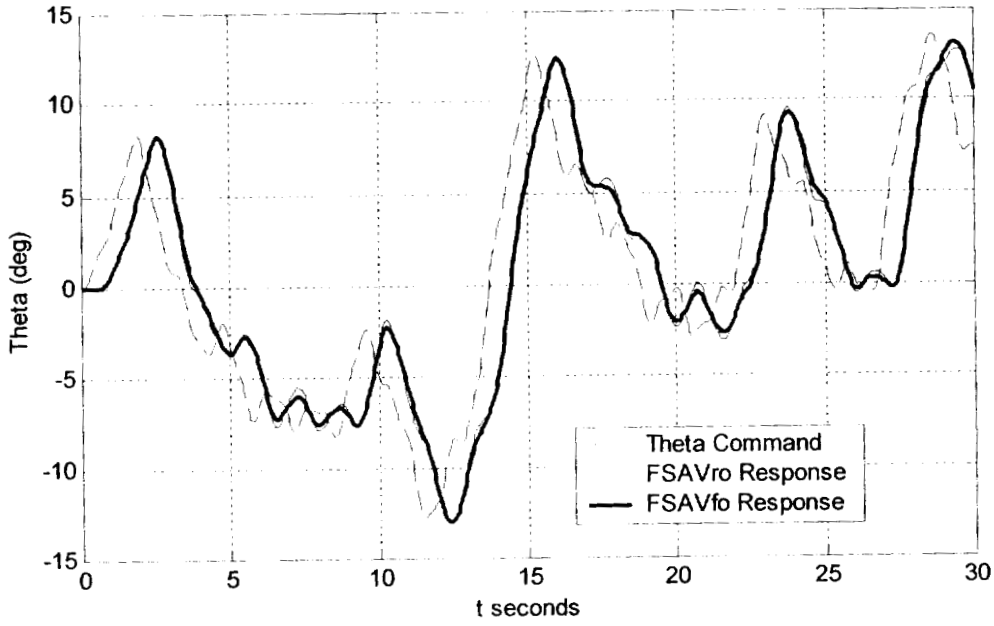

Figure 5-9: Plot of FSAVro and FSAVfo Nominal θ tracking.

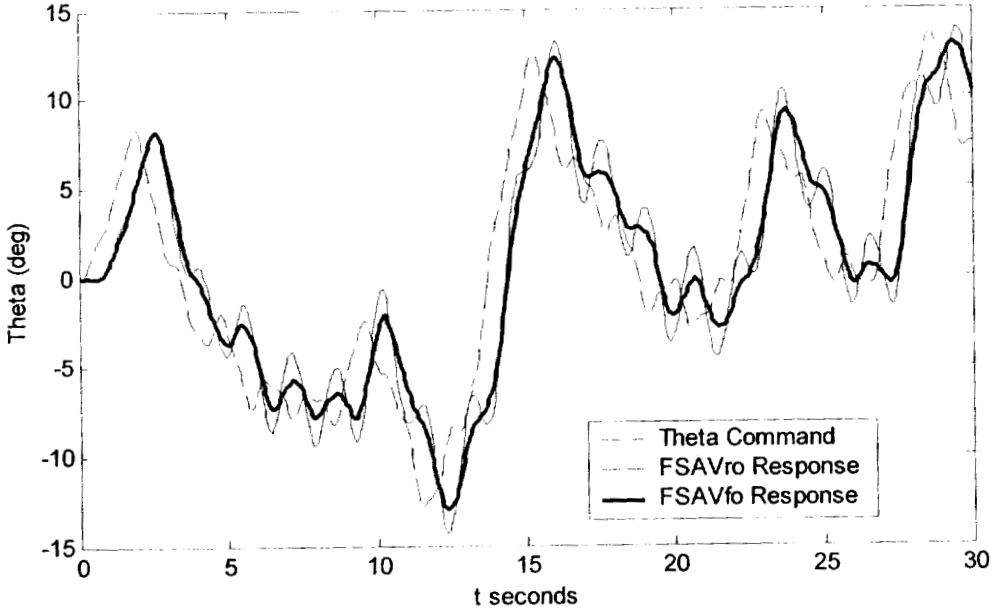

Figure 5-10: Plot of FSAVro and FSAVfo Failed θ tracking.

In the failed case of Fig. 5-10 the difference is drastic. The failure experienced by each model in this plot is *not* identical. The FSAVfo model contains a slightly slower

actuator (35 vs. 40 rad/sec), and 50% more time delay (15 vs. 10 ms). The tracking performance of the FSAVro system is stable but quite oscillatory while the FSAVfo shows very good tracking.

The noise penalty paid for the improved robustness and tracking is shown in Fig. 5-11. The plot shows nominal case on top and failed case in the lower plot. Note the time scales are different in order to improve clarity and show the scale of the noise. If the designer is willing to take this amount of jitter in the control signal, then including the first derivative in the sliding surface will improve the system performance.

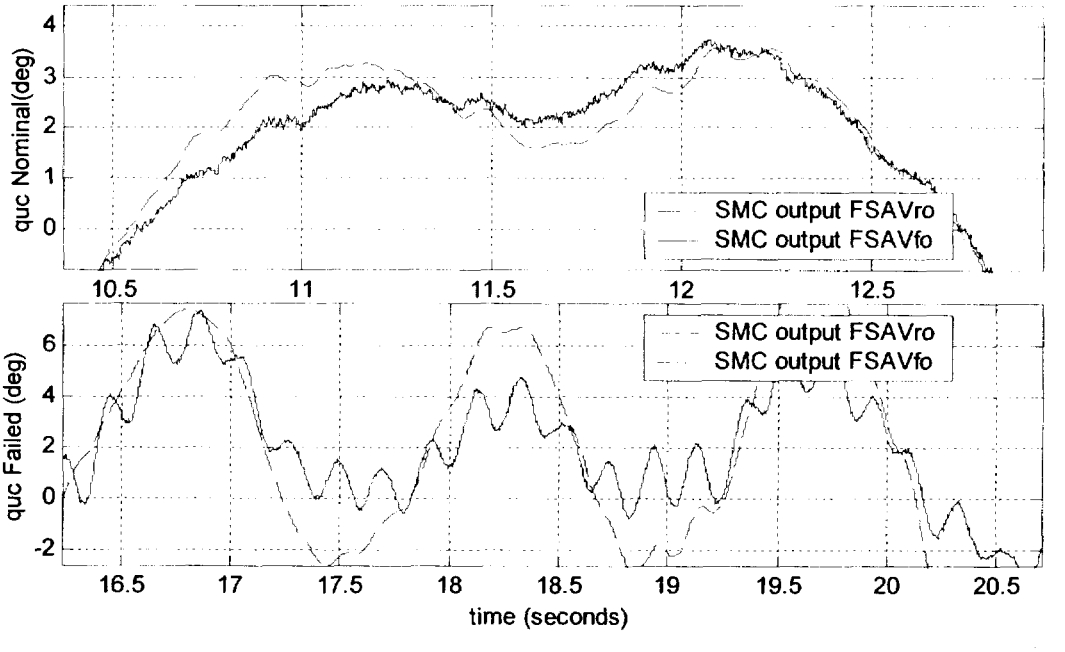

Figure 5-11: SMC output for FSAVro and FSAVfo, Nom. and Failed Conditions.

To further evaluate the effect of additive noise on the controller outputs, use the full state space model, sysCL. This time use the disturbance inputs and choose the output of the controller (u_c) as the output variable. A linear approximation of the transfer function can then easily be generated. The sysCL model does not contain the

structural modes of the wing. However, it can be shown that these modes have negligible effect on the noise transfer functions.

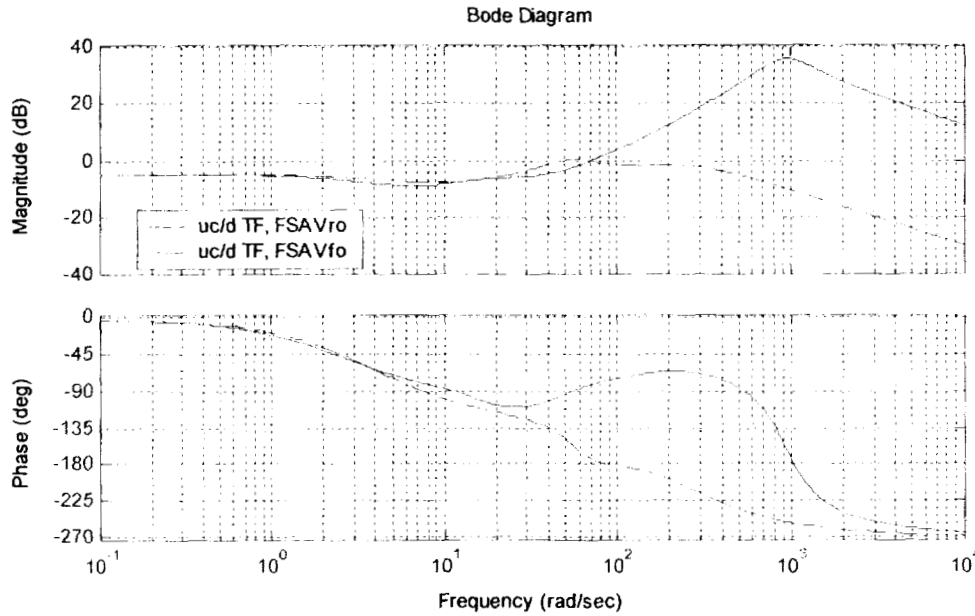

Figure	**5-12: Linear Approximation of $\frac{u_c}{d}$ TF for FSAVro and FSAVfo Model, $N_{linearize}$=1000.**

The $N_{linearize}$ term is used to convert the improper transfer function of the linearized SMC in the first order model. This has a significant effect on the loop shape as it is a large factor in determining the frequency at which the roll-off begins. The bode plot shows the difference in noise behavior and explains the fast jitter in the control found in the nominal case of Fig. 5-11 While the gain of 40 dB of the noise seems extremely large, it is noted that the power of the signal at these frequencies is quite low. This response is to a pure white noise input. Almost any noise shaping of this signal results in significantly improved bode shapes. If the filter used in Fig. 4-4 is included, the plots change shape drastically. The resulting bode diagram is seen in Fig. 5-13.

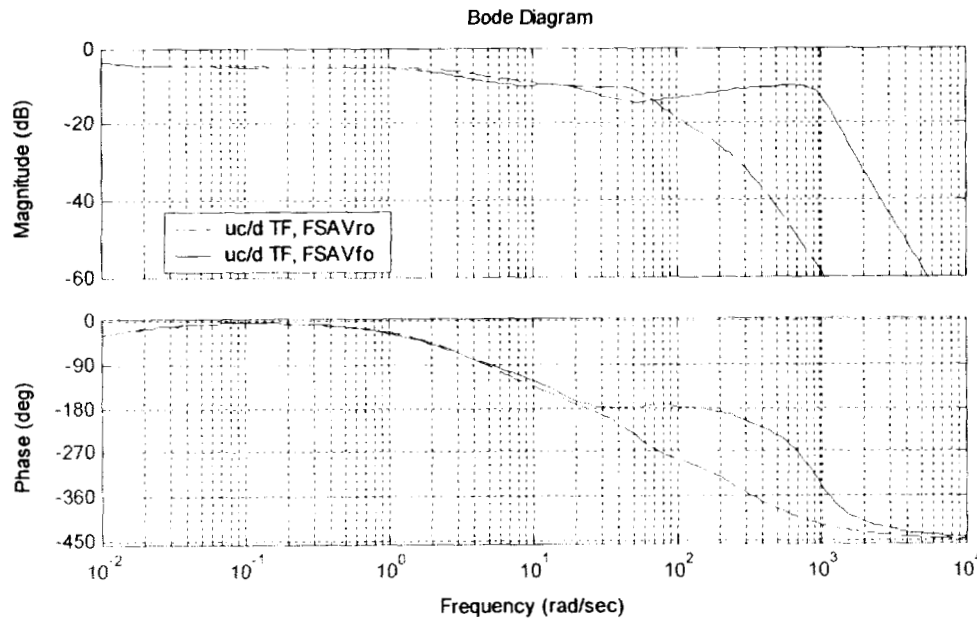

Figure	**5-13: Linear Approximation of $\frac{u_c}{d}$ TF for FSAVro and FSAVfo Model with white noise shaping, $N_{linearize}$=1000.**

Figure 5-13 shows the increase in noise with the inclusion of the derivative in the surface definition, but takes into account a limited bandwidth noise model. Since this is the filter used in all these models, this bode plot is a good representation of these systems' behavior.

This study did not delve heavily into the effect of noise on actuators, nor did it investigate or include any sophisticated attempt to filter the noise. Further study in this area could lead to positive results broadening the range of systems which can include at least one derivative in the sliding surface.

5.6 Adding Flaps: Costs and Rewards

The effect of additional actuators on robustness and performance can be remarkable or it can have only a small effect. Investigation into the use of the flaperons as a pitch control device shows that the effect on performance of the aircraft is negligible, while robustness is increased. Fig. 5-14 shows the nominal responses of the two systems.

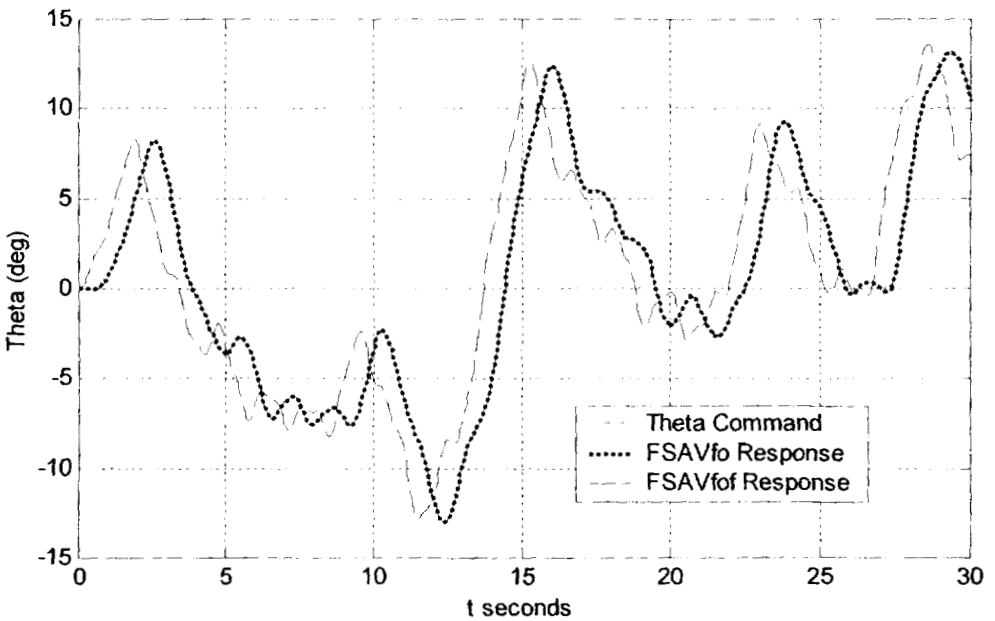

Figure 5-14: Plot of FSAVfo and FSAVfof Nominal θ tracking.

It can be seen that the difference in performance between the two systems is quite small. Magnified, the FSAVfof model may have slightly better tracking, but it is not really noticeable. Fig. 5-15 shows the failed responses.

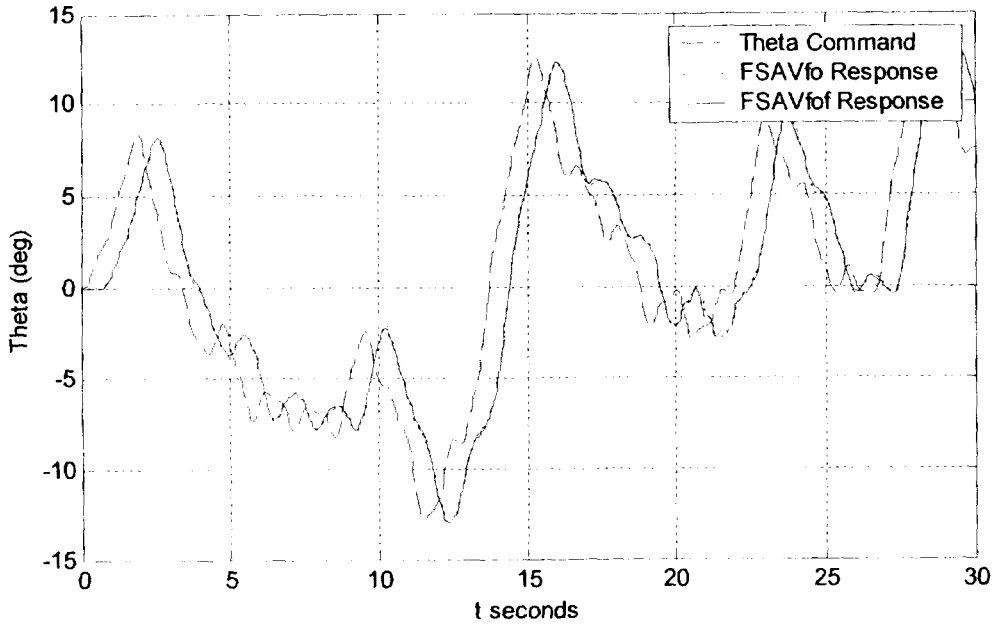

Figure 5-15: Plot of FSAVro and FSAVfo Failed θ tracking.

While larger, the difference in performance between the two systems is quite small. However, the failure which the FSAVfof model sustained causes the FSAVfo model to become unstable. Thus, the FSAVfof model maintains similar performance with increased failure.

The behavior of the FSAVfof model was quite sensitive and interesting. While a model can be constructed which uses only the flaperons as pitch control devices, models (particularly 'fo') which included the canard become unstable as the canard effectiveness is reduced, either by bandwidth or time delay. This behavior was not observed as strongly in a model created which was similar to the FSAVro model but also contained the flaperons. This behavior presents a drawback to the addition of the actuator dynamics to the plant. The addition of the model actuator to the feedback path means that those dynamics are expected in the model. As those dynamics decrease or

disappear, as in a position limit or jammed condition, the system can become unstable whereas models which include no actuator dynamics remain stable.

Hedging becomes significantly more complicated when flaps are added, particularly in the 'fo' models. The increased dynamics in the y_o state returned from the observer contains more poles and zeros then the model without flaps. While the resulting order is the same, more interactions develop between selected hedge poles/zero locations and the internal dynamics of the model. It is even more complicated in the 'fo' models because the model actuator doubles the number of pole/zero combinations. Considering the responses of the models, the benefit of multiple actuators is increased in models where the dynamics are not assumed ('ro') compared to those models which contain the dynamics ('fo'). The dynamics added to the high speed loop by the model actuators will destabilize a system which does not contain those dynamics. In a 'ro' model, where no actuator dynamics are assumed, the actuator redundancy acts to mitigate the effects of failed actuators. A possible thought process would be that in the 'ro' models the sum of the actuators must have enough power to stabilize the airplane. In the 'fo' models, they must have enough power to stabilize the airplane and be close enough to the model actuator so that they do not destabilize the controller. If the benefits of 'fo' modeling is desired and jam position and/or hard over robustness is desired, some additional form of failure detection or adaptation must be included.

Chapter 6

Conclusion

6.1 Summary

There are many motivations for investigating reconfigurable flight controllers and as many ways to implement them. Sliding Mode Control is one of the ways that offers instantaneous 'adaptation' to large parameter variation. In ideal systems, total invariance to matched parameters is possible. In real systems that include parasitic dynamics and finite bandwidth actuators, SMC becomes significantly more difficult to implement. Asymptotic observers and boundary layers on the sliding surface have been shown to partially compensate for parasitic dynamics while preserving some degree of parameter robustness. The inclusion of hedging, as a means of modifying the feedback shape, was shown to increase the ability of the SMC to handle unmodeled actuator dynamics and failures. This project presented methods for designing the sliding surface, the observers and there speeds, as well as the hedging transfer function, using the frequency domain backed up by simulations.

One of the critical question tackled in this project was, "Can SMC be used to control a highly unstable aeroelastic vehicle in the presence of real, unmodeled, limited bandwidth actuators and provide good performance and high robustness to actuator and plant variation?" It was shown that a SMC, with the addition of multiple observers and hedging, was indeed able to stabilize and provide high degrees of robustness to a highly unstable, aeroelastic model, the FSAV. Investigation into multiple design configurations

demonstrated the power and flexibility of SMC. It was shown that there are both benefits and drawbacks to the inclusion of actuator dynamics in the design of the sliding surface. Penalties of noise and failure type must be weighed against increased robustness and performance. The effect of redundant actuators was addressed showing increased robustness but more complicated design challenges, including effects from including actuator dynamics in the controller definition.

This research provides some solutions to the issues which SMC must overcome to become widely applied. In this sense, it was successful, but it was also successful in that it illuminated future options and possibilities for future investigations.

6.2 Future Questions

6.2.1 Measuring Actuators

It has been a tacit constraint throughout the design process that no measurement of actuators should be required. The added noise introduced, as well as significant questions regarding measurement failure, distinguishing between surface damage and actuator failure, as well as other issues were deemed to cloud an already complex situation. While a constraint on this research, many investigations throughout the literature measure actuator position, almost all of them make no mention of the issues which arise from this practice. Despite this warning, there is information to be obtained by measuring the actuator position. Some models were constructed which showed that fantastic results in both performance and robustness could be obtained for certain failures if actuator position was measured and included in the feedback system. The inclusion of this measurement increases the complexity of the failures which must be investigated. However, the potential for increased performance and robustness,

particularly to rate and position limits, suggests that this is a potentially fruitful direction for continued research.

6.2.2 Model Reference Hedging and Actuator Limits

While the concept of model reference hedging was initially applied to this model, it was morphed into a very useful, but slightly different actuator hedger. While the new system still serves the original purpose of hiding unmodeled dynamics, it has lost the global character previously desired. The sensitivity of the models presented to position limits, even without failures, was perhaps the largest shortcoming of the design. The application of true model reference hedging, where the system does not command rates or positions which cannot be obtained or will lead to instability, is still open for investigation. This seems like one of the most promising methods of dealing with actuator position limits and could drastically broaden the robustness of the entire system.

Along the same lines as model reference hedging, would be to investigate the effect of a feed forward term in the reference model. During the construction of the state space model a second identical reference model was accidentally included in the model. This appeared in the output as pure phase lag. This accentuated that the reference model does impose a time delay from the command. The control then attempts to track the new signal when there exists information (which is not used) about what will be coming. The entire system is lagged by 20 ms at the pilot bandwidth of 1.5 rad/sec, 80 at 5 rad/sec and 160 ms at 10 rad/sec. The information which is lagged could be used to improve model reference tracking and perhaps contribute to true model reference hedging.

6.2.3 Dynamic Everything

The entire investigation has focused on a single flight condition, with all of the subsystems as predefined. The robustness and performance of SMC is amazing however, in certain failures, or if the flight condition changes enough, a different controller could outperform the nominal SMC. The observer, the hedger, and the control allocation are all designed at a certain flight condition, the ability to reconfigure these system elements, as well as potentially the sliding surface, while maintaining the quick adaptation and general robustness of SMC is an exhilarating thought. Many of the current reconfiguring schemes for observers, and control allocation require parameter identification. While this method has many issues, the problem of incomplete adaptation, and the time delay required for adaptation would possibly be contained within the ability of the SMC to stabilize the system.

For simplicity, throughout this investigation a simple ganging was used in the control allocation matrix despite the fact that the model was responsive to changes in the control allocation matrix. The FSAVfof model was particularly sensitive compared to a FSAVrof model (a FSAVro model with flaperons added). As the canard was slowed or jammed, the control allocation matrix continued to send the command signal back through the observer which could drive the system unstable. The addition of a dynamic, reconfigurable control allocation scheme could improve the robustness and performance while optimizing control surface use.

Dynamic hedge gains present some interesting challenges. Initial work shows that the system is dramatically sensitive to the rate of change of hedge gain, so sensitive that the gain cannot be changed fast enough to be of much use. However, the modification

of the gain is not what is truly needed. It has been shown that, for optimality the dynamics need to be reshaped to adapt to slower or failed actuators. Continued research into adaptable hedge shapes could improve robustness and performance in failed conditions.[28]

Reconfigurable observers present the most understood and perhaps largest benefits to the ability of the system to adapt to huge changes in flight regime and long term system changes. Even simple gain scheduling of observers could easily allow the system to adapt to various flight regimes. It is highly possible that parameter identification could benefit from this subsystem adaptation, but again the delay and incomplete adaptation of the parameter identification scheme could almost certainly be dealt with effectively by the SMC structure.

6.3 Conclusion

Research into reconfigurable control and other means of obtaining increasing robustness and performance continues to march forward in many universities and throughout industry. With growing research into Sliding Mode Control as a means to simpler, higher performance and safer aircraft, it is hoped that this research has taken one step along the path toward a feasible and elegant solution.

Bibliography

[1]Eslinger, R. A., and Chandler, P. R., "Self-Repairing Flight Control System Program Overview," *Proceedings of National Aerospace and Electronics Conference*, IEEE, 1988, pp. 504-511.

[2]Chandler, P. R., Pachter, M., and Mears, M., "System Identification for Adaptive and Reconfigurable Control," *Journal of Guidance, Control, and Dynamics*, Vol. 18, No. 3, 1995, pp. 516-524.

[3]Urnes, J., Yeager, R. B., and Stewart, J., "Flight Demonstration of the Self-Repairing Flight Control System in a NASA F-15 Aircraft," *Proceedings of National Aerospace and Electronics Conference*, Dayton, OH, 1990.

[4]Caglayan, A. K., et al., "Detection, Identification, and Estimation of Surface Damage/Actuator Failure for High Performance Aircraft," *Proceedings of American Control Conference*, Atlanta, GA, Jun 1988, pp. 2206-2212.

[5]Morelli, E. A., "Real-Time Parameter Estimation in the Frequency Domain," *Proceedings of Guidance, Navigation, and Control Conference*, AIAA-99-4043, AIAA, Portland, OR, 9-11 Aug 1999.

[6]Siwakosit, W., Snell, S. A., and Hess, R. A., "Robust Flight Control Design with Handling Qualities Constraints Using Scheduled Linear Dynamic Inversion and Loop-Shaping," *IEEE Transactions on Control Systems Technology*, Vol. 8, No. 3, 2000, pp. 483-494.

[7]Shtessel, Y. B., Buffington, J. M., Pachter, M., Chandler, P. R., and Banda, S. S., "Reconfigurable Flight Control on Sliding Modes Addressing Actuator Deflection and Deflection Rate Saturation," *Proceedings of Guidance, Navigation, and Control Conference*, AIAA-98-4112, AIAA, Boston, MA, Aug 1998, pp. 127-137.

[8]Shtessel, Y. B., Buffington, J. M., and Banda, S. S., "Tailless Aircraft Flight Control Using Multiple Time Scale Re-Configurable Sliding Modes," *Proceedings of Guidance, Navigation, and Control Conference*, AIAA-99-4136, AIAA, Portland, OR, 9-11 Aug 1999, pp. 966-976.

[9]Shtessel, Y. B., Buffington, J. M., and Banda, S. S., "Multiple Time Scale Flight Control Using Re-configurable Sliding Modes," *Proceedings of 37th Conference on Decision and Control*, Vol. 4, IEEE, Tampa, FL, 16-18 Dec 1998, pp. 4196-4201.

[10]Shtessel, Y. B., Buffington, J. M., and Banda, S. S., "Multiple Timescale Flight Control Using Reconfigurable Sliding Modes," *Journal of Guidance, Control, and Dynamics*, Vol. 22, No. 6, 1999, pp. 873-883.

[11]Young, K. D., Utkin, V. I., and Özgüner, Ü. "A Control Engineer's Guide to Sliding Mode Control," *IEEE Transactions on Control Systems Technology*, Vol. 7, No. 3, 1999, pp. 328-342.

[12]Utkin, V. I., "Variable Structure Systems with Sliding Mode," *IEEE Transactions on Automatic Control*, Vol. AC-22, No. 2, 1977, pp. 212-222.

[13]Gilbert, M. G., "Dynamic Modeling and Active Control of Aeroelastic Aircraft," Purdue University, 1982.

[14]Itkis, Y., *Control Systems of Variable Structure*, Wiley, New York, NY, 1976.

[15]Slotine, J.-J. E., and Li, W., *Applied Nonlinear Control*, Prentice Hall, Englewood Cliffs, NJ, 1991.

[16]Edwards, C., and Spurgeon, S. K., *Sliding Mode Control*, Taylor & Francis Ltd, Bristol, PA, 1998.

[17]Shtessel, Y. B., and Tournes, C. H., "Flight Control Reconfiguration on Sliding Modes," *Proceedings of Guidance, Navigation, and Control Conference*, AIAA-97-3632, AIAA, New Orleans, LA, Aug 1997, pp. 1288-1298.

[18]Shtessel, Y. B., and Tournes, C. H., "Nonminimum Phase Output Tracking in Dynamic Sliding Manifolds with Application to Aircraft Control," *Proceedings of 35th Conference on Decision and Control*, Vol. 2, IEEE, Kobe, Japan, 11-13 Dec 1996, pp. 2071-2076.

[19]Shtessel, Y. B., and Lee, Y.-J., "New Approach to Chattering Analysis in Systems with Sliding Modes," *Proceedings of 35th Conference on Decision and Control*, Vol. 4, IEEE, Kobe, Japan, 11-13 Dec 1996, pp. 4014-4019.

[20]Shtessel, Y. B., and Buffington, J. M., "Continuous Sliding Mode Control," *Proceedings of American Control Conference*, Vol. 1, IEEE, Philadelphia, PA, 24-26 Jun 1998, pp. 562-563.

[21]Shtessel, Y. B., and Buffington, J. M., "Finite-Reaching-Time Continuous Sliding Mode Controller for MIMO Linear Systems," *Proceedings of 37th Conference on Decision and Control*, Vol. 2, IEEE, Tampa, FL, 16-18 Dec 1998, pp. 1934-1935.

[22]Hess, R. A., Wells, S. R., and Vetter, T. K., "MIMO Sliding Mode Control as an Alternative to Reconfigurable Flight Control Designs," *Proceedings of American Control Conference*, IEEE, Anchorage, AK, 8-10 May 2002.

[23]Hess, R. A., and Wells, S. R., "Sliding Mode Control Applied to Reconfigurable Flight Control Design," *Proceedings of 40th AIAA Aerospace Sciences Meeting and Exhibit*, AIAA-2002-7751, AIAA, Reno, NV, 14-17 Jan 2002.

[24]Hess, R. A., Siwakosit, W., and Chung, J., "Accommodating a Class of Actuator Failures in Flight Control Systems," *Journal of Guidance, Control, and Dynamics*, Vol. 23, No. 3, 2000, pp. 412-419.

[25]Hess, R. A., Siwakosit, W., and Chung, J., "Accommodating Actuator Failures in Flight Control Systems," *Proceedings of 37th Aerospace Sciences Meeting*, AIAA-99-0634, AIAA, Reno, NV, 1999.

[26]Wells, S. R., and Hess, R. A., "A Frequency-Domain Interpretation of Robustness in Sliding Mode Control Design with Boundary Layers," *IEEE Transactions on Control Systems Technology*, submitted.

[27]Wells, S. R., and Hess, R. A., "MIMO Sliding Mode Control for a Tailless Fighter Aircraft, An Alternative to Reconfigurable Architectures," *Proceedings of Guidance, Navigation, and Control Conference*, AIAA, Monterey, CA, submitted.

[28]Wells, S., "Application of Sliding Mode Methods to the Design of Reconfigurable Flight Control Systems," Dissertation Thesis, University of California, Davis, Davis, CA, 2002.

[29]Filippov, A. F., "Differential Equations with Discontinuous Right Hand Sides," *Am. Math Soc. Transl.*, Vol. 42, 1964, pp. 193-231.

[30]Johnson, E. N., Calise, A. J., El-Shirbiny, H. A., and Rysdyk, R. T., "Feedback Linearization with Neural Network Augmentation Applied to X-33 Attitude Control," *Proceedings of Guidance, Navigation, and Control Conference*, AIAA-2000-4157, AIAA, Denver, CO, 14-17 Aug 2000, pp. 1-11.

[31]The Author would like to thank Seth Dutter for his insight in to this solution.

[32]Hess, R. A., "Unified Theory for Aircraft Handling Qualities and Adverse Aircraft-Pilot Coupling," *Journal of Guidance, Control, and Dynamics*, Vol. 20, No. 6, 1997, pp. 1141-1148.

[33]Kish, B. A., Mosle, W. B., III, Remaly, A., Seo, J., Cabiati, R., and Kromberg, J., "A Limited Flight Test Investigation of Pilot-Induced Oscillation Due to Elevator Rate Limiting (HAVE LIMITS)," USAF TPS/EDB, AFFTC-TR-97-12, Edwards AFB, CA, June, 1997.

[34]Hess, R. A., and Stout, P. W., "Assessing Aircraft Susceptibility to Nonlinear Aircraft-Pilot Coupling/Pilot-Induced Oscillations," *Proceedings of Atmospheric Flight Mechanics Conference*, AIAA-97-3496, AIAA, 1997.

[35]Hess, R. A., "A Unified Theory for Aircraft Handling Qualities and Adverse Aircraft-Pilot Coupling," *Proceedings of 35th Aerospace Sciences Meeting and Exhibit*, AIAA-97-0454, AIAA, Reno, NV, 6-10 Jan 1997, pp. 1-12.

Index

V

X

UNIVERSITY OF CALIFORNIA, DAVIS

BERKELEY • DAVIS • IRVINE • LOS ANGELES • MERCED • RIVERSIDE • SAN DIEGO • SAN FRANCISCO SANTA BARBARA • SANTA CRUZ

DEPARTMENT OF MECHANICAL AND
AERONAUTICAL ENGINEERING
TELEPHONE: (530) 752-0580
FAX: (530) 752-4158
http://mae.engr.ucdavis.edu

ONE SHIELDS AVENUE
DAVIS, CALIFORNIA 95616-5294

DELINQUENT FINAL REPORT
Summary of Research

September 28, 2002

ATTN: Carol Dancy, Document Processing Section
NASA Center for AeroSpace Information (CASI)
7121 Standard Drive
Hanover MD 21076-1320

Dear Ms Dancy

This concerns NASA Cooperative Agreement NCC-1-01010. Enclosed are copies of two graduate theses completed under the identified agreement. Also enclosed are copies of three manuscripts that have also been completed under the agreement. These latter manuscripts are under review by, or will be submitted to, technical journals for publications. All these documents are intended to serve as the Summary of Research for the agreement identified above.

Sincerely,

Ronald A. Hess
Professor and Vice Chairman

cc: René H. Domino